AD743180

MODELS OF RADIATION TRANSPORT IN AIR –

THE ATR CODE

INTERIM REPORT

1 April 1970 through 15 November 1971

by

R. J. Harris, Jr.
J. A. Lonergan
L. Huszar

HEADQUARTERS
Defense Nuclear Agency
Washington, D.C. 20305

D. D. C.

JUN 12 1972

B
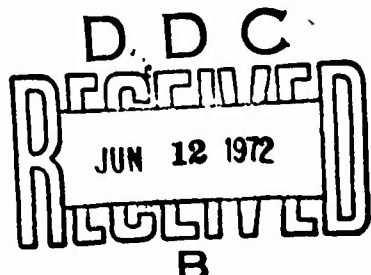
Contract DASA01-70-C-0090

Approved for public release; distribution unlimited.

SCIENCE APPLICATIONS, INCORPORATED

P.O. Box 2351, 1250 Prospect St., La Jolla, Calif. 92037 (714) 459-0211

ₗₗ9

APPROVED FOR PUBLIC RELEASE; DISTRIBUTION UNLIMITED

DESTROY THIS REPORT WHEN IT IS NO

LONGER NEEDED. DO NOT RETURN TO SENDER.

DNA 28031

MODELS OF RADIATION TRANSPORT IN AIR —

THE ATR CODE

by

R. J. Harris, Jr.
J. A. Lonergan
L. Huszar

Security Classification

DOCUMENT CONTROL DATA - R & D

(Security classification of title, body of abstract and indexing annotation must be entered when the overall report is classified)

1 ORIGINATING ACTIVITY *(Corporate author)*	2a. REPORT SECURITY CLASSIFICATION
Science Applications, Inc. P.O. Box 2351, 1250 Prospect Street La Jolla, California 92037	UNCLASSIFIED
	2b GROUP

3 REPORT TITLE

Models of Radiation Transport in Air - The ATR Code

4 DESCRIPTIVE NOTES *(Type of report and inclusive dates)*

Final Report

5 AUTHOR(S) *(First name, middle initial, last name)*

Robert J. Harris, Jr., James A. Lonergan and Louis Huszar, Jr.

6 REPORT DATE	7a. TOTAL NO OF PAGES	7b. NO OF REFS
November 1971	123	81

8a. CONTRACT OR GRANT NO DNA01-70-C-0090	9a. ORIGINATOR'S REPORT NUMBER(S)
b PROJECT NO NWED Subtask Code PB045	SAI-71-557-LJ
c Work Unit Code 02	9b OTHER REPORT NO(S) *(Any other numbers that may be assigned this report)*
d	DNA 2803I

10 DISTRIBUTION STATEMENT

Approved for public release; distribution unlimited.

11 SUPPLEMENTARY NOTES	12 SPONSORING MILITARY ACTIVITY
	Defense Nuclear Agency Washington, D. C. 20305

13 ABSTRACT

This interim report describes the work to date on development of the ATR computer code - a user-oriented code for calculating quickly and simply radiation environment problems at all altitudes in the atmosphere. The ATR code is based on parametric models of a comprehensive data base of air transport results which was generated using rigorous transport techniques for infinite homogeneous air. The effects of an air-ground interface and non-uniform air density are treated as perturbation corrections on homogeneous-air results. The data base has been generated for neutrons, secondary gamma-rays, high-energy photons and low energy photons as a function of space, energy and angle out to ranges of 550 gm/cm^2 of air. Parametric models have been developed for all of this data base except photon angular distribution and a version of ATR has been completed for neutron and secondary gamma-ray transport.

DD FORM 1473

Security Classification

14 KEY WORDS	LINK A		LINK B		LINK C	
	ROLE	WT	ROLE	WT	ROLE	WT
ATR Computer Code						
Radiation Transport in Air						
Neutron						
Secondary Gamma-Ray						
Photon						
Parametric Models						
Air-Ground Interface						
Non-Uniform Air Density						

ABSTRACT

This interim report describes the work to date on development of the ATR computer code - a user-oriented code for calculating quickly and simply radiation environment problems at all altitudes in the atmosphere. The ATR code is based on parametric models of a comprehensive data base of air transport results which was generated using rigorous transport techniques for infinite homogeneous air. The effects of an air-ground interface and non-uniform air density are treated as perturbation corrections on homogeneous-air results. The data base has been generated for neutrons, secondary gamma-rays, high-energy photons and low energy photons as a function of space, energy and angle out to ranges of 550 gm/cm^2 of air. Parametric models have been developed for all of this data base except photon angular distribution and a version of ATR has been completed for neutron and secondary gamma-ray transport.

TABLE OF CONTENTS

LIST OF FIGURES

LIST OF FIGURES (Cont'd)

LIST OF FIGURES (Cont'd)

LIST OF FIGURES (Cont'd)

LIST OF FIGURES (Cont'd)

LIST OF TABLES

I. INTRODUCTION

This report describes research performed at Science Applications, Inc. over the past year to develop parametric models for efficiently calculating radiation transport in the atmosphere. The fundamental problem being solved is to represent the free-field radiation environment for monoenergetic sources by parametric equations so that free-fields for arbitrary source spectra can be calculated quickly by simple folding operations.

Our general approach was to develop detailed parametric models by curve fits to rigorous transport data for infinite homogeneous air, and to include the effects of an air-ground interface and exponential air density as perturbation corrections. The end result of this effort is the ATR computer code which has been designed as a user-oriented code to calculate a wide variety of radiation environment problems at all altitudes in the atmosphere.

The work to date includes: (1) the development of a comprehensive data base of homogeneous air transport results as a function of source energy, space, energy and angle for neutrons, secondary gamma-rays, high-energy photons and low-energy photons; (2) parametric models for the entire data base except for photon angular distribution; (3) corrections to homogeneous air results for neutrons and secondary gamma-rays and; (4) a completed version of ATR for neutrons and secondary gamma-rays. Detailed discussions of these items are given in subsequent sections.

II. DATA BASE FOR RADIATION TRANSPORT IN HOMOGENEOUS AIR

Although many volumes of data for radiation transport in the air have been compiled over the years (see Appendix A) much of it has been out-dated because of newer cross-section data. Even more recent results are often available only in tabulated form or only for a selected range of values in the independent variables. All of these factors make it difficult to assemble a consistent comprehensive data base from existing results which is suitable for production-processing by computer. For this reason, we have generated a complete and uniform data base at SAI using rigorous transport codes based on the most recent cross-section data available. These calculations will be described in this section including selected comparisons with other calculated results and experiments. It is anticipated that the complete data base will be available in published form at the end of this contract year.

2.1 Neutron and Secondary Gamma-Rays

The data base for neutron and secondary gamma-ray transport was based on Straker's results[13] published in ORNL 4464. These data were considered to be the most definitive and comprehensive set of calculations available at the time and have been thoroughly documented including detailed comparisons with integral experiments. The SAI data base was generated using the identical P5S16 air cross-sections of ORNL 4464 provided by Straker in 22 neutron groups and 18 gamma groups.

The SAI calculations were made with ANISN for 18 monoenergetic source bands and for a maximum range of 5000 meters at a uniform air density of 1.11 mg/cm^2. Since these calculations were made, recently evaluated cross-sections for nitrogen and oxygen have become available from the work of Young. Selected calculations were performed using Young's cross-sections to determine their effect on the existing data base. The dose versus distance results for neutron and secondary gamma-rays are shown in Fig. 1 and Fig. 2, respectively, for a 14 MeV neutron source. The largest discrepancy occurs for secondary gamma-rays with the results obtained using Young's cross-sections being lower than Straker's by as much as a factor of 2. The source of this difference is indicated in Fig. 3 which shows Young's gamma-production cross-sections being lower than Strakers by a factor of two. The question of which is the more accurate cross-section data seems unclear at this time because of conflicting conclusions between theory-experiment comparison. Secondary gamma-ray results from the HENRE experiment[17] are in good agreement with Straker's cross-sections, but the recent re-analysis of LN_2 experiments by Reynolds[16] is in better agreement with Young's cross-sections. It is anticipated that this discrepancy will be resolved soon and allow the data base for ATR to be updated accordingly.

2.2   High-Energy Photons

The photon transport data base is needed for a wide range of energies extending from about 10 keV up to 10 MeV. Two separate

4.
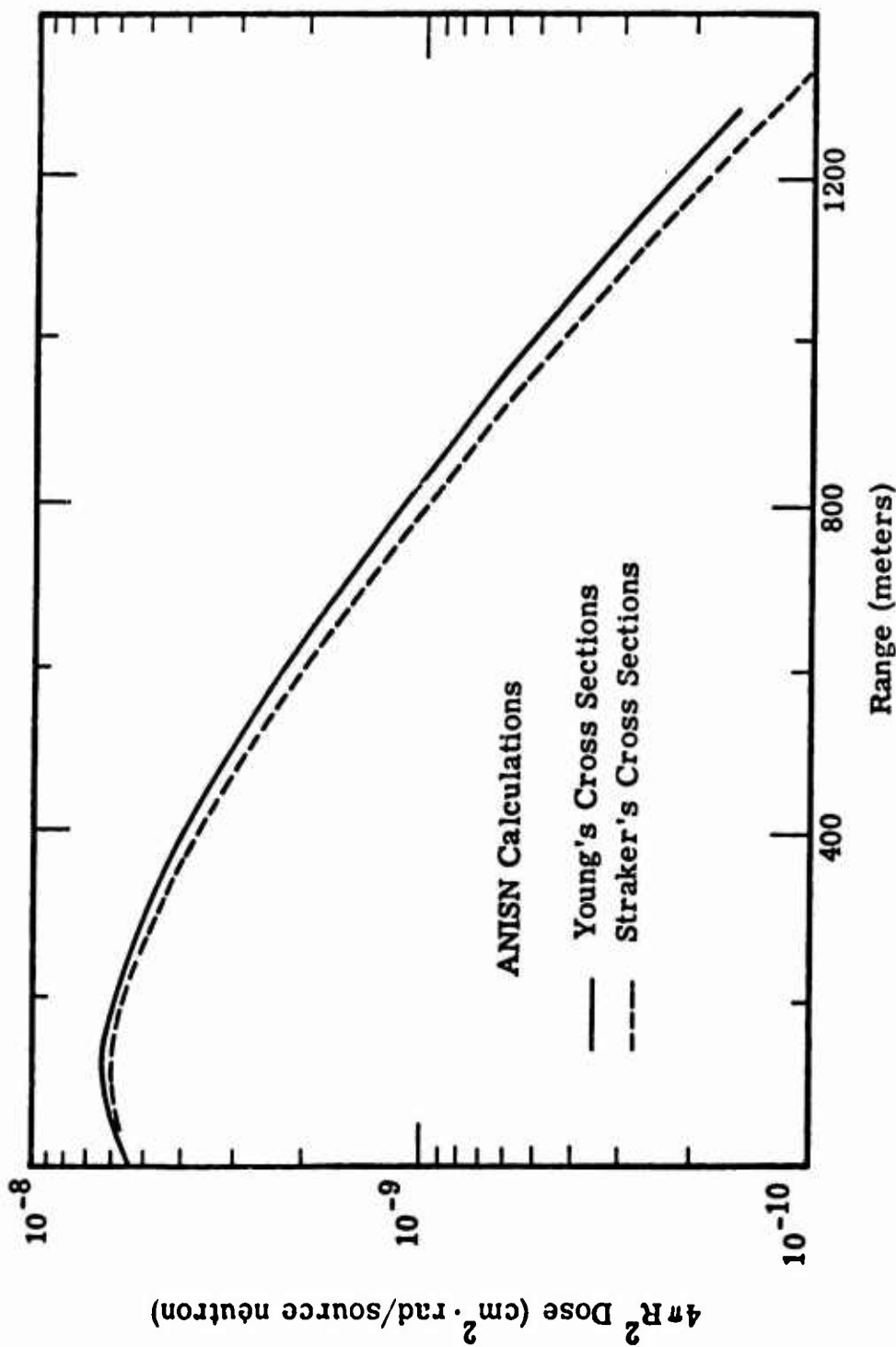
Fig. 1. $4\pi R^2$ neutron dose versus range for a point isotropic 14 MeV source in infinite homogeneous air.

5.
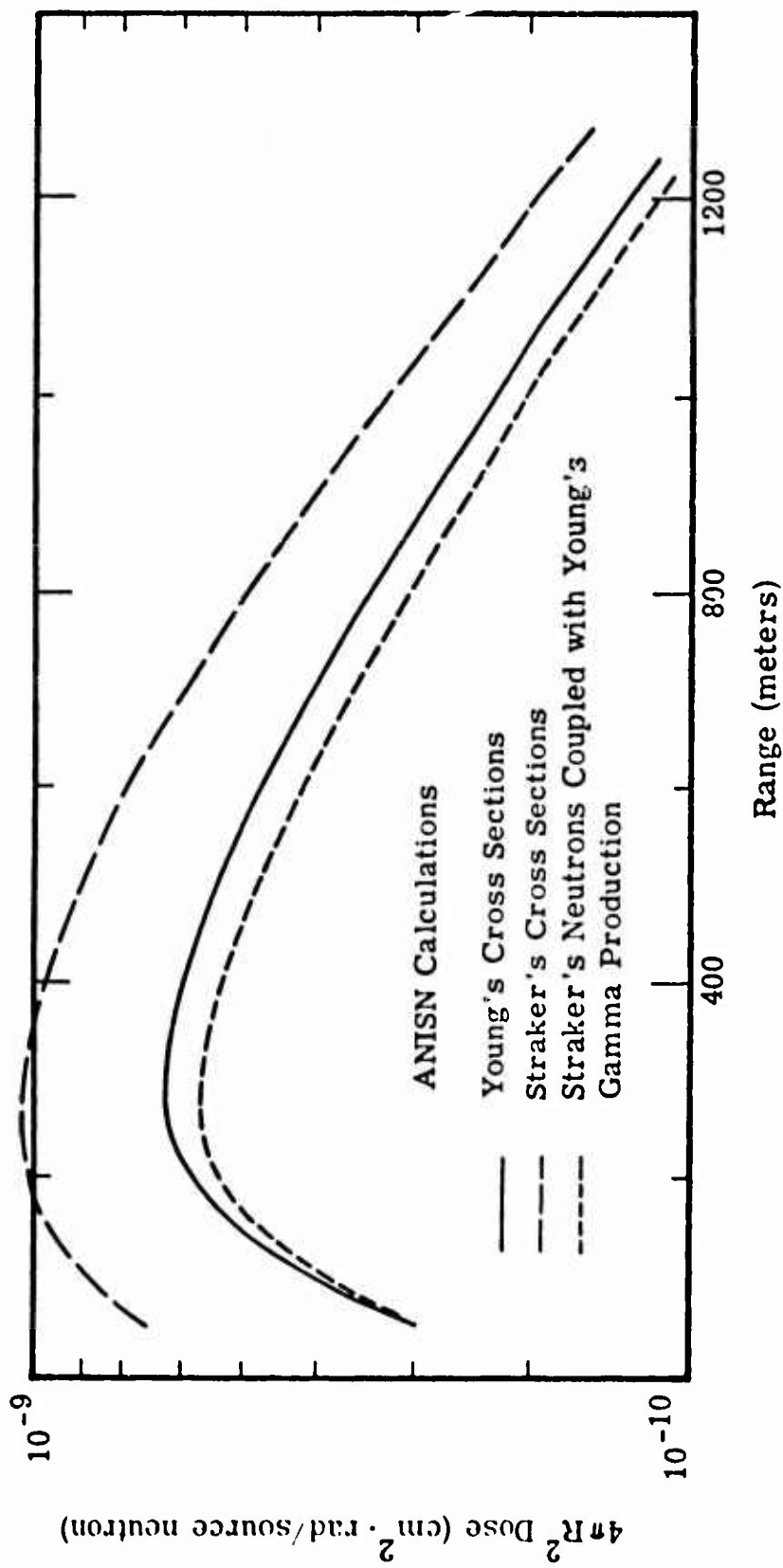
Fig. 2. $4\pi R^2$ secondary gamma-ray dose versus range for a point isotropic 14 MeV source in infinite homogeneous air.

6.
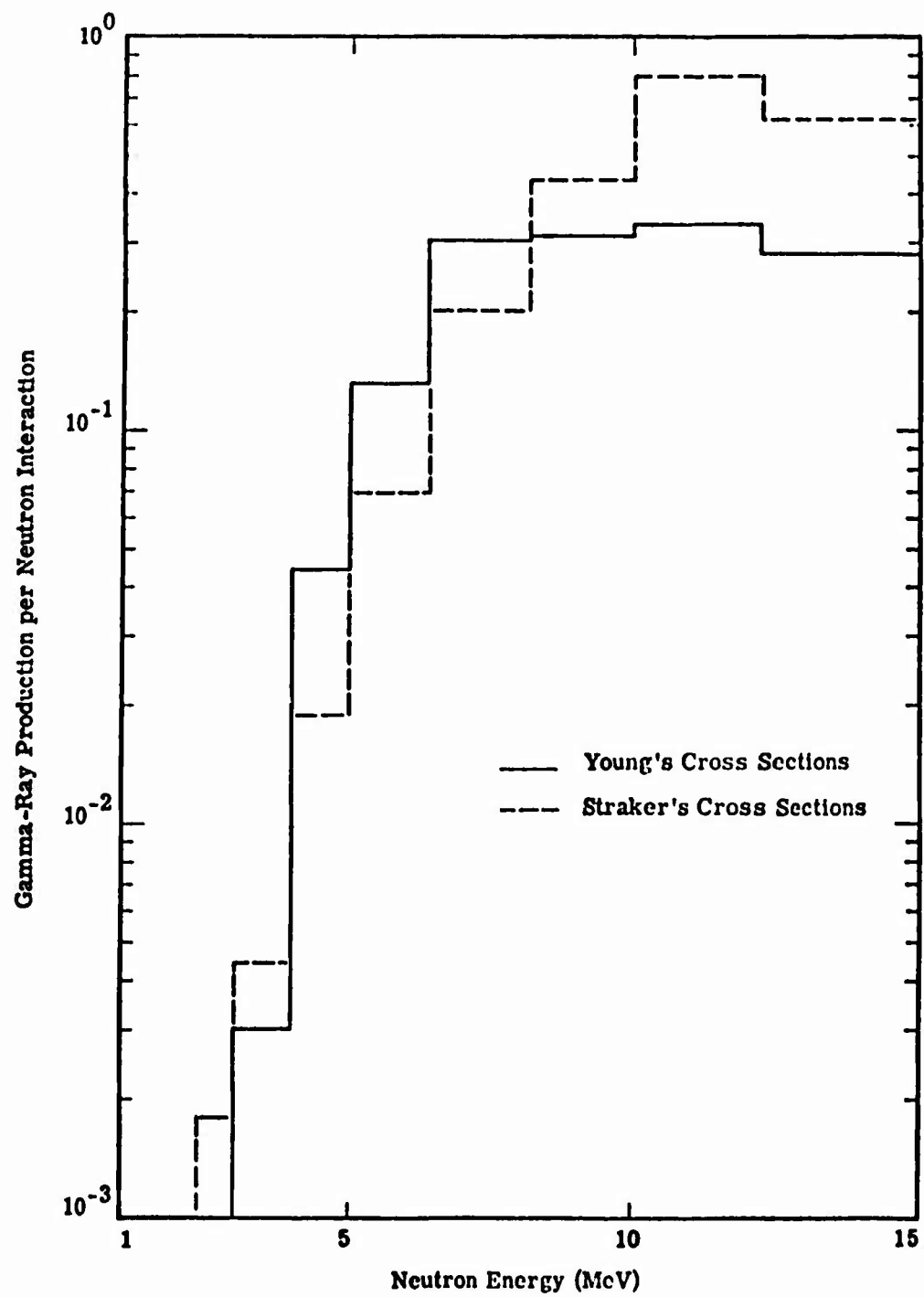
Fig. 3. Comparison of Young's and Straker's gamma-ray production cross sections.

transport calculations were made in order to achieve an optimum group structure for both the high and low photon energy ranges. The high-energy photon transport data base was calculated using DTFXRAY in the P5S16 approximation with an analytical first-collision source. The group structure was the same 18 group representation from .02 to 10 MeV used for the secondary gamma-rays and the maximum range was 5000 meters in air of density 1.11 mg/cm^3. GAMLEGX with pair production was used to prepare multigroup cross-sections. The air composition by weight was 0.2318 for oxygen, 0.7553 for nitrogen and 0.0129 for argon. Input absorption cross-sections were taken from Hubbell[78] for energies above 1 MeV and from McMaster[79] for energies below 1 MeV. Scattering cross-sections are calculated internally in GAMLEGX by the Klein-Nishina formula. All photon transport calculations were made without coherent scattering since GAMLEGX can only treat coherent scattering as isotropic. This approximation tends to be poor at low energies where coherent scattering is the most important.

Before generating the high energy photon data base, several test calculations were performed to test the overall sensitivity of the results to choice of cross-section data and transport code. Figure 4 shows a comparison of dose versus distance results calculated with different codes and cross-sections sets. A maximum difference of about 20% occurs at 100 gm/cm^2, with the ANISN, DTFXRAY and OGRE results being in very close agreement with each other.

8.
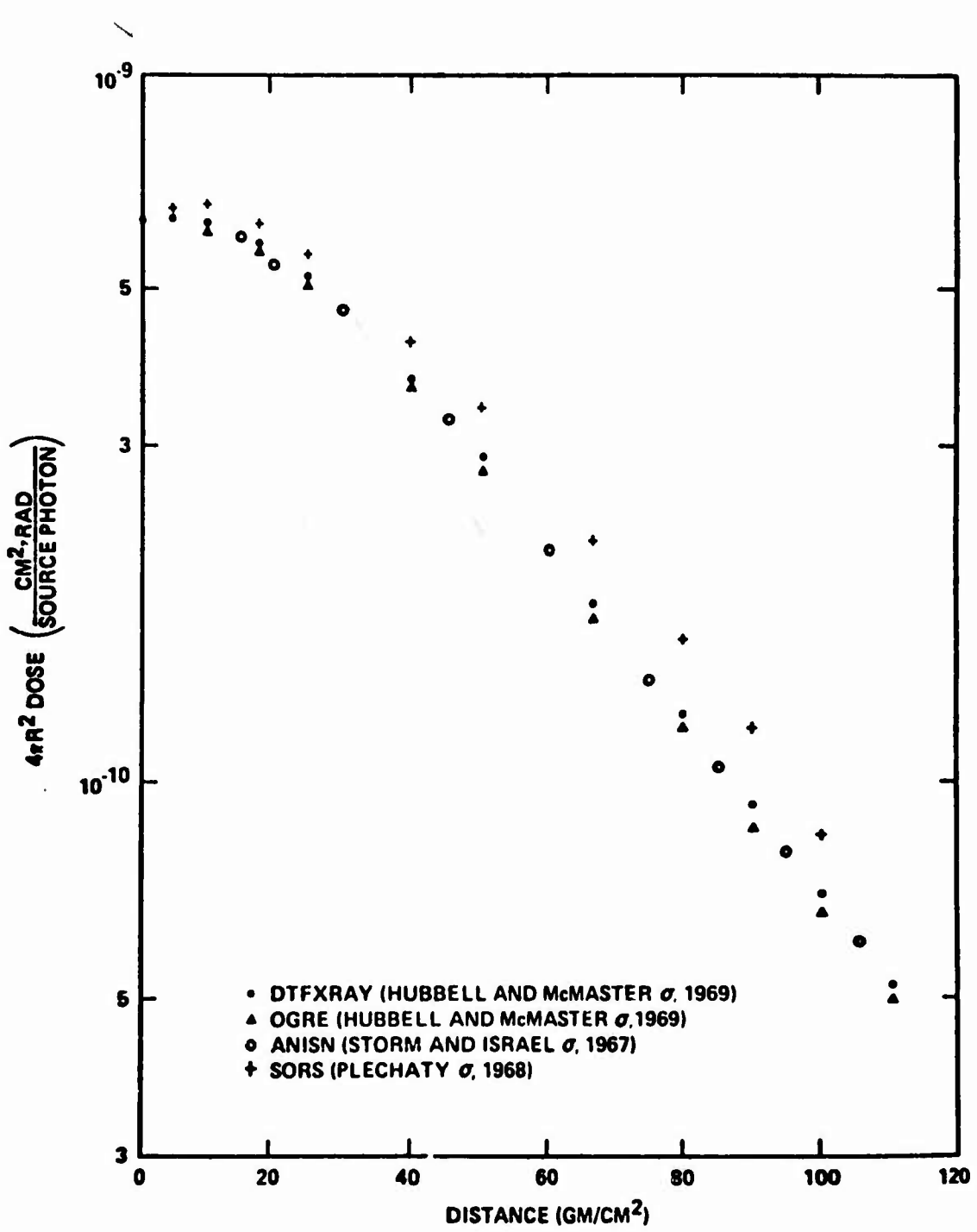
Fig. 4. Comparison of dose vs distance calculations
for a prompt fission source.

9.

Figures 5 and 6 are typical computer-generated plots taken from the high-energy photon data base and illustrate the general transport behavior. Figure 5 is a plot of the scattered fluence versus distance for each of the 18 sources. The systematic decrease in scattered fluence near the maximum range (~ 550 gm/cm^2) is due to leakage out of the system caused by the vacuum boundary condition. All parametric fitting was extended out to only ~ 530 gm/cm^2 to avoid errors due to this flux depression. Figure 6 is a plot of the scattered energy spectra for an 8.0-6.5 MeV source at distances of 1, 3 5, 7, and 10 MFP of the source energy. These data all show a small peak at 0.5 MeV due to the annihilation quanta in pair-production.

2.3 Low-Energy Photons

The low-energy photon transport data base covers the energy range from 300 to 10 keV and was generated using DTFXRAY as described in Section 2.2. The McMaster cross-section compilation was used for energies below 1 MeV, and was selected as being the most accurate for air transport based on a series of sensitivity calculations and comparisons. The largest differences in basic cross-section data for the three elemental constituents of air being considered occur in the absorption values for nitrogen at energies below 100 keV. Six different compilations of cross-section data were compared for the energy range 20-100 keV and are given in Table I. The maximum
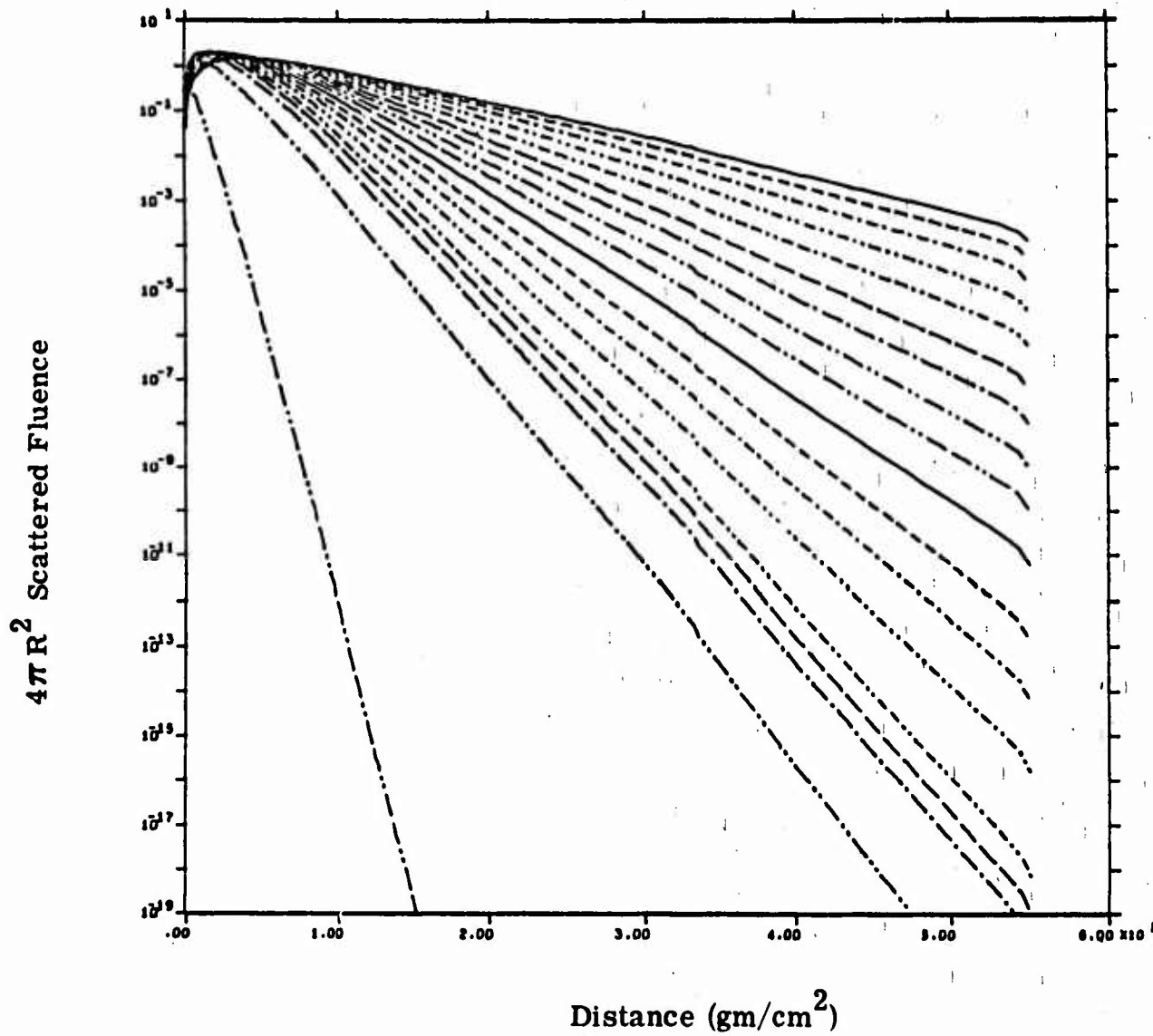
Fig. 5. DTFXRAY results for the scattered fluence vs distance for 18 sources from 10 MeV - 0.02 MeV.
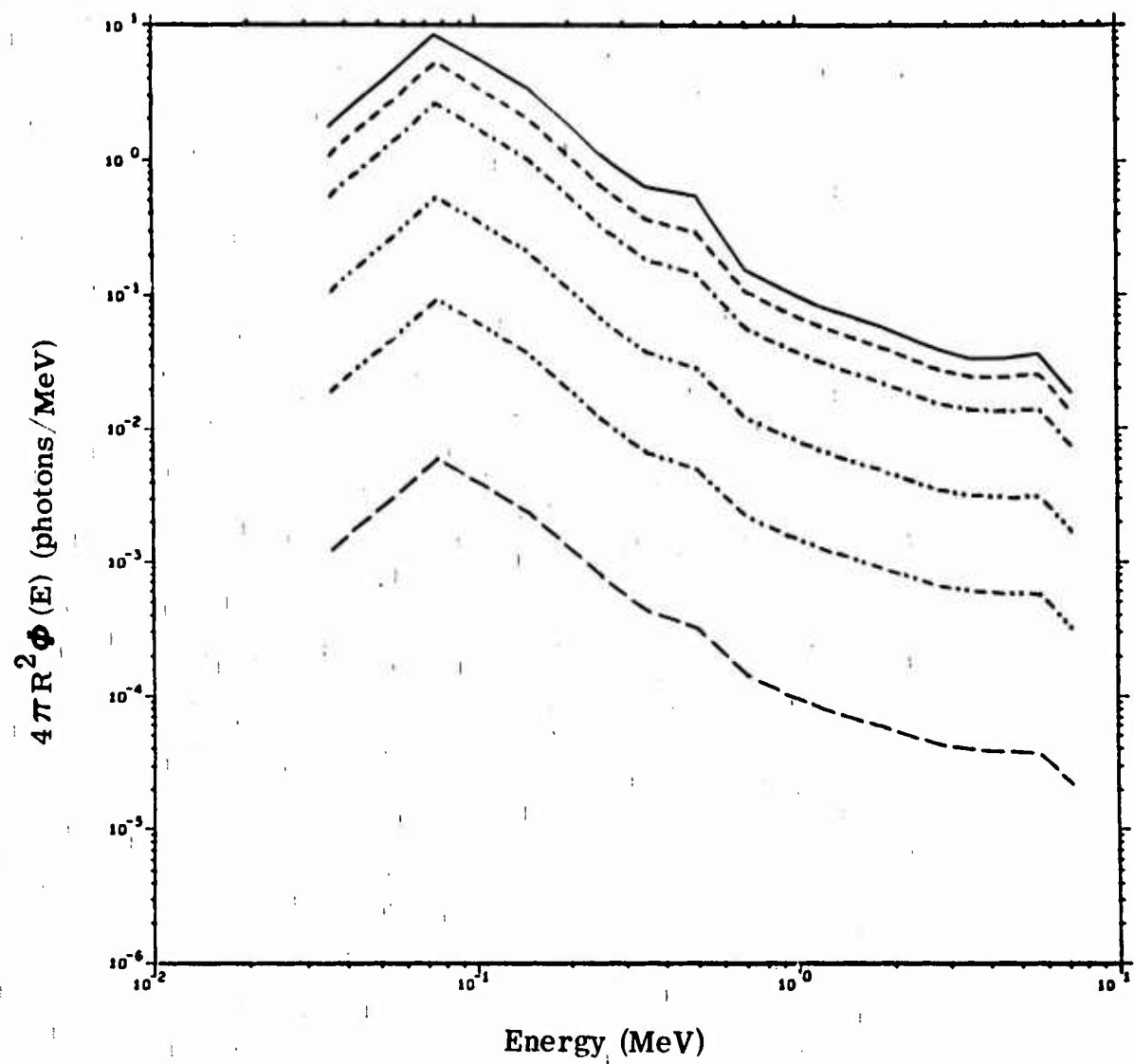
Fig. 6. DTFXRAY results for the scattered
photon spectra from a 8.0 - 6.5 MeV
photon source.

TABLE I.

Photoelectric cross-sections in N^{14} from
different compilations.   Values in
barns/atoms.

E (keV)	1968 LRL Plechaty	1969 LRL McMaster	1969 NBS Hubbell	1967 LASL Storm	1967 LRL McMaster	1957 NBS Gradstein
20	7.30	7.90	8.26	8.02	8.70	8.21
30	1.86	2.06	2.23	2.06	2.31	2.15
40	0.706	0.792	0.878	0.790	0.898	0.81
50	0.334	0.379	0.425	0.377	0.432	0.38
60	0.182	0.208	0.238	0.204	0.238	0.21
80	0.0702	0.0810	0.094	0.0790	0.0932	0.082
100	0.0339	0.0393	0.0454	0.0373	0.0453	0.041

values occur in 1968 Plechaty compilation and the minimum values for the
1969 Hubbell compilation. The relative difference between the maximum
and minimum absorption values at 60 keV is approximately 30%, which
results in a 100% difference in the total calculated fluence at 20 MFP. In
order to select the most appropriate cross-section set, comparisons were
made between deep-penetration photon transport experiments[23] in LN_2 and
calculations based on the discrete ordinates code DTFXRAY and the Monte
Carlo code OGRE. The experiment consisted of measuring the forward
number current as a function of distance from an Am^{241} isotopic source
(59.57 keV gamma energy) in a LN_2 dewar that was 16 feet high by 8 feet
in diameter. The comparison of results are shown in Fig. 7. The three
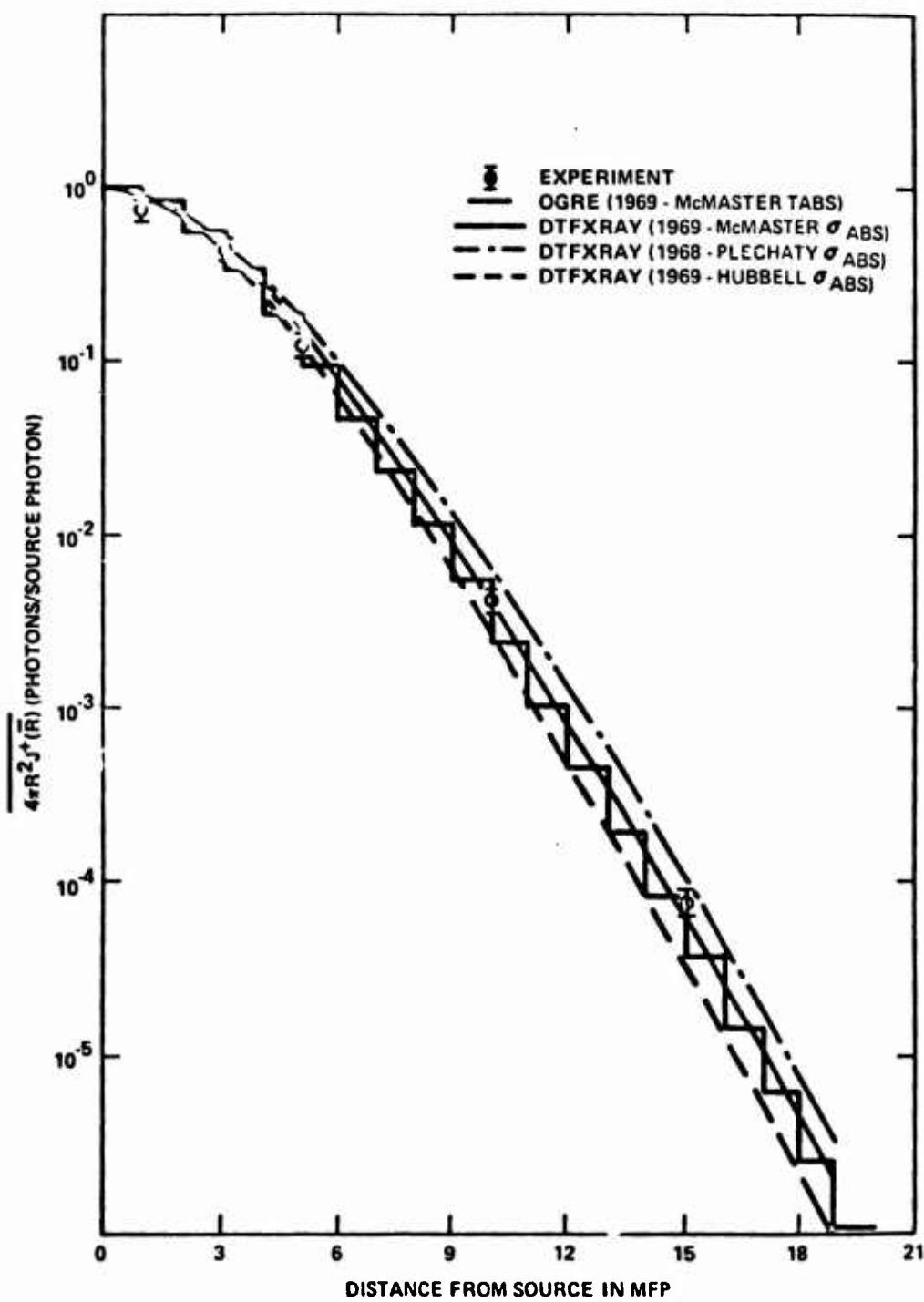
Fig. 7.   Comparison of different calculations with LN$_2$ photon transport experiment.

14.

DTFXRAY calculations used the maximum (1968-Plechaty), minimum (1969-Hubbell) and average-value (1969-McMaster) cross-section sets. The OGRE calculations[80] also used the average-value 1969-McMaster compilations. Figure 7 demonstrates good agreement between experiment and theory for the 1969-McMaster absorption cross-sections. In addition, there is also good agreement between OGRE and DTFXRAY for the same cross-sections. The OGRE calculation used importance sampling with 10^5 histories, and resulted in statistical errors on the forward current of several percent at deep penetrations.

Additional comparisons between calculations were made for photon transport in air and are illustrated in Fig. 8 for the energy fluence build-up as a function of source energy at 10 MFP. The OGRE[81] and DTFXRAY results agree within 10% for most energies, but differ from the Kaman Nuclear Monte Carlo results[19] by as much as a factor of 2. The source of this large discrepancy is not known, however, the small number of initial histories (2000) and lack of importance sampling in the Kaman Nuclear calculations suggests that large statistical errors could be present at deep penetrations.

Computer plots representative of the low-energy photon data base generated with DTFXRAY are shown in Figs. 9 and 10. Figure 9 illustrates the scattered fluence vs distance for each of the 18 sources from 10-300 keV; Fig. 10 shows plots of scattered photon spectra vs energy for a 300-260 keV source and for eight distances from 1 to 20 MFP.

15.
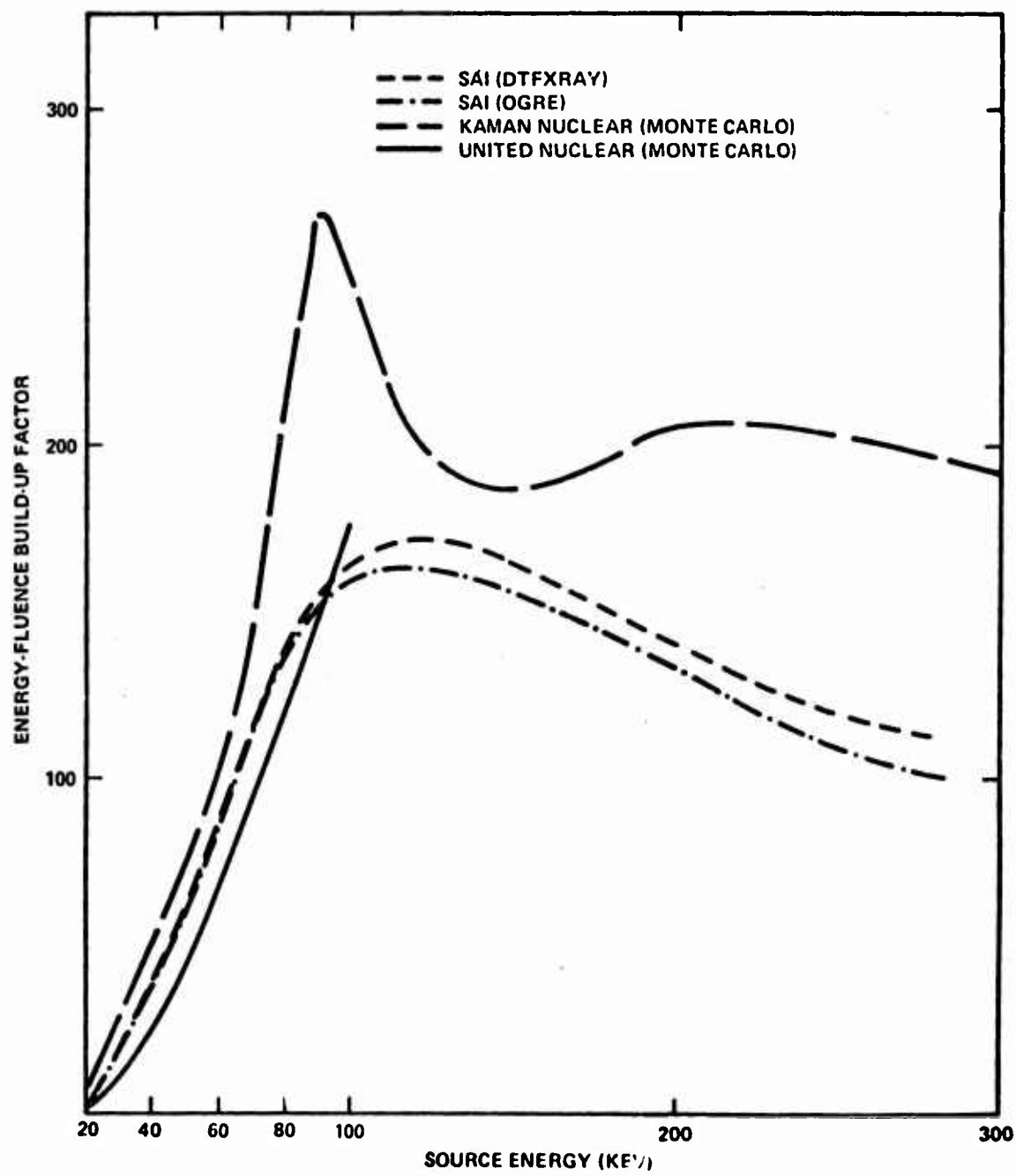
Fig. 8. Comparison of build up factor calculations vs source
energy for low energy photons.

16.
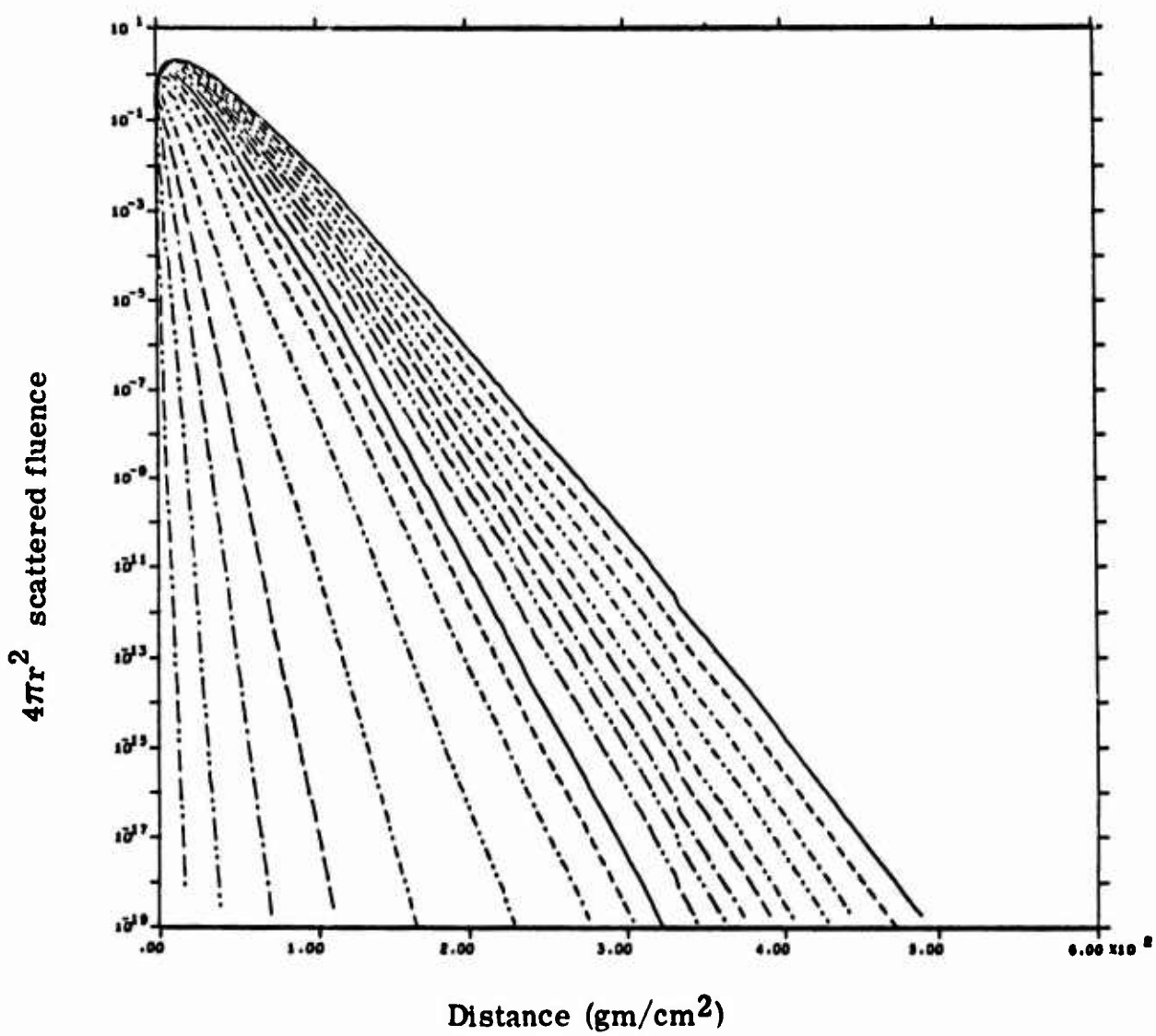
Fig. 9. DTFXRAY scattered fluence vs distance
for source energies from 10 to 300 keV.
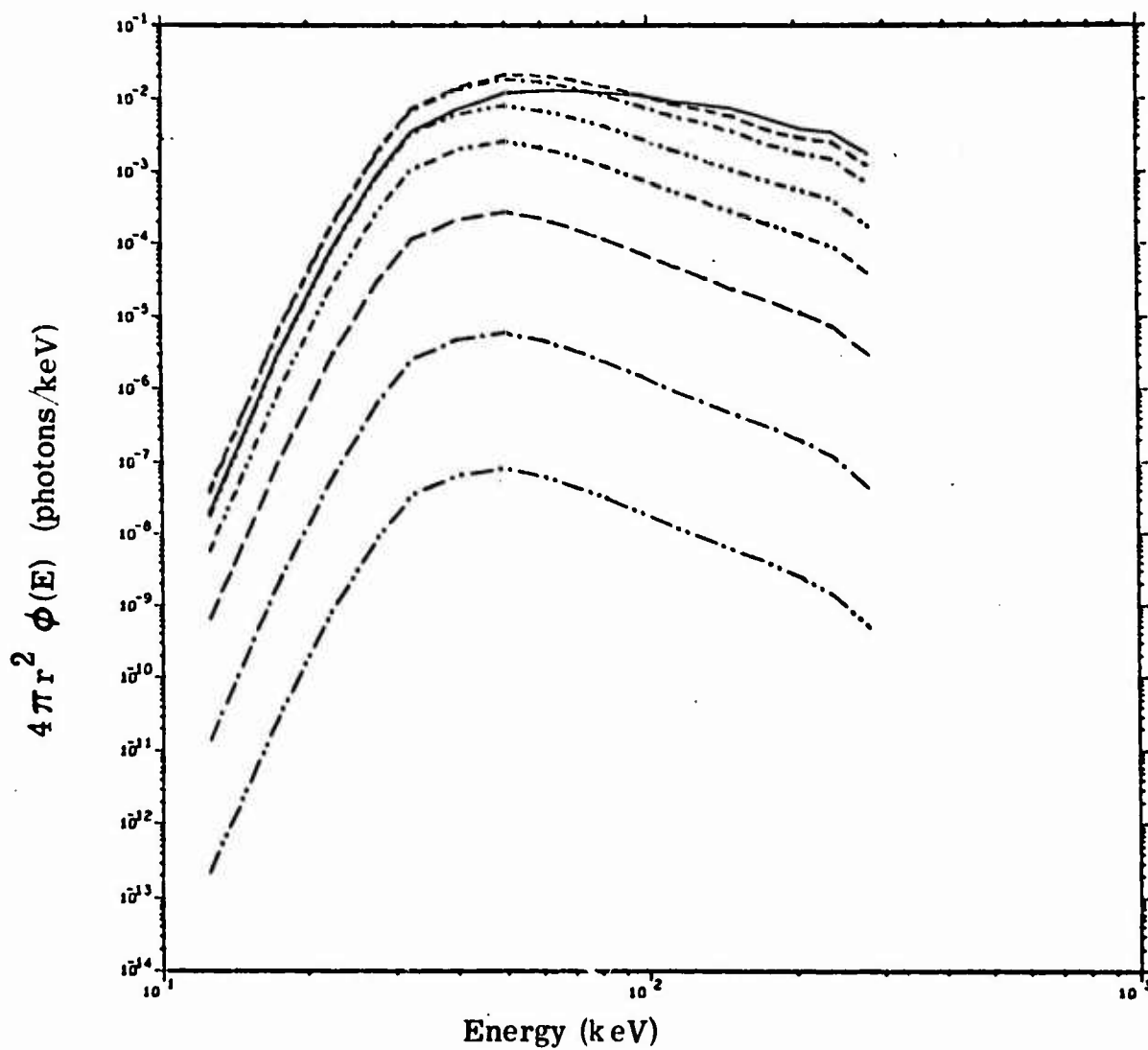
Fig. 10.   DTFXRAY scattered photon spectra
for a 220-260 keV source at distance
of 1 to 20 MFP.

18.

III.   PARAMETRIC MODELS OF THE DATA BASE

The fundamental problem being solved is to represent the free-field radiation environment $\phi(E_s, E, \Omega, r)$ for monoenergetic sources E_s by parametric equations so that free-fields for an arbitrary source spectrum $W(E_s)$ can be generated simply and quickly by the folding integral:

$$\Phi(E, r, \Omega) = \int W(E_s)\, \varphi(E_s, E, \Omega, r)\, dE_s$$

Folding monoenergetic source data from raw flux dump tapes is used frequently to calculate radiation transport, however, computer storage is quickly exausted in most systems before a complete data base can be stored. The neutron, secondary gamma-ray and photon data base being used at SAI contains nearly 10^7 flux values. In addition to storage problems, the manipulation of tapes is slow and often cumbersome. The aim of the parametric modeling approach is to reduce the size of the calculational problem considerably. This reduction would allow air transport problems to be calculated from a self-contained, fast running, easy to use computer code. More emphasis can be placed on flexibility in the different types of problems that can be calculated, in addition to designing a code oriented to the needs of the user.

The one dominant factor which makes parametric modeling of a large data base feasible is the slowly - changing, asymptotic behavior

characteristic of radiation transport in large homogeneous systems.
Thus, although structure may exist in energy spectra, at a given range,
the propagation of this structure at other ranges occurs in a systematic
slowly-changing manner. This behavior was illustrated in the previous
plots of Section II.

The general approach used is to describe the free-field quantities
in terms of shape functions and the areas or fluences under these shapes.
This approach makes the different parts of the problem separable and
allows greater flexibility in manipulating and displaying the data to
determine optimum parametric equations. The general form of the
equations used in ATR to represent the angular flux is:

$$\varphi\ (E_s, r, E, \Omega) = S\ (E_s, r, E) \cdot F_{SCATT}\ (E_s, r) \cdot R\ (E_s, E, r, \Omega)$$

$$+ \frac{e^{-\mu(E_s)r}}{4\pi r^2 \Delta E_s \Delta \Omega_0}\ \delta_{E, E_s} \cdot \delta_{\Omega, \Omega_0}$$

where

$$R\ (E_s, E, r, \Omega) = \frac{\varphi(E_s, r, E, \Omega)}{\int \varphi(E_s, r, E, \Omega)\ d\Omega}$$

20.

and

φ = angular flux; particles/$cm^2 \cdot$ MeV $\cdot$ steradian $\cdot$ source neutron.

F = fluence functions; particles/$cm^2 \cdot$ source neutron.

S = Scalar flux shapes; fraction/MeV, integral over energy equal unity.

R = ratio of angular to scalar flux at each energy E for a
given angular direction, range and monoenergetic source
energy; fraction/steradian, integral over solid angle equal unity.

$\mu(E)$ = total neutron cross section (cm^{-1}) at energy E and air
density of 1.11 mg/cm^2

Ω_0 = solid angle corresponding to the zero-degree direction.

The parametric modeling consisted of making curve fits to three basic
quantities for each monoenergetic source band: (1) scattered fluences
$F_{SCATT}(R)$; (2) scattered spectrum shapes S(E, R) and; (3) angular ratio
functions R(E, r, Ω).

3.1   Fluence

Each set of fluence data was fit with parametric equations for
the entire range of 180 spatial intervals from 0-550 gm/cm^2 of air using
6 coefficients for each of the 18 source energies. No simple functional
form was found to fit all of the data to the desired accuracy ($\pm 2\%$) for all
source energies. Two basic functions were used for the fits (in semi-log
space); one was a coupled quadratic and the other the following:

$$\varphi(R) = a_1 + a_2\sqrt{R} + a_3 R + \frac{a_4}{R} + \frac{a_5}{R^2} + \frac{a_6}{R^3}$$

Figures 11 through 14 are plots of the raw data and the parametric fit for fluences of neutrons, secondary gamma-rays, high energy photons and low energy photons, respectively. This comparison is typical of all fits to fluence data and shows typical errors in the fit of several percent.

3.2   Energy Distribution

The spectral shape functions were more complicated to determine since simultaneous variations in energy and distance occur for each source energy. Various plots of the data were first studied to determine where systematic behavior occured and what functional forms might be appropriate. Figure 15, which illustrates the general behavior, is a plot of normalized neutron spectral data for ten distances from 0-550 gm/cm^2 for a 14 MeV neutron source. The nearly constant asymptotic shape is apparent for ranges $\gtrsim 100$ gm/cm^2. Two-dimensional fits in energy and distance were made to these data by first fitting the data with piece-wise continuous functions versus energy for each radius, and then fitting each resulting coefficient as a function of radius. Separate piece-wise continuous functions were used for the fits versus energy to minimize the total number of parameters required. Thus, only 6 coefficients were required in most cases to fit the variation in energy for a given distance and source energy. In log-log space, the functions were (1) a linear term for energies below $E \leq 0.1$ MeV,

22.
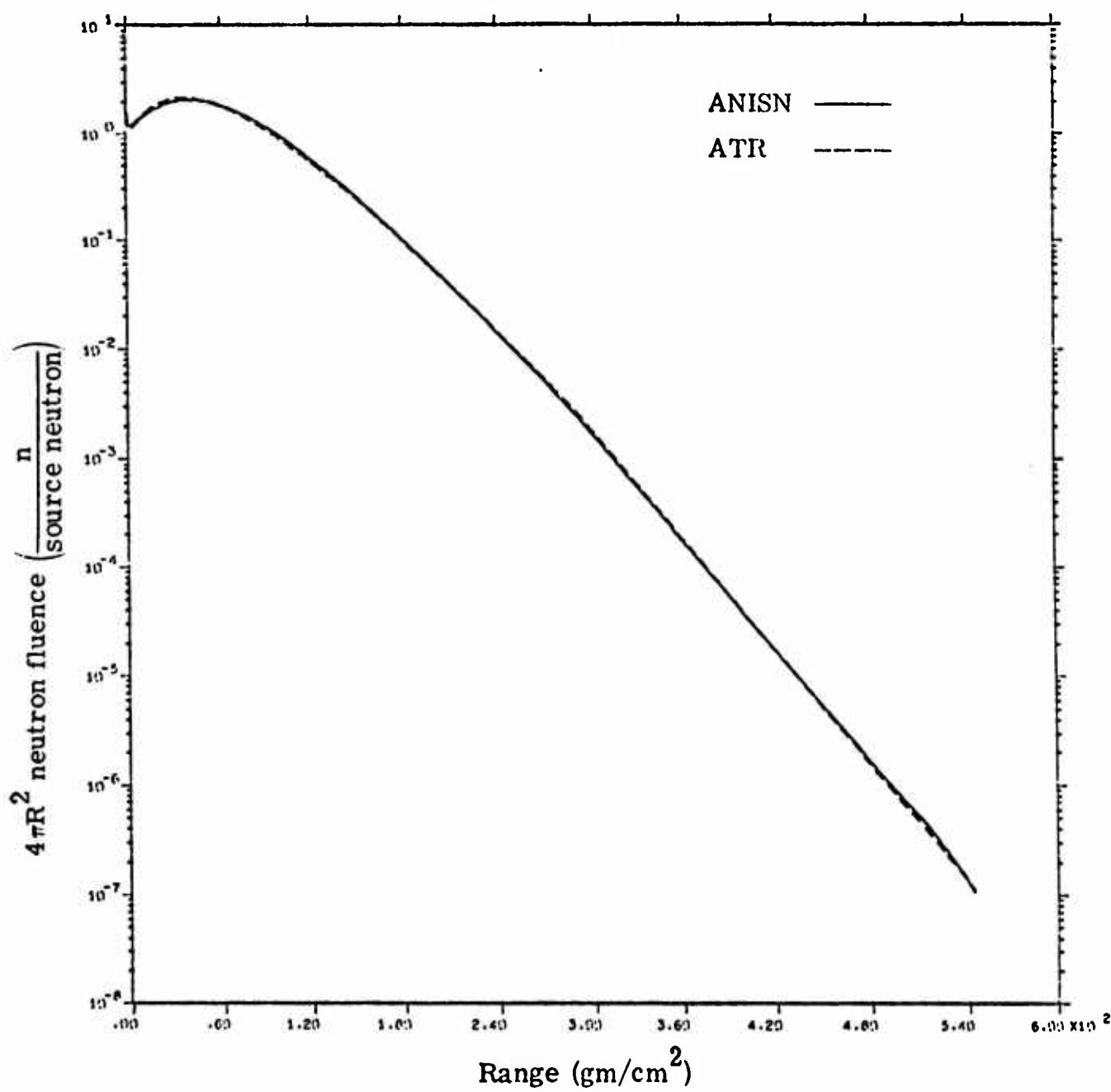
Fig. 11. Neutron fluence vs range for a 12.2-15 MeV
neutron source.
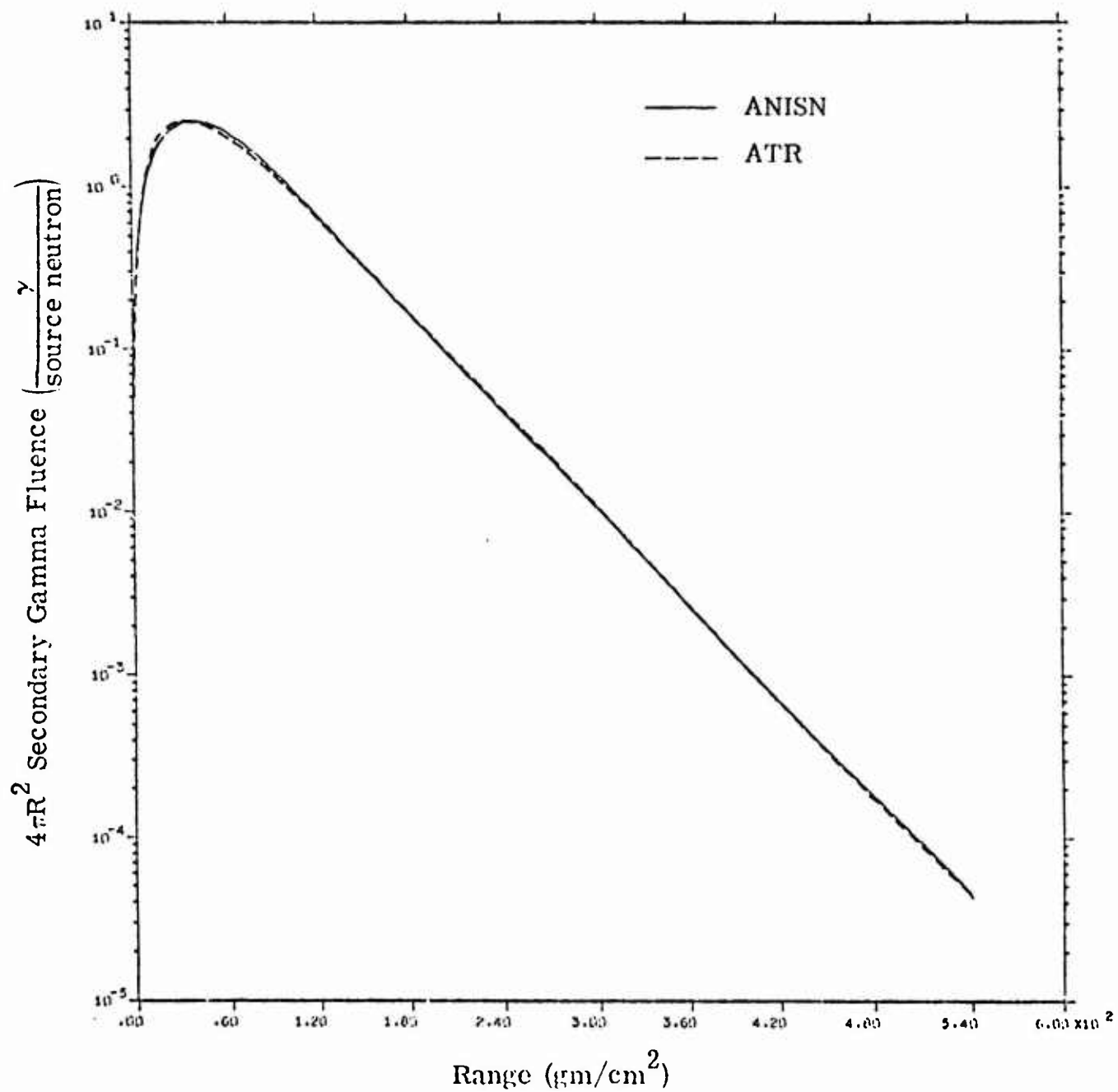
Fig. 12. Secondary gamma-ray fluence vs range for
12.2-15 MeV neutron source.

24.
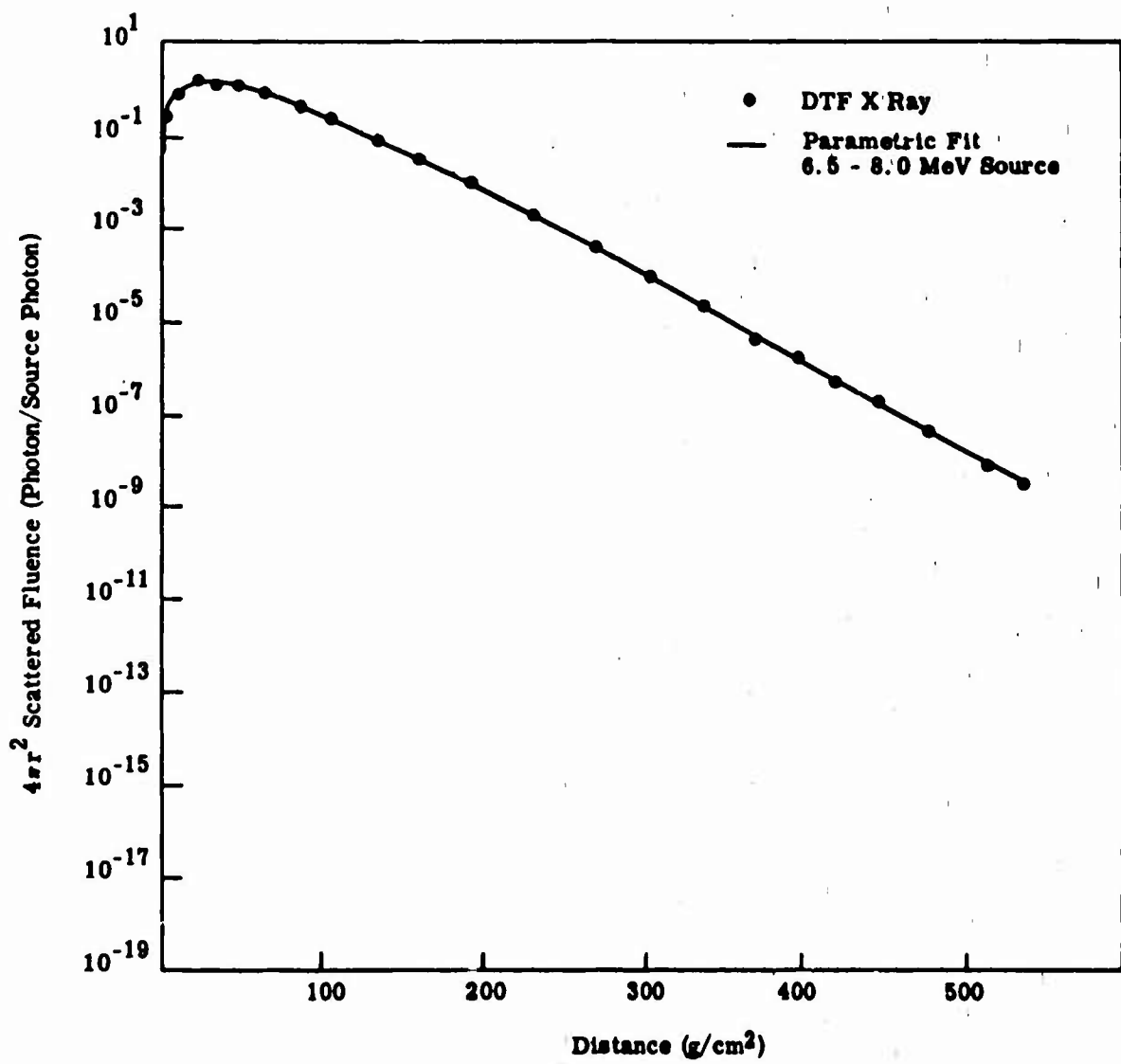
Fig. 13.   Parametric fit to scattered fluence for a
6.5-8.0 MeV photon source.
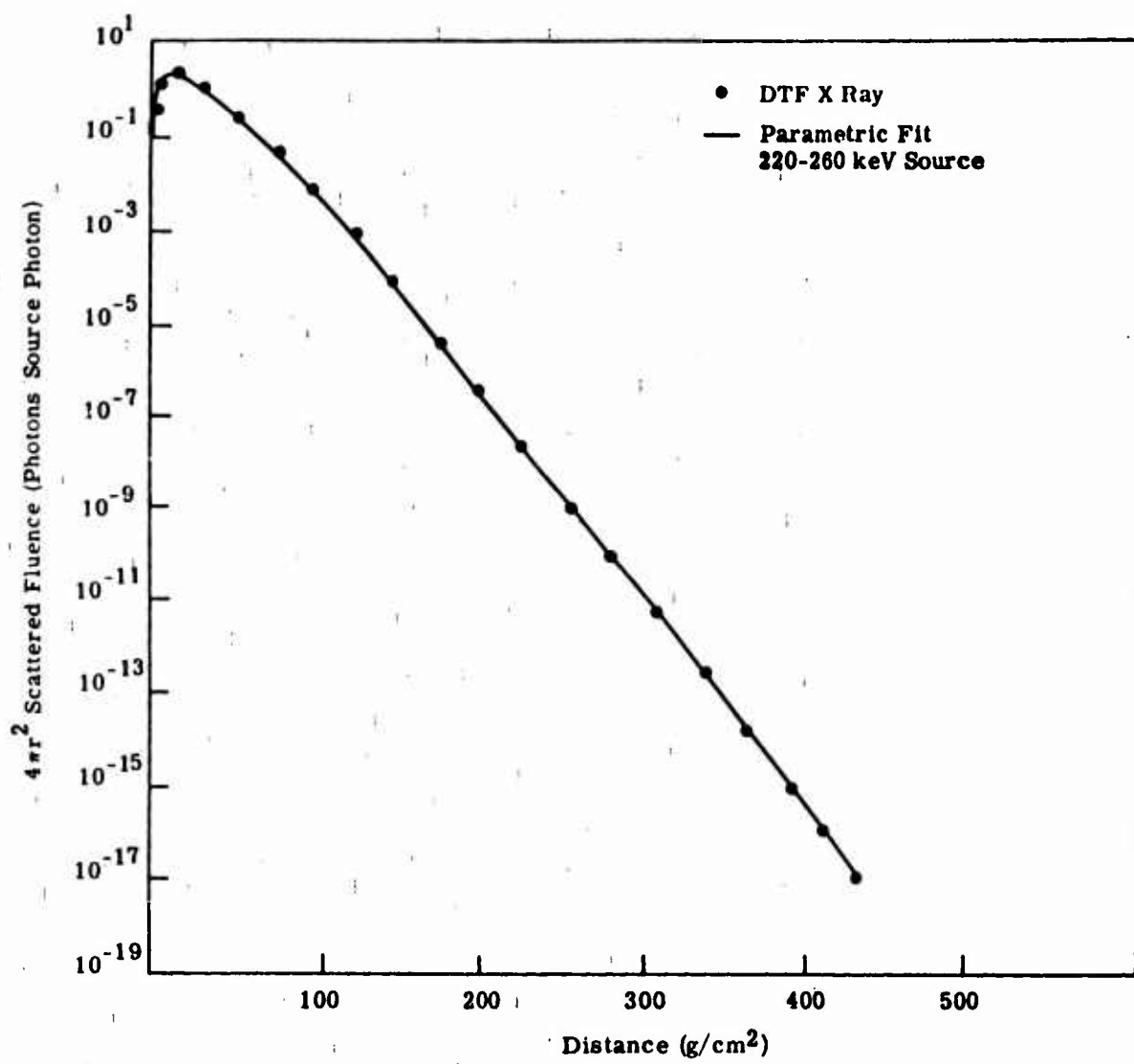
Fig. 14. Parametric fit to the scattered fluence for a 220-260 keV photon source.

26.
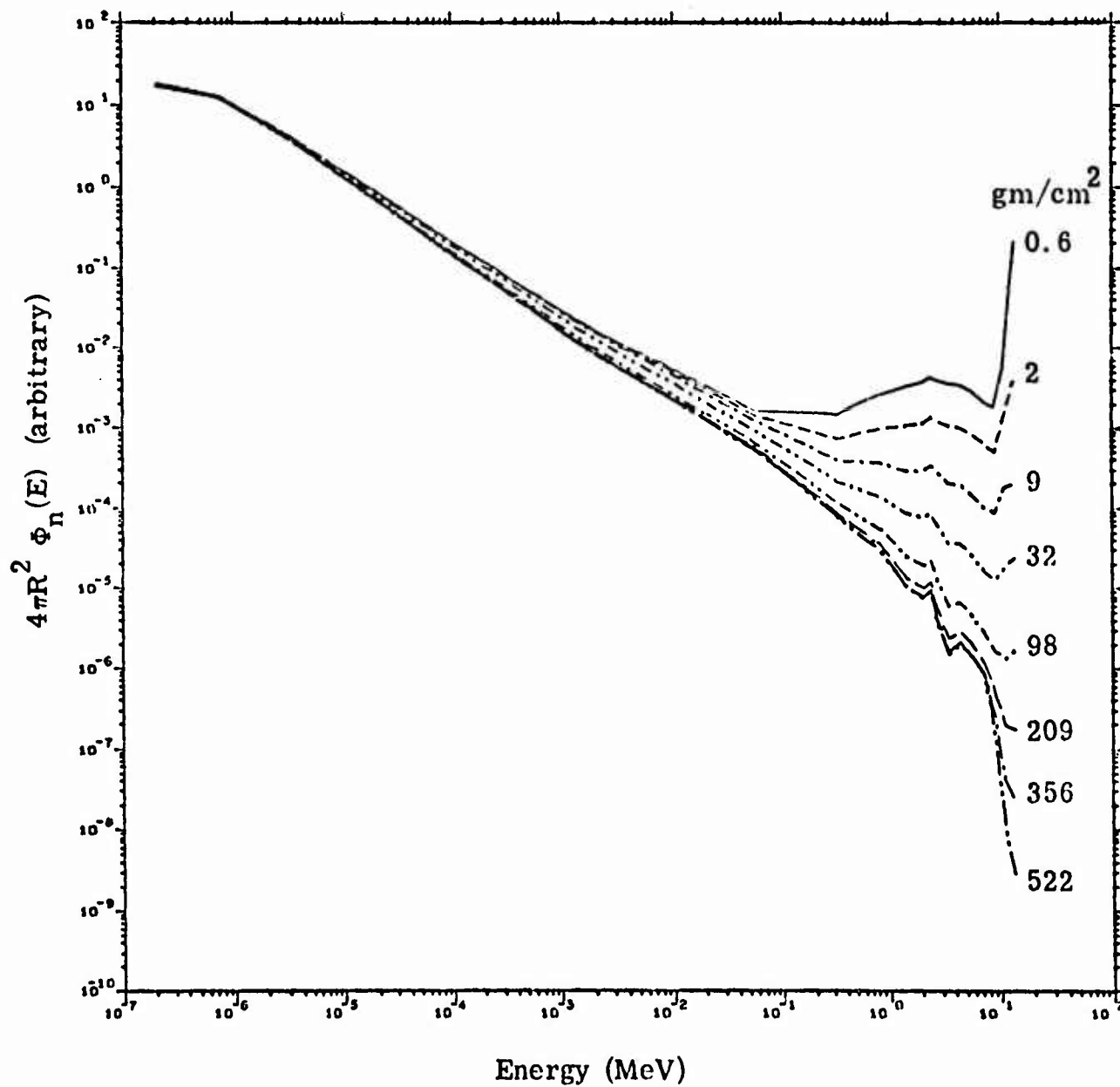
Fig. 15. Neutron spectra calculated by ANISN for a 12.2-15
MeV neutron source at different ranges from 0-550
gm/cm^2 of air. Data normalized at low energies.

(2) a quadratic for 0.1 MeV $< E < E_s$ and (3) a constant for E_s . The resulting six coefficients for each radius were then fit vs radius using the same 6 parameter functions used in the fluence fits. Thus, approximately 36 total coefficients were typically used to describe the spectral shape vs distance for each source energy giving a total of $36 \times 18 = 648$ coefficients. The actual number of coefficients from these fits was usually much less due to the nearly constant spectral shape for the last 80 or so radii. The parametric fits then, reduced the original $\phi(18 \times 22 \times 180)$ array of 71,280 neutron fluxes by more than a factor of 100 to approximately 700 coefficients and several equations.

The uncertainty in the parametric fits was small ($\sim10\%$) except at energies where "peaked" structure existed. Errors at these points were usually systematic as a function of distance and were corrected by a separate correction subroutine which fit the difference between the raw data and parametric representation at these points. The features of this subroutine allow fine-tuning of the fit and can also be used to convert ATR from one data base to another without having to go through the entire parametric fitting procedure. This in fact was done early in the program to convert fits from a LASL flux tape to the existing data base.

Figures 16 through 21 illustrate neutron spectra calculated by the parametric equations in ATR for a 14 MeV source at distances from 300-4800 meters in air at a density of 1.11 mg/cm^3. The solid histogram

28.
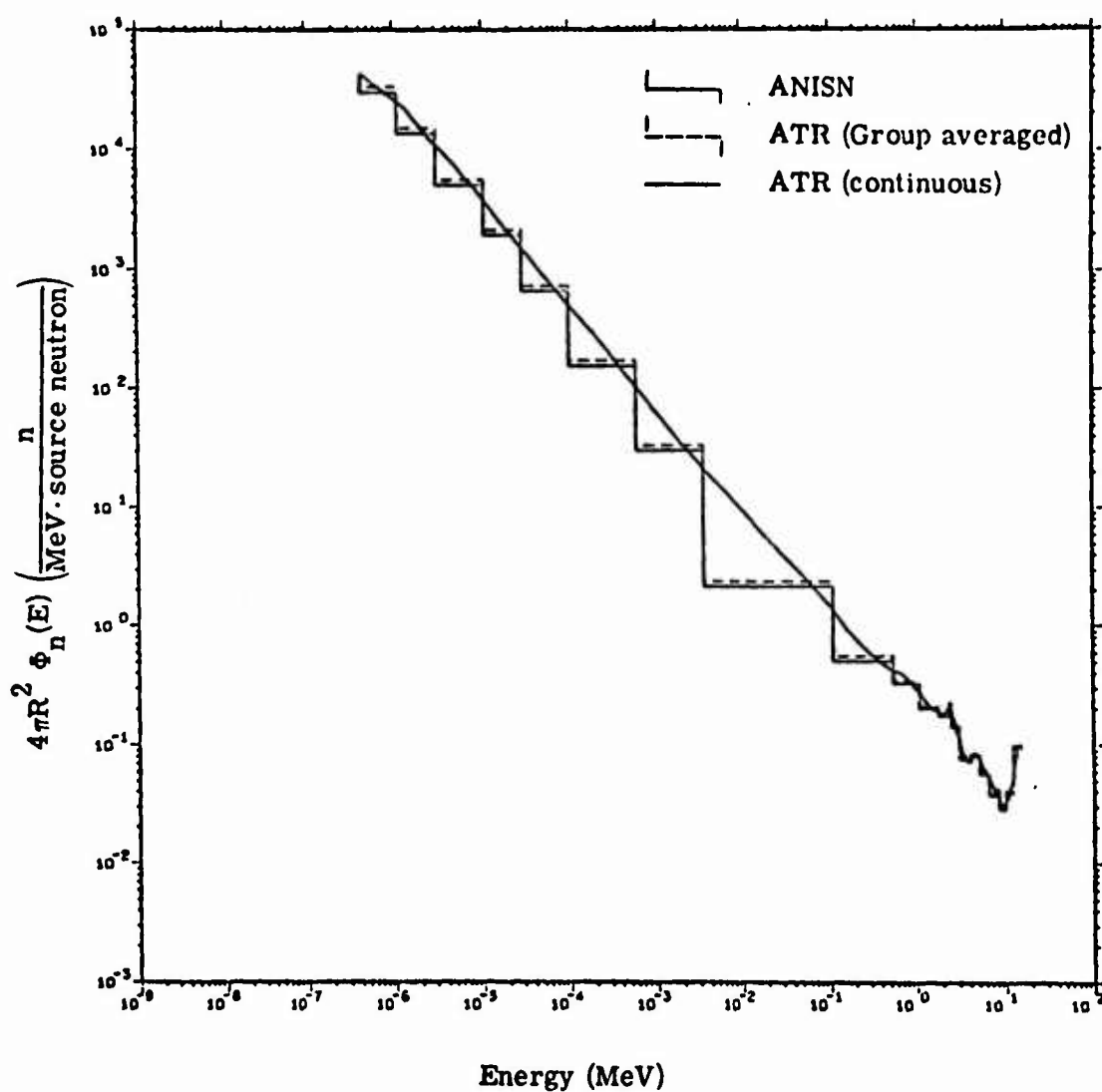
Fig. 16. Comparison of neutron spectra calculated by ATR and the ANISN data base for a 12.2-15 MeV neutron source at 300 meters in air of density 1.11 mg/cm³.
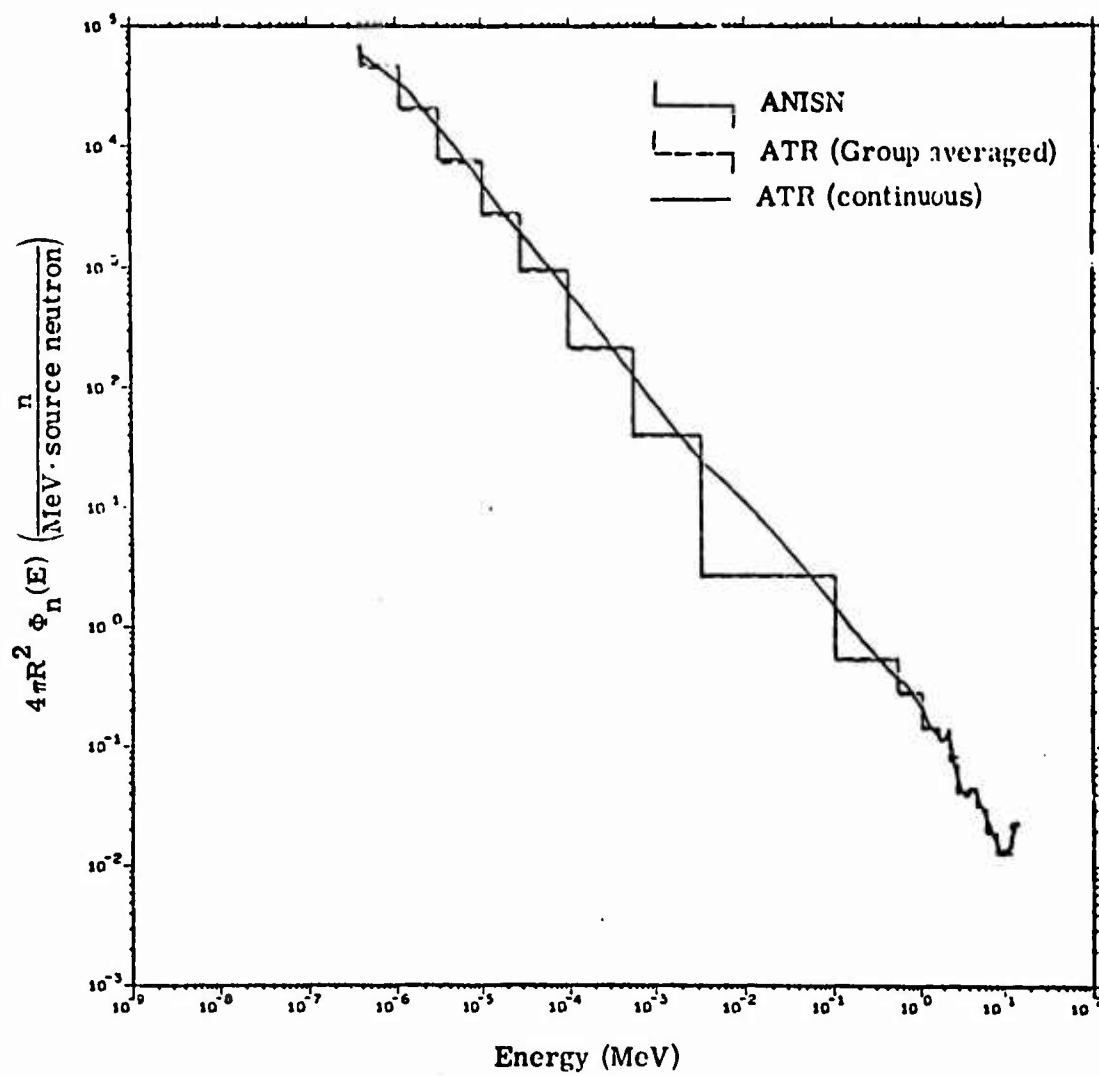
Fig. 17. Comparison of neutron spectra calculated by ATR and
the ANISN data base for a 12.2-15 MeV neutron source
at 600 meters in air of density 1.11 mg/cm^3.

30.
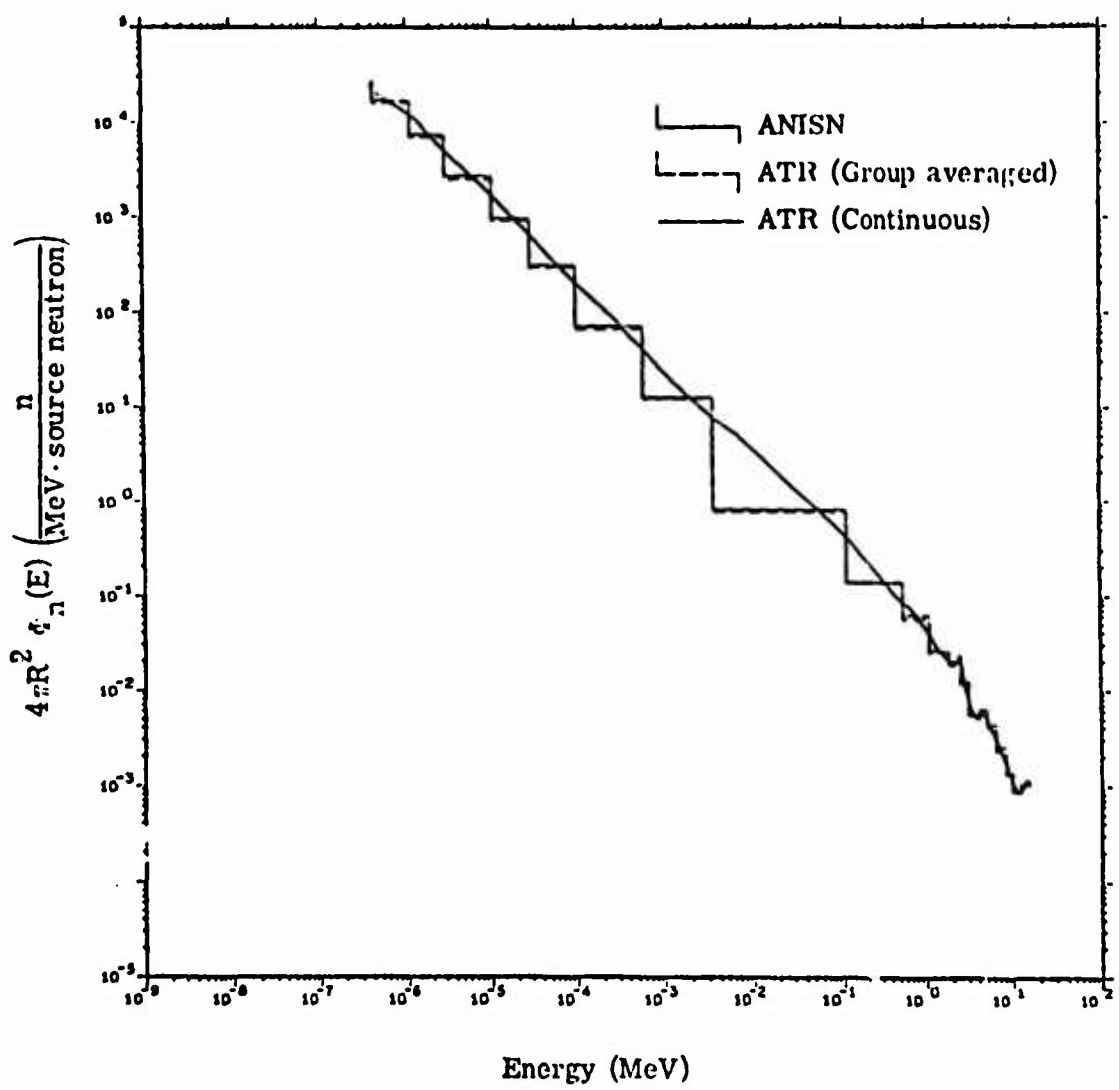
Fig. 18. Comparison of neutron spectra calculated by ATR and the
ANISN data base for a 12.2-15 MeV neutron source at
1200 meters in air of density 1.11 mg/cm³.
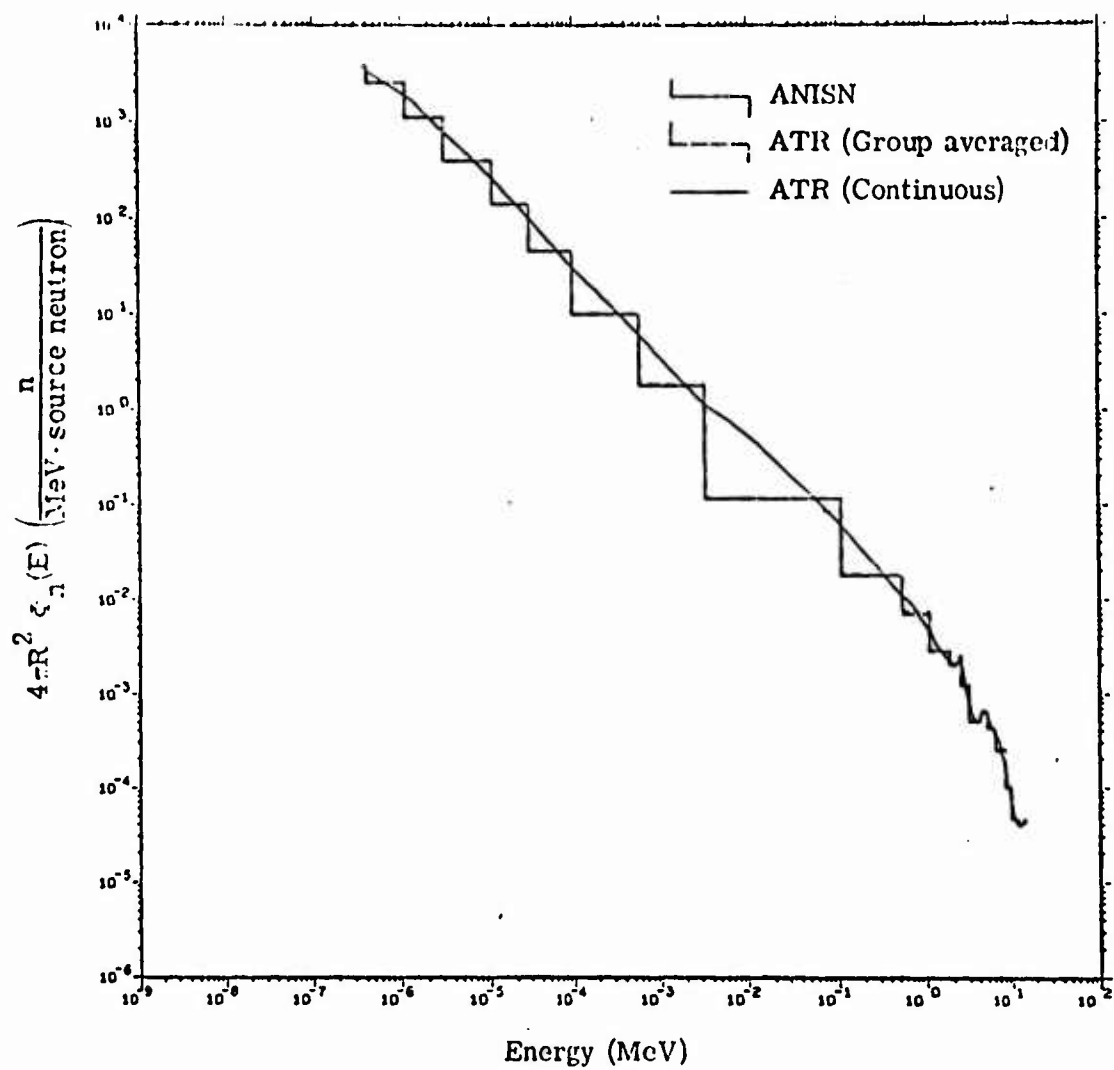
Fig. 19. Comparison of neutron spectra calculated by ATR and the ANISN data base for a 12.2-15 MeV neutron source at 1800 meters in air of density 1.11 mg/cm^3.
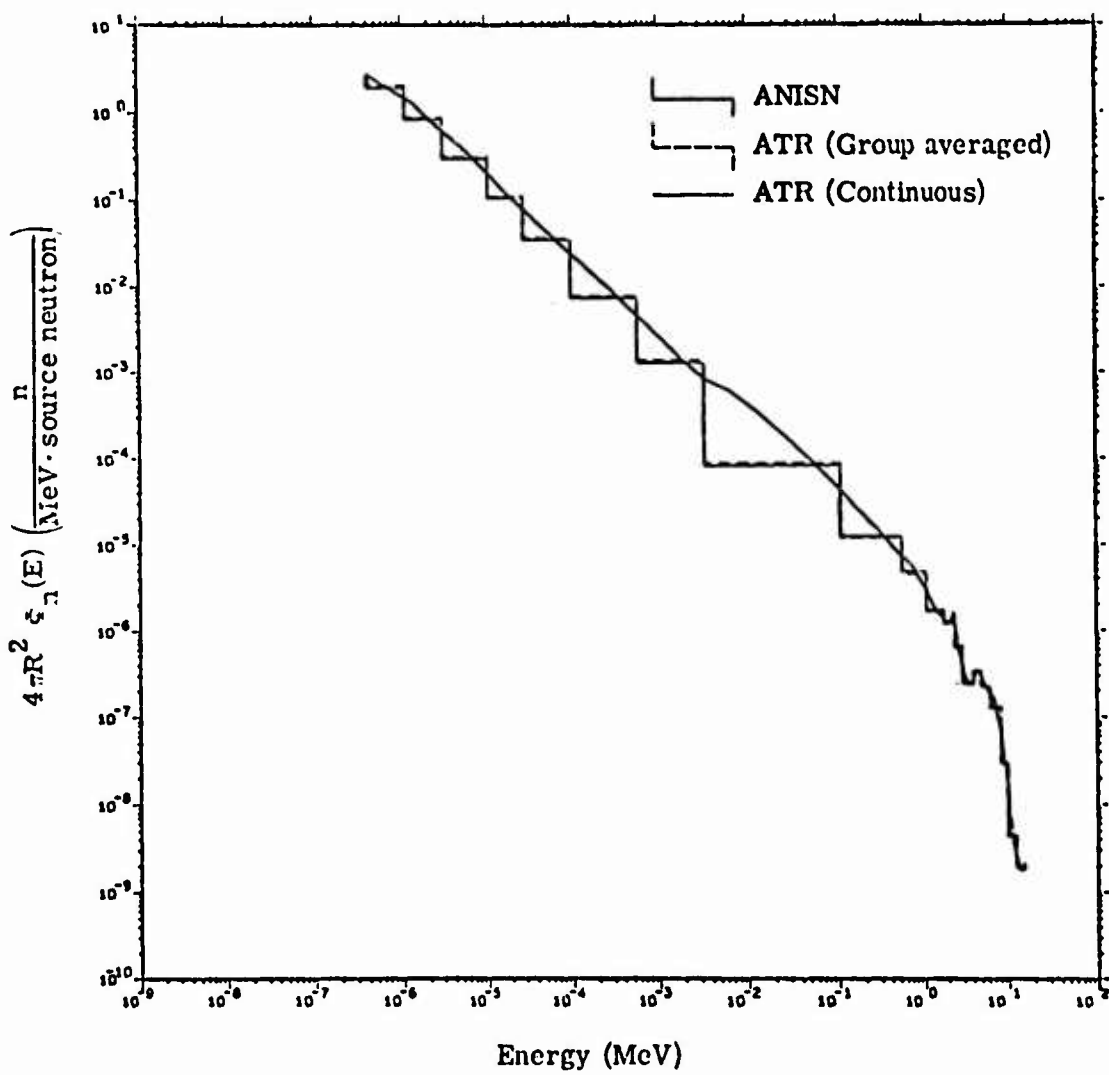
Fig. 20. Comparison of neutron spectra calculated by ATR and the ANISN data base for a 12.2-15 MeV neutron source at 3600 meters in air of density 1.11 mg/cm³.
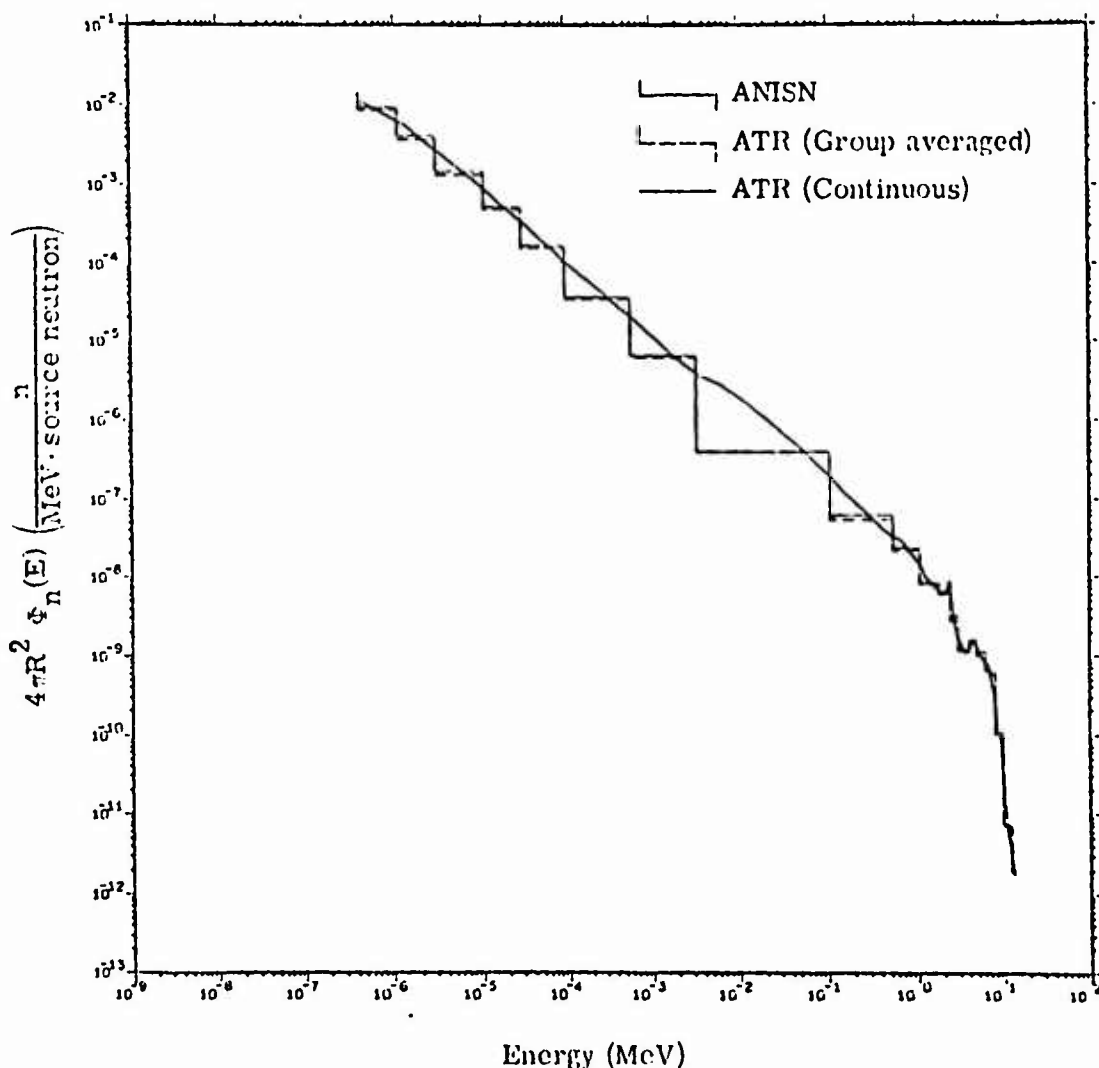
Fig. 21. Comparison of neutron spectra calculated by ATR and
the ANISN data base for a 12.2-15 MeV neutron source
at 4800 meters in air of density 1.11 mg/cm^3.

is the raw ANISN data, the dashed histograms are ATR values for the ANISN group structure and the smooth curve is the continuous ATR representation. The differences between ATR and ANISN are typically less than 10%.

Spectral shapes for secondary gamma-ray data displayed a similar asymptotic behavior vs distance as neutron spectra and are illustrated for a 14 MeV neutron source in Fig. 22 for normalized data. Two-dimensional fits to these shapes were made using a fourth order polynomial in energy whose coefficients were then fit vs distance using one of the six-parameter fluence type functions described in the previous section. The structure in the shapes at short ranges was taken into account by using the correction routine to fit differences between the polynomial fit and raw data. Final errors in the parametric fits of spectral shapes were less than 10%. Figures 23 through 28 are plots of secondary gamma-ray spectra from ATR and ANISN for a 14 MeV neutron source and ranges of 300 m to 4800 m in air at density 1.11 mg/cm^3.

Normalized spectra shapes for 8 radii are shown in Figs. 29 and 30 for representative high and low-energy photon sources, respectively. Unlike neutron and secondary gamma-ray transport data, the photon spectra displayed a reasonably smooth asymptotic behavior which lends itself to a different, more economical fitting approach. The procedure used for each source, to model both high and low-energy photon transport, was to generate spectral shapes for all distances from a reference shape obtained

35.
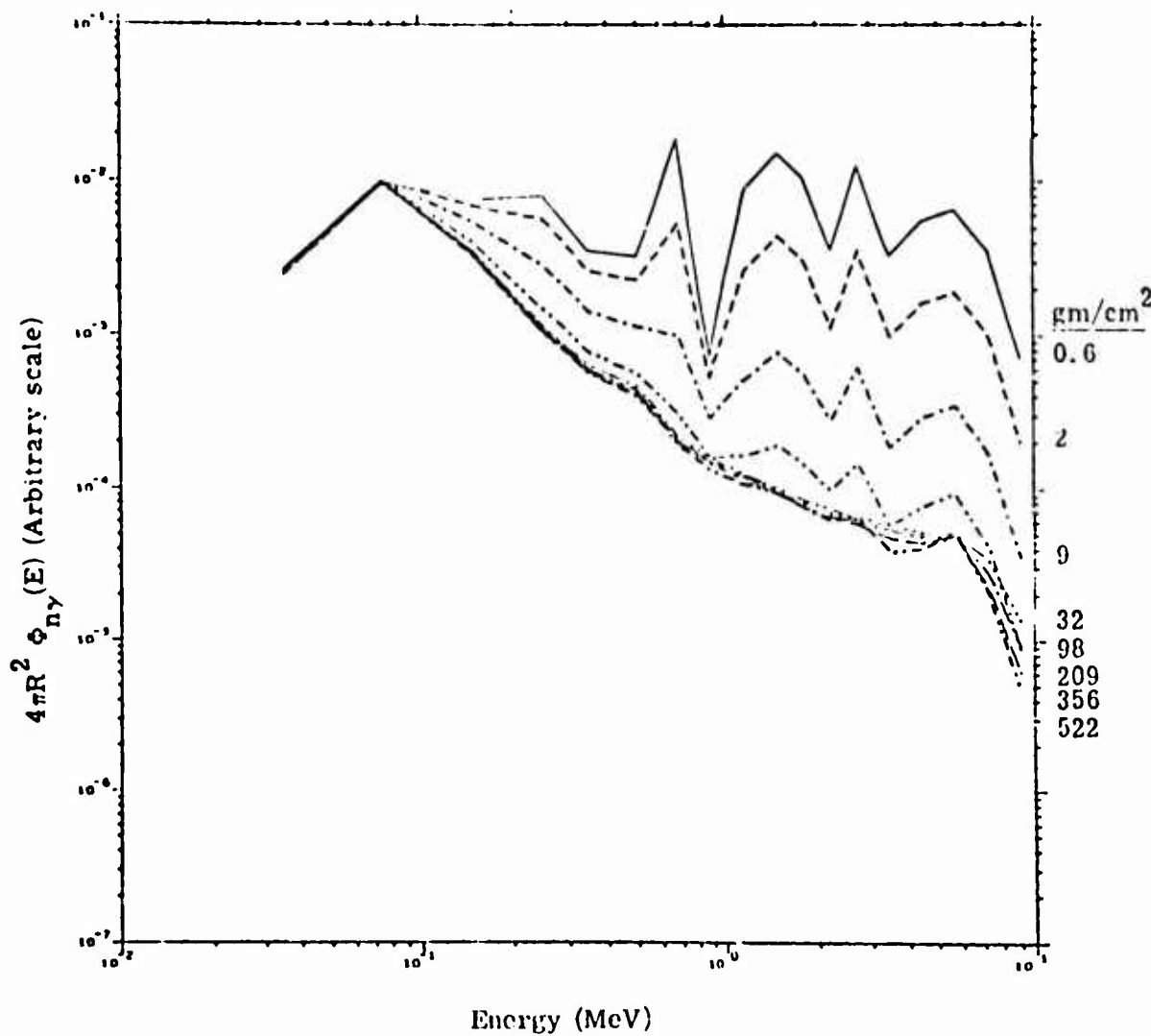
Fig. 22. Secondary gamma-ray spectra calculated by ANISN for a 12.2-15 MeV neutron source at different ranges from 0-550 gm/cm^2 of air. Data normalized at low energies.

36.
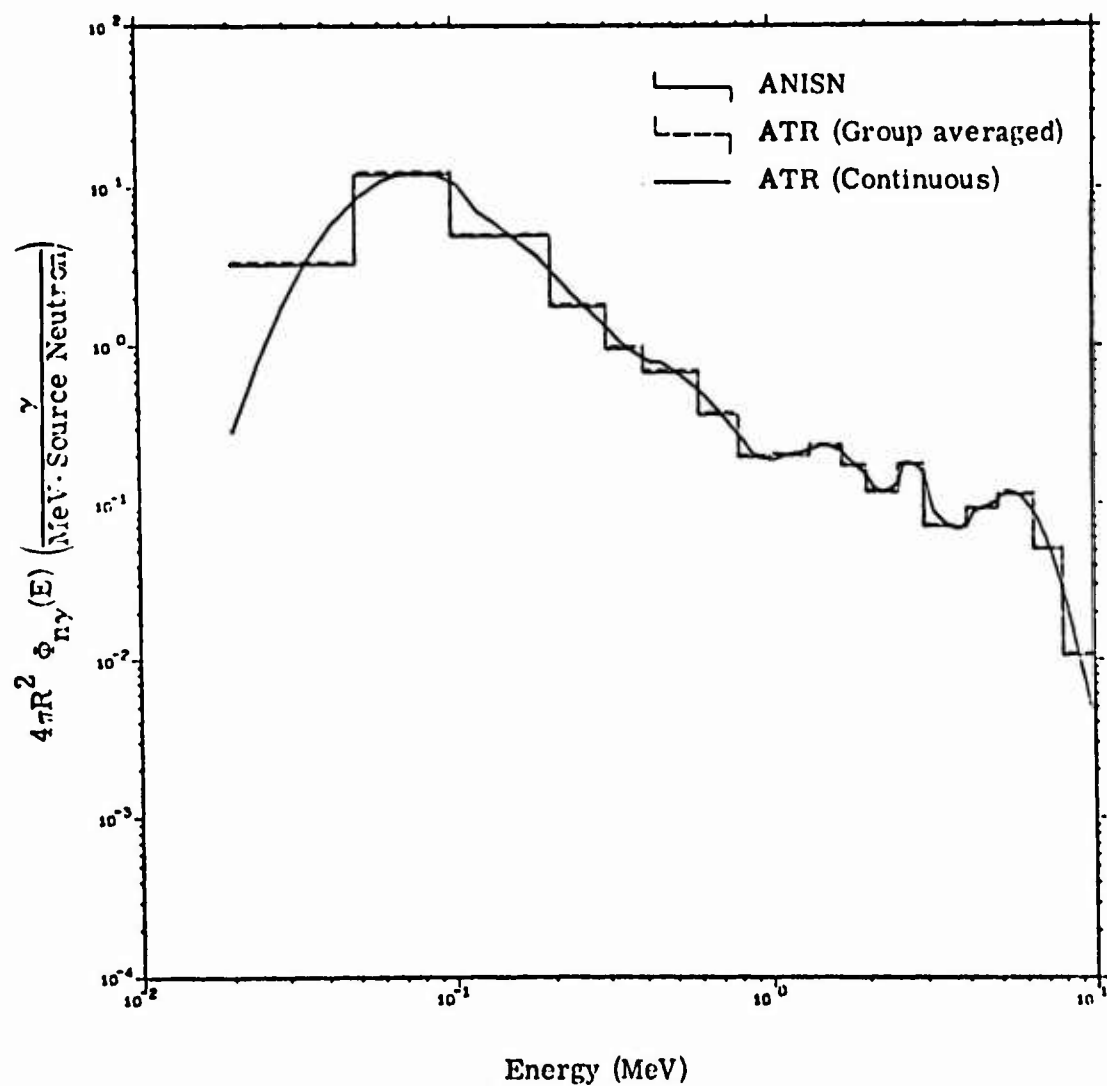
Fig. 23. Comparison of secondary gamma-ray spectra calculated
by ATR and the ANISN data base for a 12.2-15 MeV neu-
tron source at 300 meters in air of density 1.11 mg/cm^3.
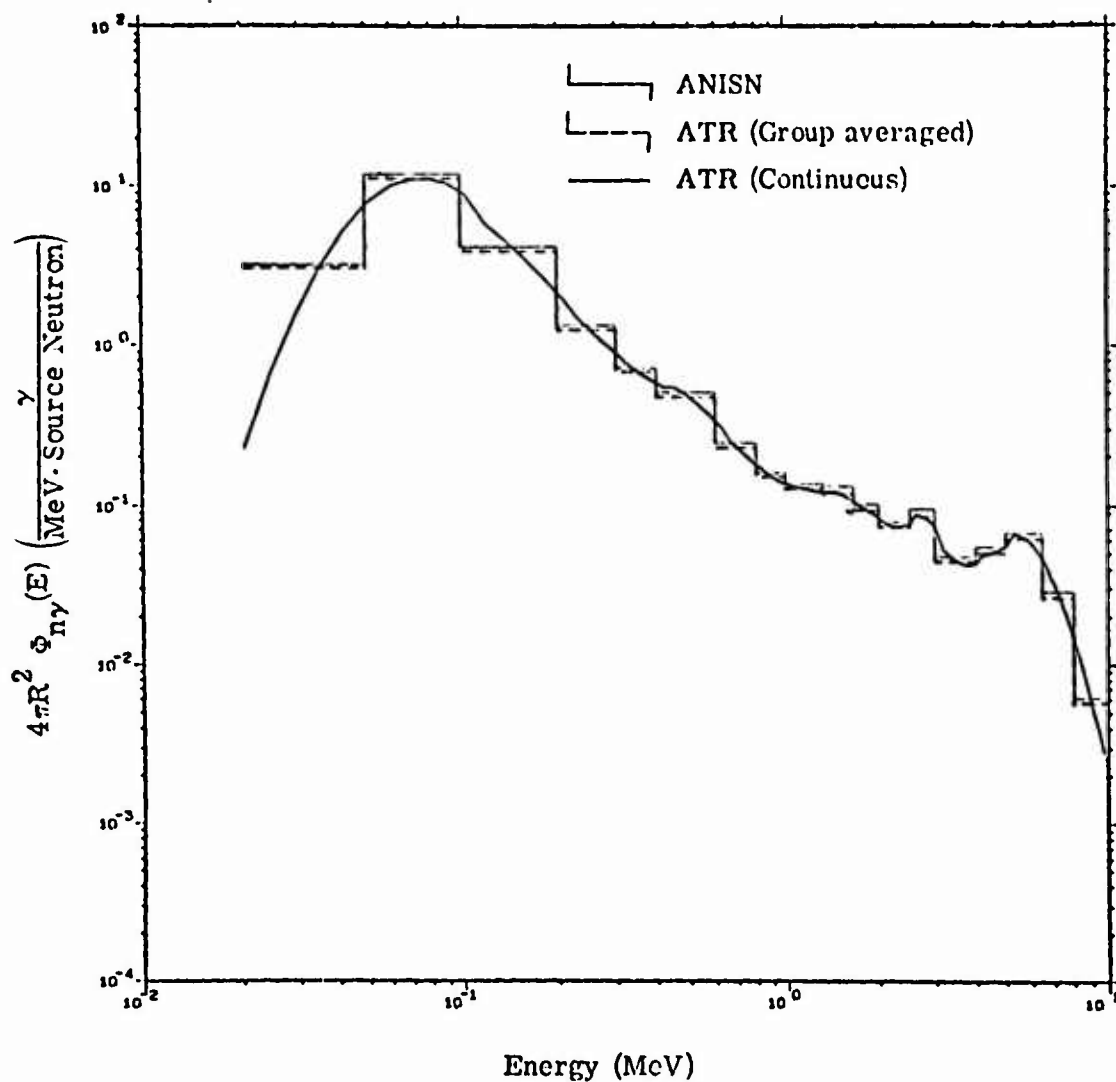
Fig. 24. Comparison of secondary gamma-ray spectra calculated by ATR and the ANISN data base for a 12.2-15 MeV neutron source at 600 meters in air of density 1.11 mg/cm^3.

38.
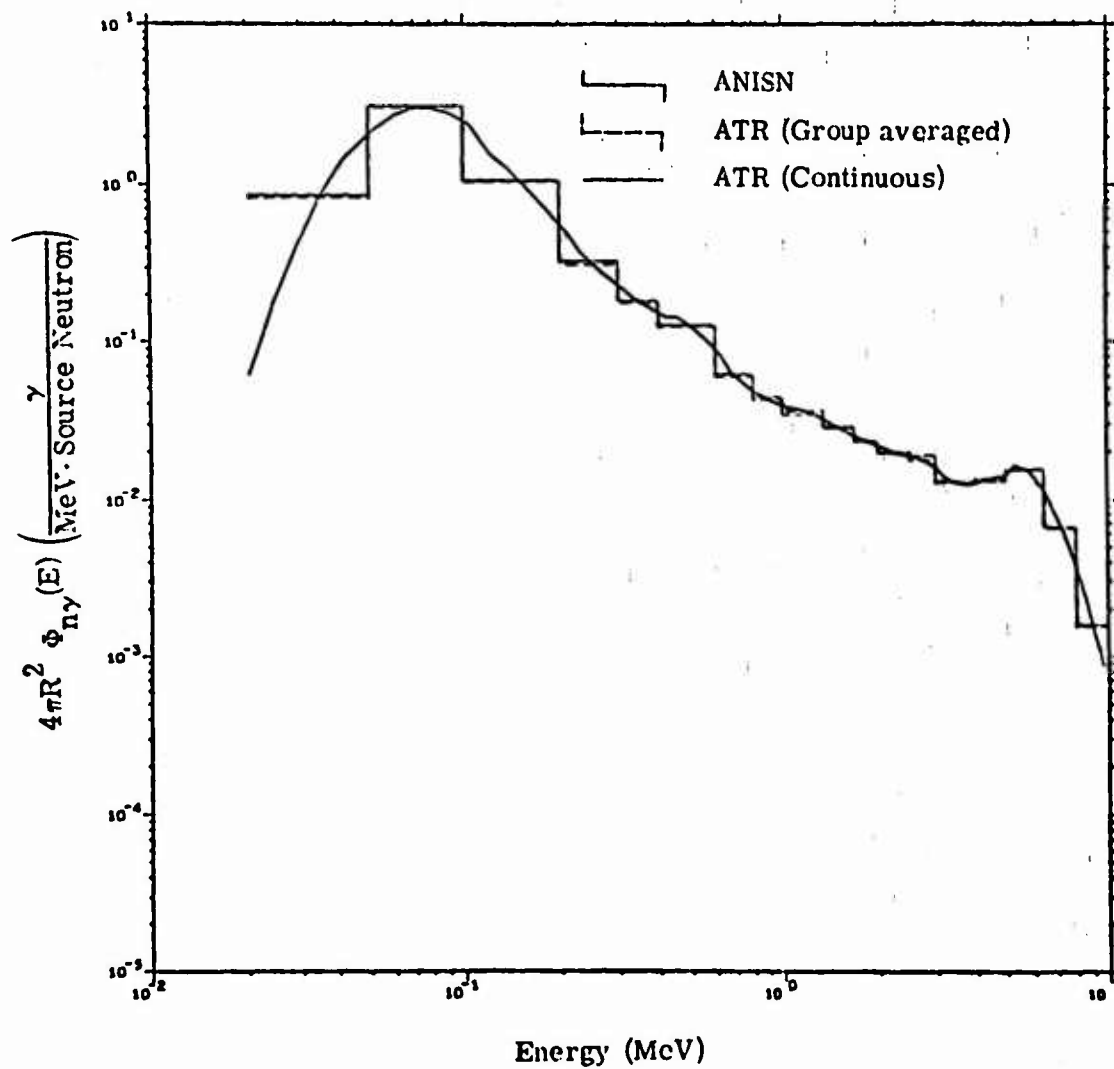
Fig. 25. Comparison of secondary gamma-ray spectra calculated by ATR and the ANISN data base for a 12.2-15 MeV neutron source at 1200 meters in air of density 1.11 mg/cm³.
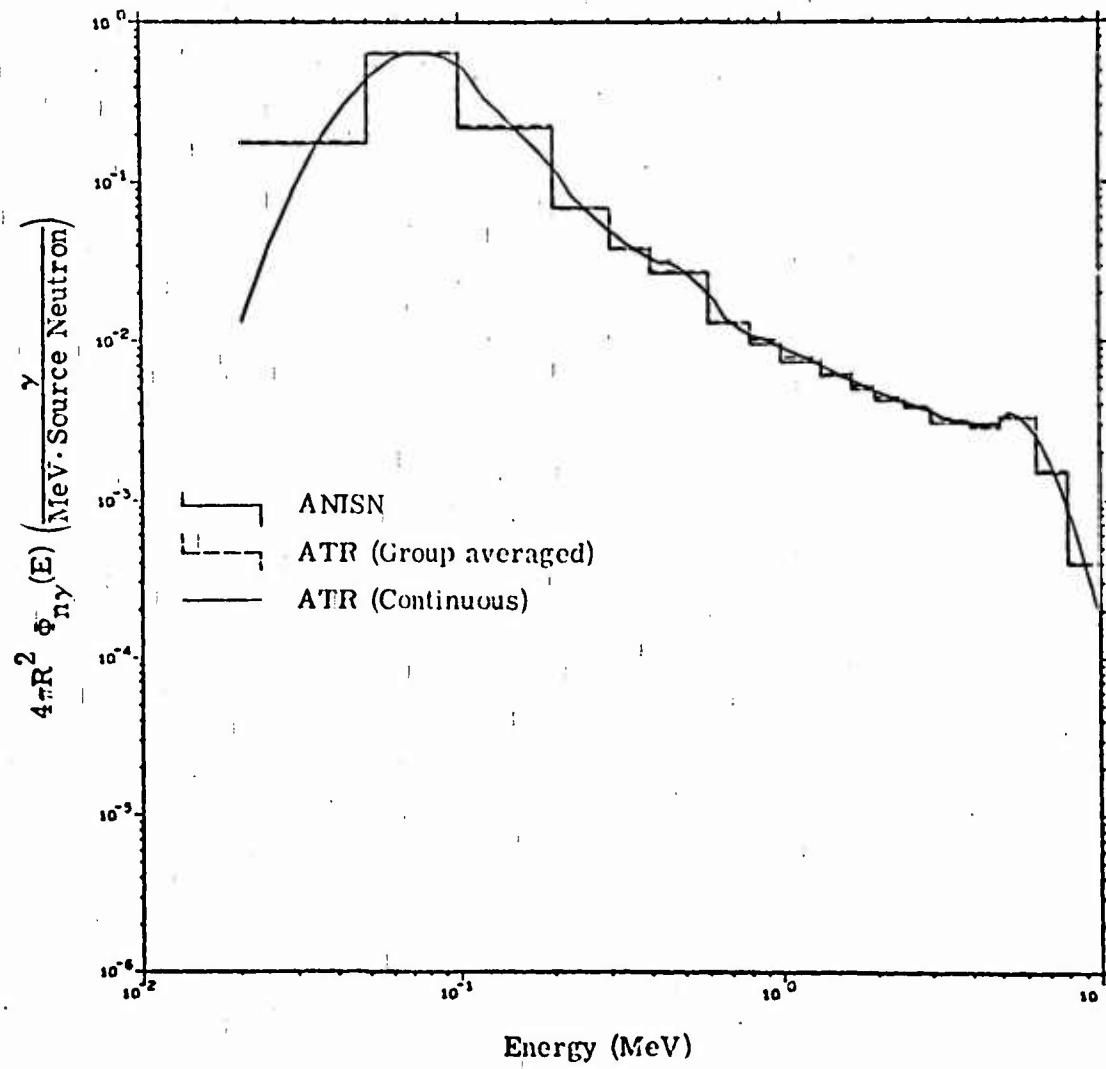
Fig. 26. Comparison of secondary gamma-ray spectra calculated by ATR and the ANISN data base for a 12.2-13 MeV neutron source at 1800 meters in air of density 1.11 mg/cm^3.

40.
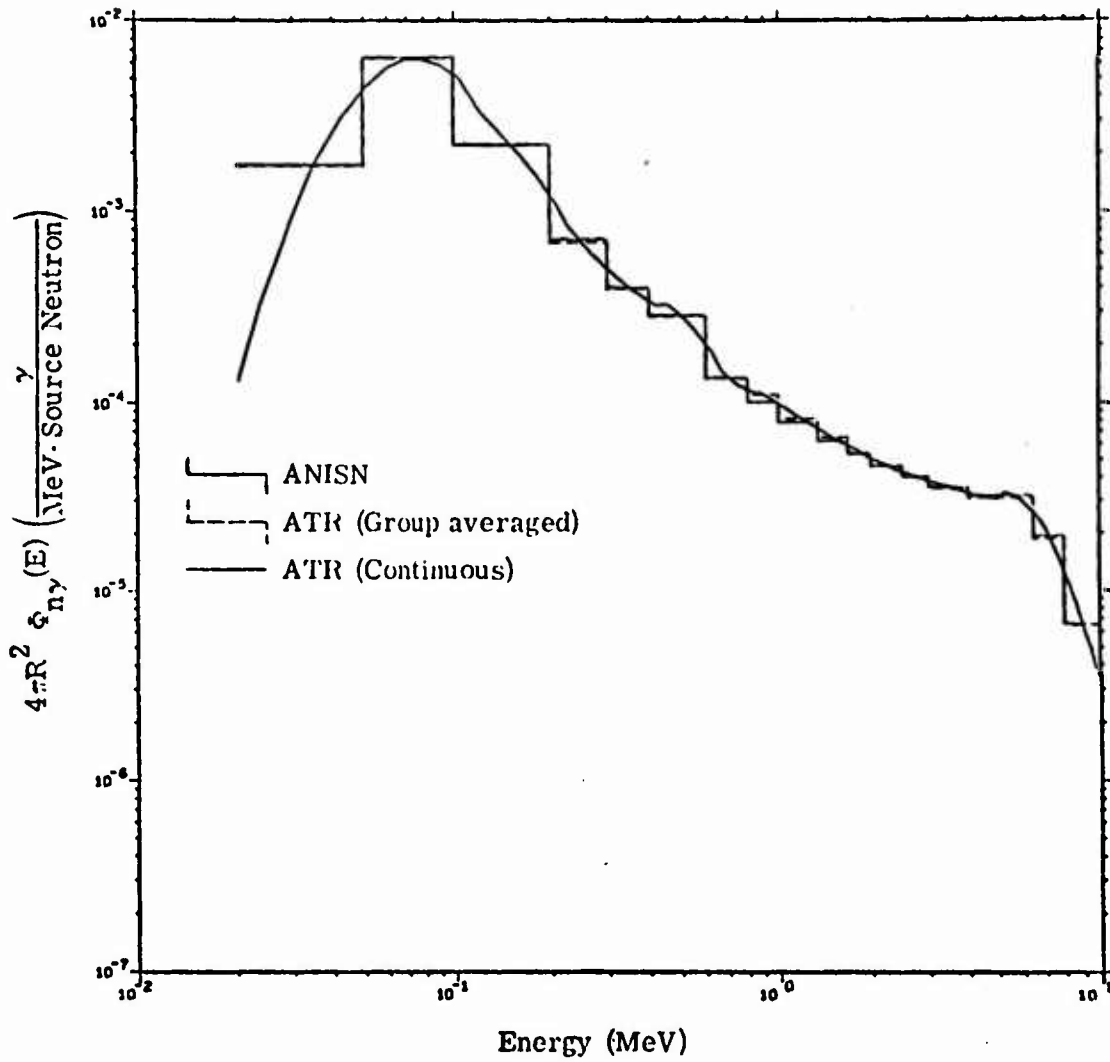
Fig. 27. Comparison of secondary gamma-ray spectra calculated
by ATR and the ANISN data base for a 12.2-15 MeV neu-
tron source at 3600 meters in air of density 1.11 mg/cm^3.
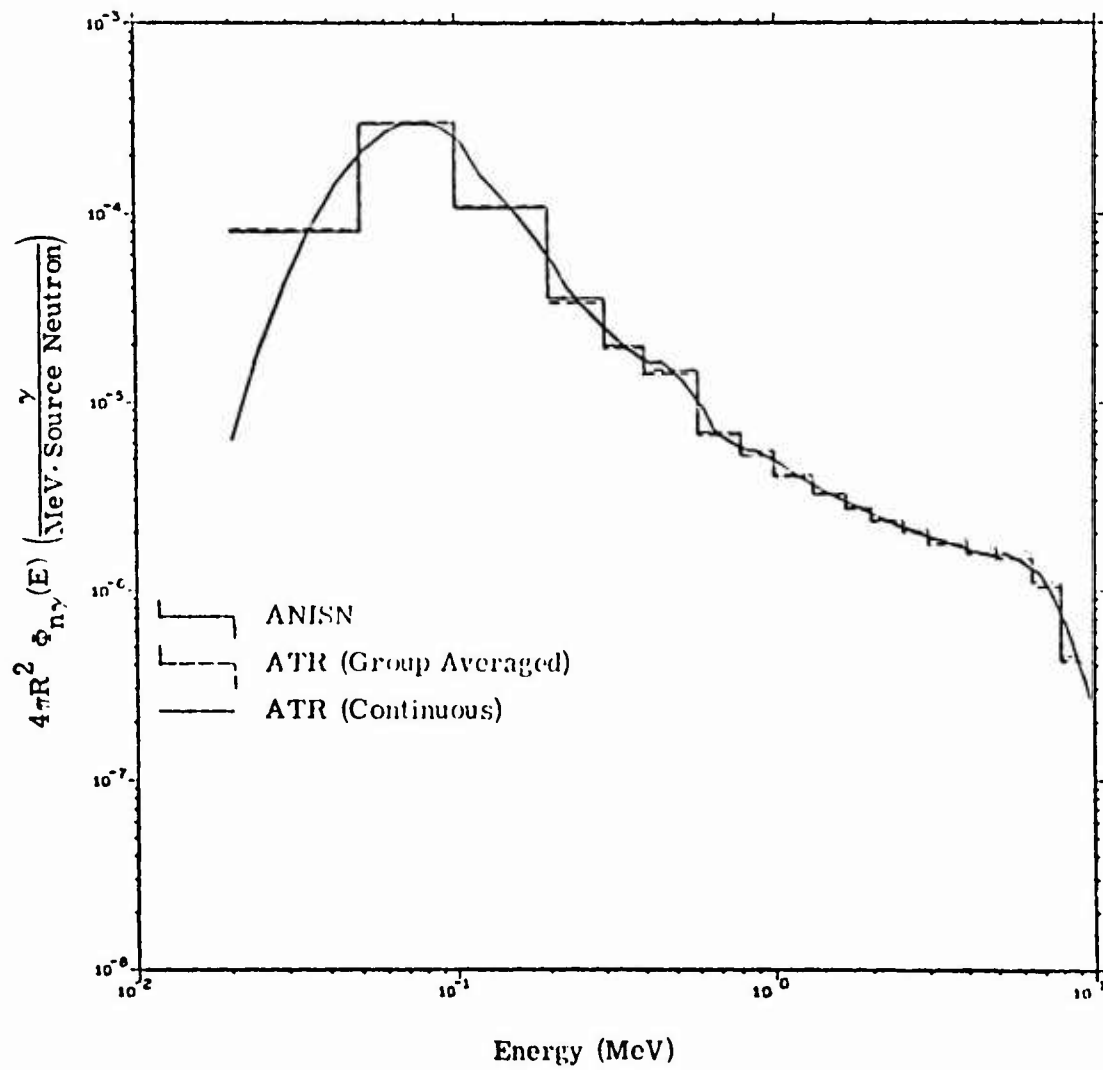
Fig. 28. Comparison of secondary gamma-ray spectra calculated by ATR and the ANISN data base for a 12.2-15 MeV neutron source at 4800 meters in air of density 1.11 mg/cm^3.

42.
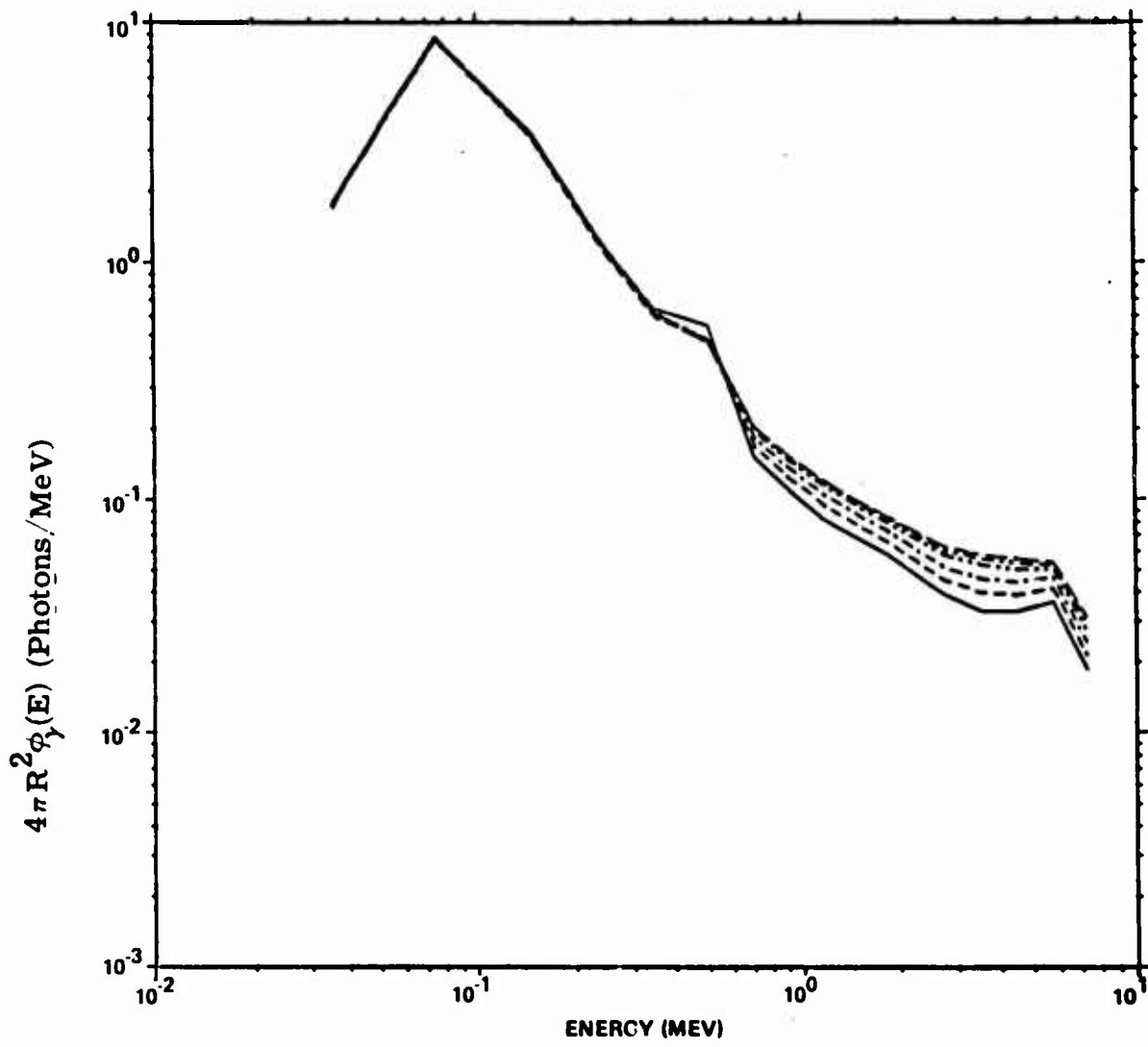
Fig. 29.   Normalized spectral shapes for a photon source
of 6.5-8.0 MeV at distance of 1 to 15 MFP.

43.
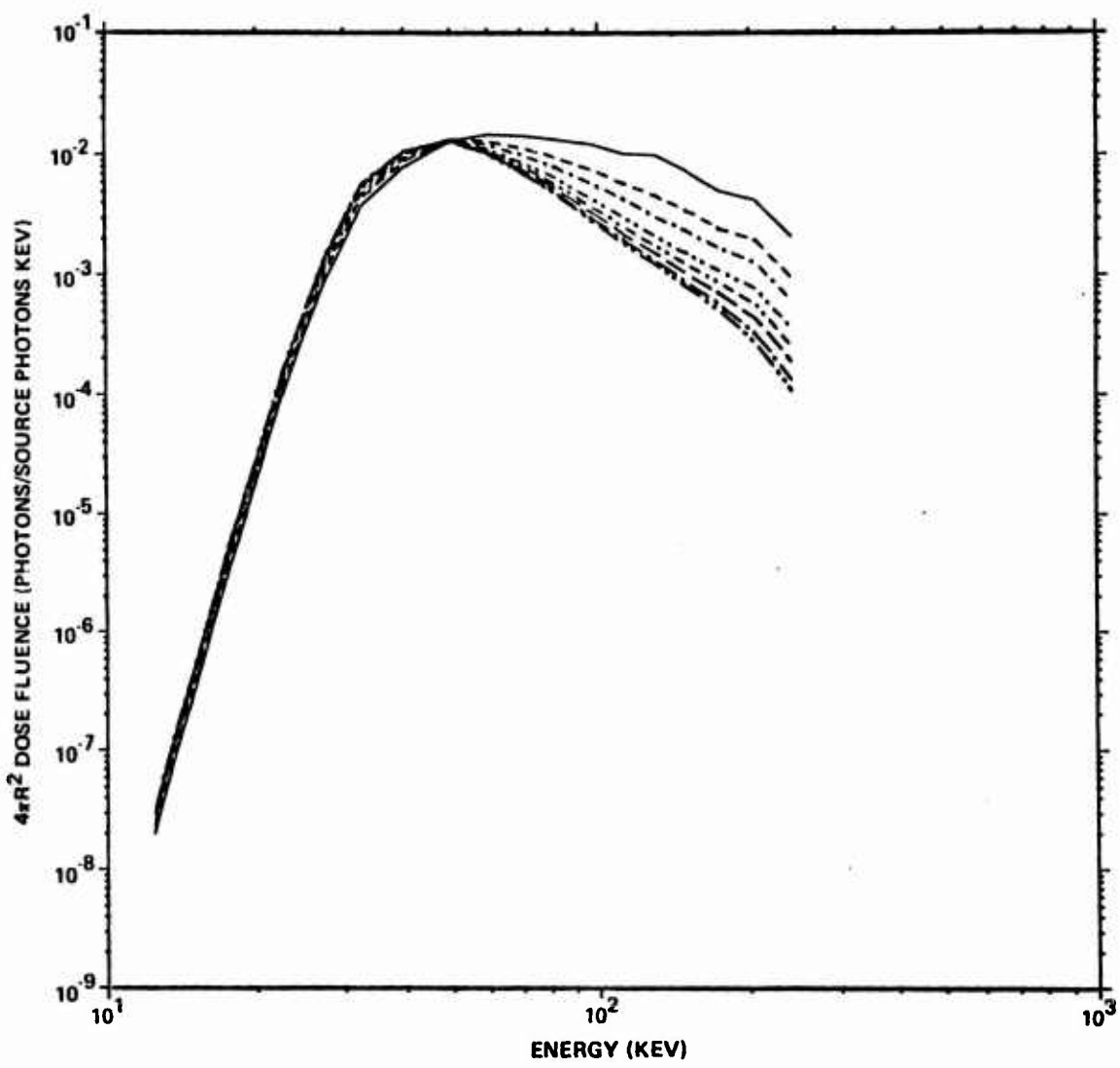
Fig. 30. Normalized spectral shapes for a photon source
of 260-220 keV at distances of 1 to 20 MFP.

44.

by curve-fitting the spectrum vs energy at one distance. The fixed distance was usually chosen to be at least several mean free paths from the source.

For high energy photon sources, the reference shape was obtained by curve-fitting a cubic equation in log-log space to the spectral data for $E_{NORM} \leq E < E_{MAX}$. The flux at this minimum energy point $(E_{NORM}-1)$ was assumed to be constant, and at the maximum energy point E_{MAX}, was fit vs distance using one of the two polynomials used in the fluence fits. Spectral shapes at an arbitrary distance were generated by linear interpolation from the reference shape. Thus, in the region above 0.5 MeV where spreading occurs in the spectral shapes vs distance and energy, an arbitrary spectral shape is calculated from:

$$S(E,r) = \exp\left\{ \ln S_0(E,r_0) + \left(\frac{\ln E - \ln E_1}{\ln E_{MAX-1} - \ln E_1}\right)\left[\ln S(E_{MAX}, r) - \ln S(E_{MAX}, r_0)\right]\right\}$$

where E_1 = 0.5 MeV energy point.

$$S_0(E, r_0) = \exp\left\{ A_1 + A_2 \ln E + A_3 (\ln E)^2 + A_4 (\ln E)^3 \right\}$$

is the reference shape,

$$S(E_{MAX}, r) = \exp\left\{ B_1 + B_2 \ln r + B_3 (\ln r)^2 + B_4 (\ln r)^3 + B_5 (\ln r)^{-1}\right\}$$

is the fit vs distance for the flux at E_{MAX}.

The differences between the parametric shapes and the raw data were small except at the 0.5 MeV peak. This difference was reduced to less than 10% for all ranges except very close-in by introducing a constant correction at 0.5 MeV.

A similar scheme to the above was used for low energy photons except for energies below the normalization point where the data were not constant (Fig. 30) but exhibited a nearly constant displacement vs energy for different radii. A constant displacement vs energy was assumed for this region of the spectra and was obtained in parametric form as a function of distance by fitting a quadratic at one energy at the fourth energy point (27 keV). A cubic equation also worked well for fitting the reference shape in the low-energy photon data base.

An arbitrary spectral shape for a given source energy was calculated in an analogous manner to the above equation for $E \geqslant E_{NORM}$. For $E < E_{NORM}$, the reference shape was shifted by an amount determined from the fit vs distance for the fourth energy point, i.e. for $E < E_{NORM}$,

$$S(E, r) \cdot \exp \left\{ \ln \left| S_0(E, r_0) \right| + \ln \left| S(E_4, r) \right| - \ln \left| S(E_4, r_0) \right| \right\}$$

46.

where $S_0(E, r_0)$ is the reference shape at r_0 determined by a cubic fit vs energy, and the fourth-point fit vs distance is

$$S(E_4, r) = \exp\left\{ C_1 + C_2 \ln r + C_3 (\ln r)^2 \right\}.$$

3.3 Angular Distribtuions

The energy-angle coupling of the scattered flux was taken into account by parametrizing the following ratio function:

$$R(E_S, \ E, \ r, \ \Omega) = \frac{\Phi(E_S, \ r, \ E, \ \Omega)}{\int \Phi(E_S, \ r, \ E, \ \Omega)\, d\Omega}$$

where R is the ratio of the angular flux to the scalar flux at each energy E for a given angular direction, range and monoenergetic source energy. The use of the ratio function to represent angular dependence tends to "smooth out" the energy structure and also maintains the slowly-varying behavior of the flux as a function of distance and angle. The "smoothing" occurs because the qualitative shape of a scalar flux spectrum does not differ grossly from the spectrum shape for each angle. These factors allowed the energy-angle coupling to be modeled with a minimum number of parameters.

Parametric modeling for energy-angle coupling has been completed for neutrons and secondary gamma-rays, and is discussed below. The general behavior of the energy-angular flux is shown in Figs. 31 through 35 at 100 meter and 2400 meter for a 12.2-15 MeV neutron source. Figure 36 illustrates the variation of angular flux vs distance for the 6.36-8.19 MeV detector group at 6 angles. These plots were generated by computer from the raw data base and demonstrate the variation in energy spectra for each of the 17 angles used in the ANISN calculations. A significant feature of these plots is the irregular behavior for small flux components which tends to occur in the backward directions becoming negative for some cases. This behavior is apparently due to the truncation of the Legendre expansion at P5 in the angular scattering representation of the discrete ordinates calculations. These irregular components make it difficult to initiate a curve fitting scheme on a production basis, however, they should be included for completeness in any model. Therefore, as a first step toward modeling the energy-angle coupling, a new angular flux tape was created in which the negative fluxes and irregular behavior were corrected by extrapolation and interpolation. This procedure was carried out subject to the constraint that the integrated fluence was conserved for each angle. The important differential flux data in the forward four angles (0-40°) was essentially unchanged by this operation.
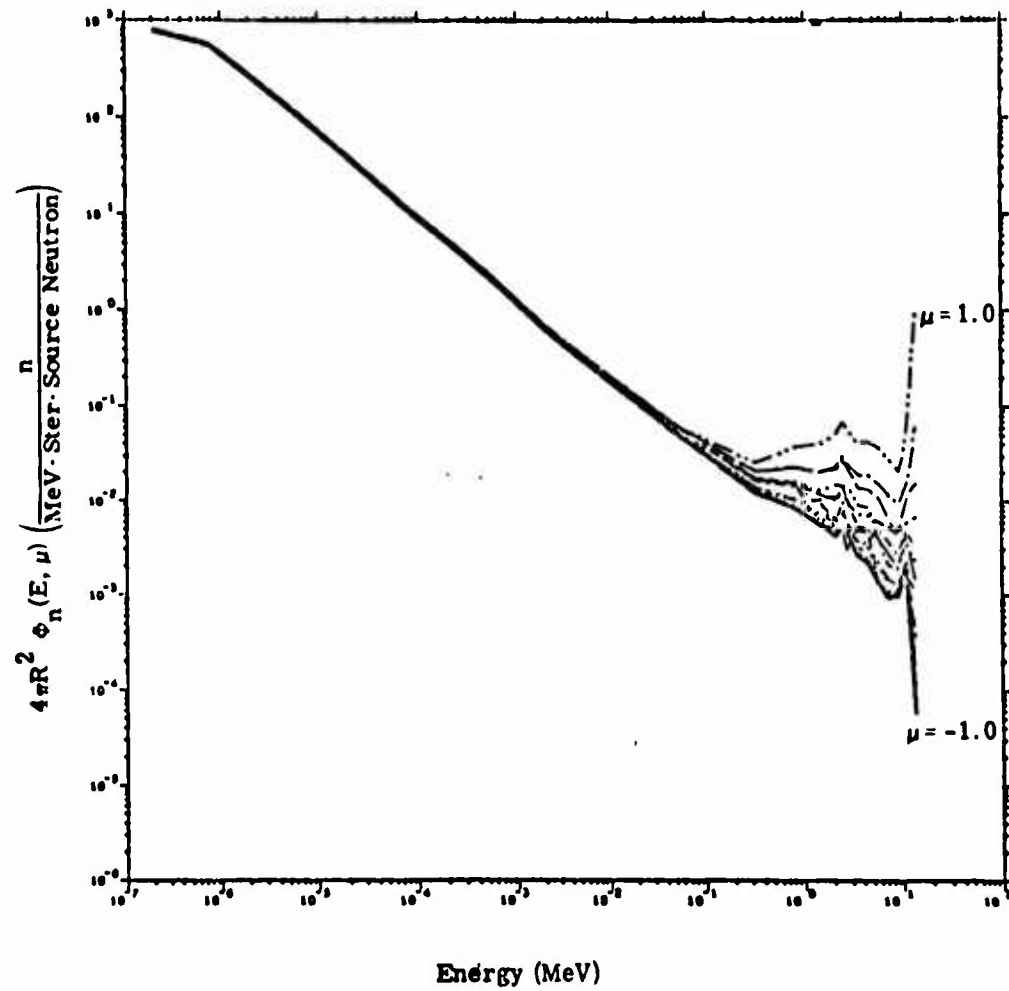
Fig. 31. Neutron angular flux spectra calculated with ANISN
at 17 angles for a 12.2-15 MeV neutron source at a
range of 100 meters in air of density of 1.11 mg/cm^3.
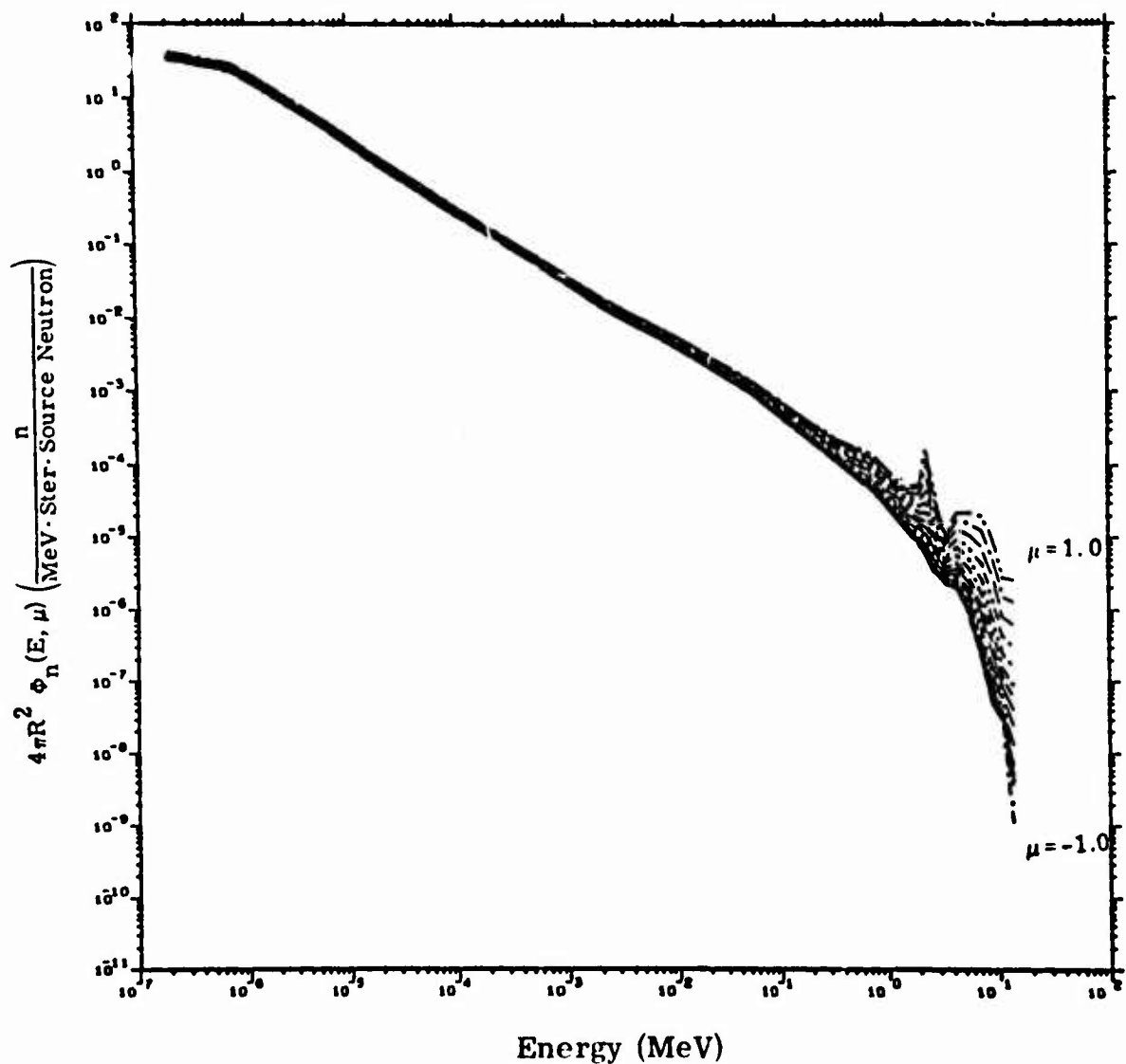
Fig. 32. Neutron angular flux spectra calculated with ANISN
at 17 angles for a 12.2-15 MeV neutron source at a
range of 2400 meters of air.

50.
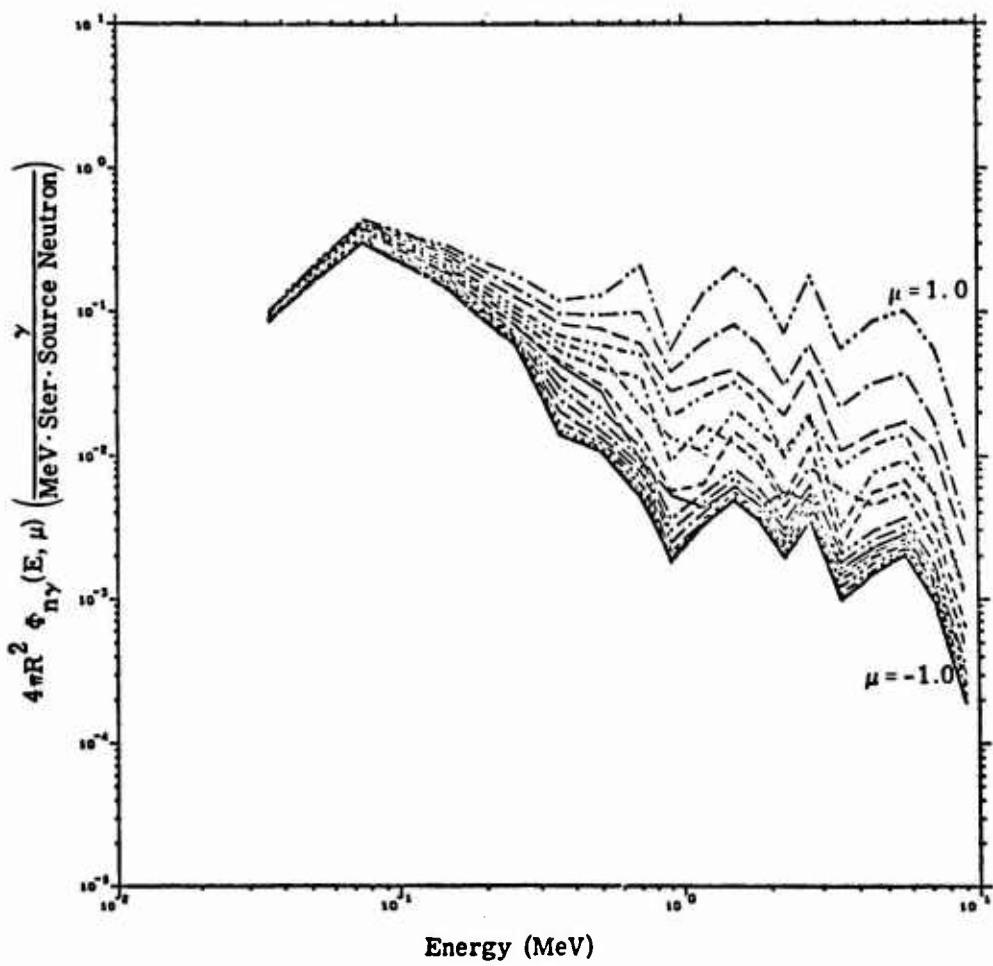
Fig. 33. Secondary gamma-ray angular flux spectra calculated with ANISN at 7 angles for a 12.2-15 MeV neutron source at a range of 100 meters in air of density 1.11 mg/cm^3.
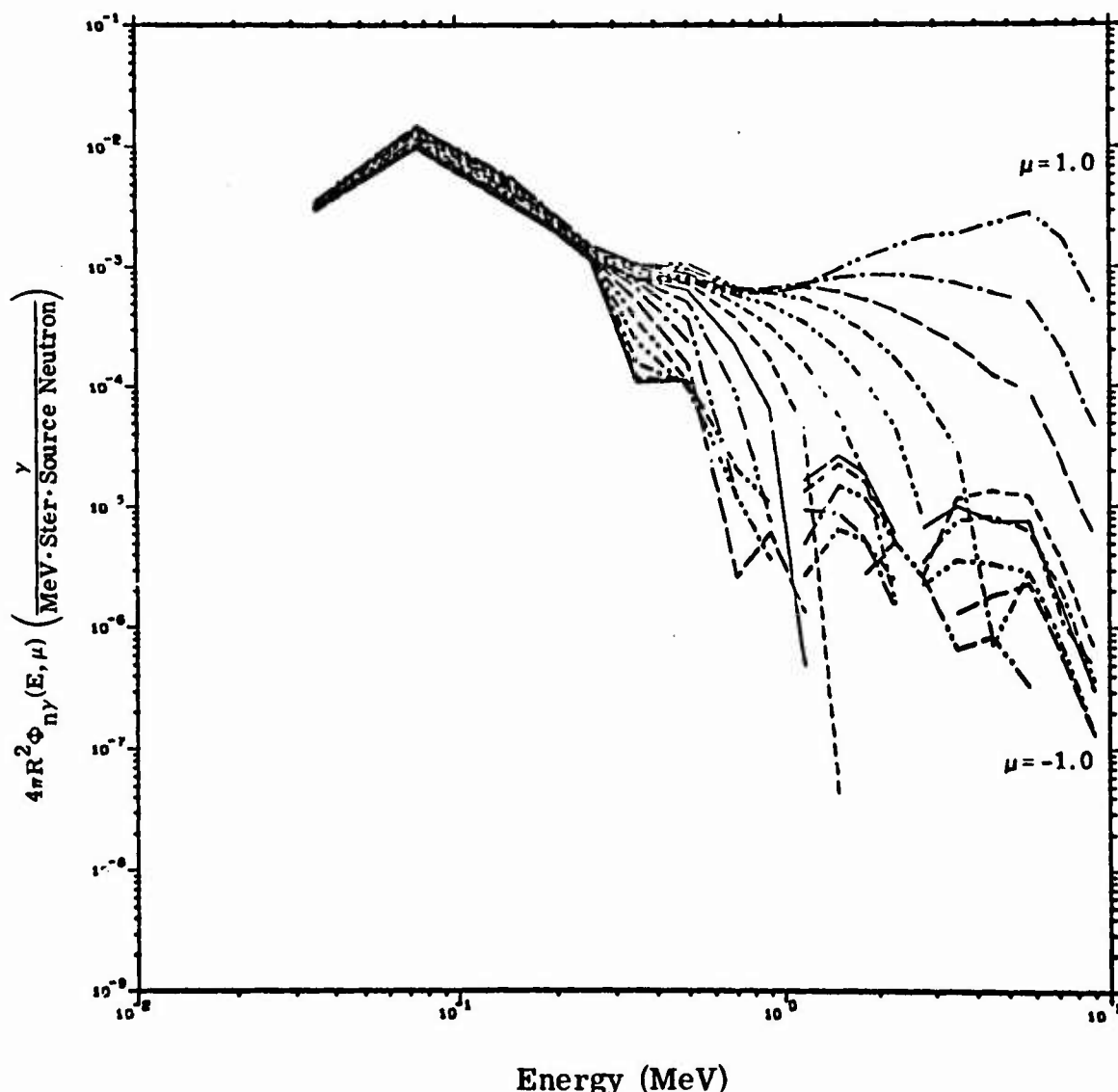
Fig. 34. Secondary gamma-ray angular flux
spectra calculated with ANISN at 17
angles for a 12.2-15 MeV neutron
sources at a range of 2400 meters.
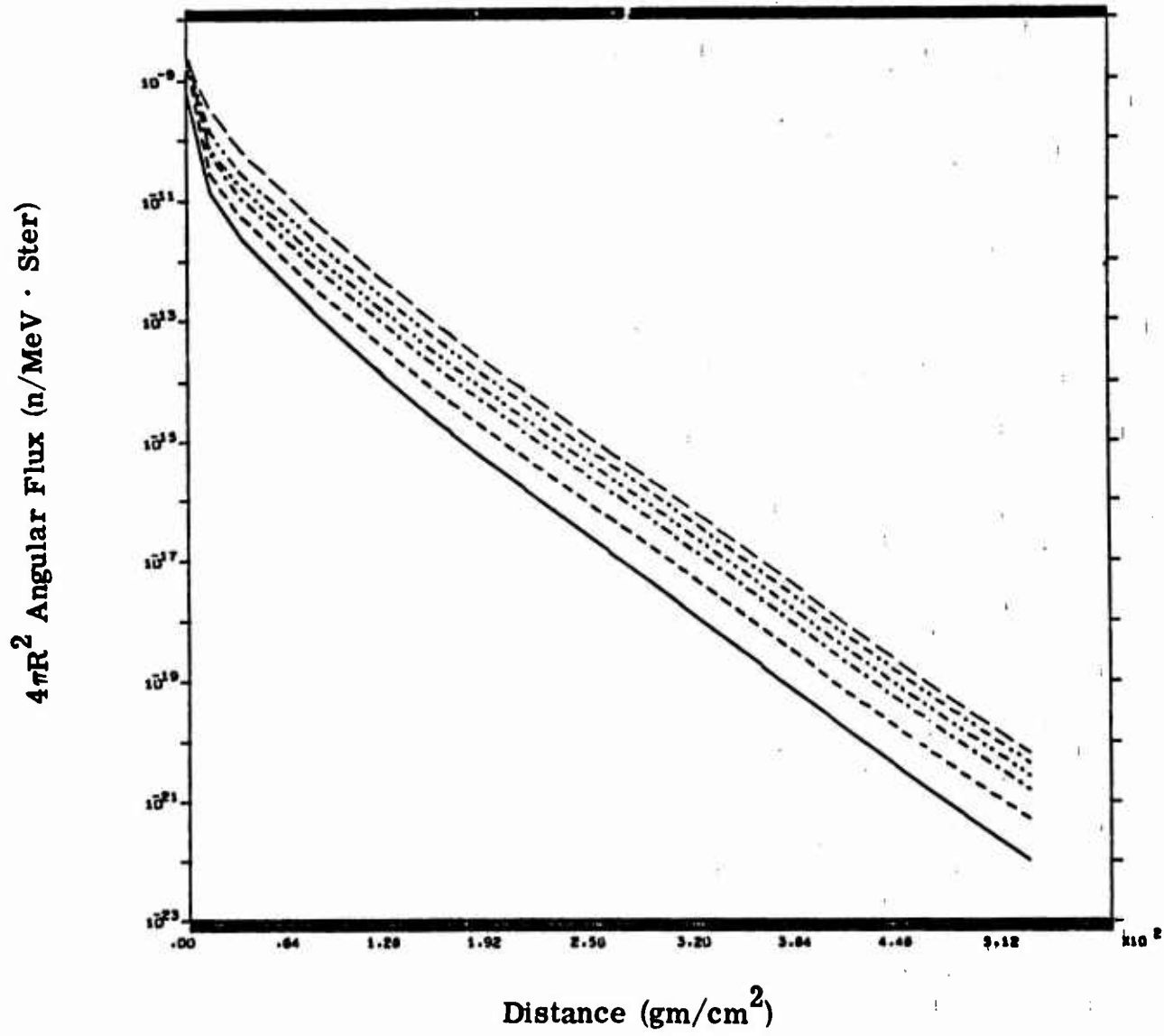
Fig. 35. Variation of angular flux vs distance for
the 6.36 to 8.19 MeV detector group and
12 to 15.2 MeV neutron source.

Ratio functions as defined earlier were formed into a data base $R(E_S, E, r, \mu)$ for modeling and are illustrated in the representative plots of Figs. 36 and 37 for neutrons and secondary gamma-rays, respectively, at 300 meters from a 14 MeV source. These curves show clearly the smoothing effect as a function of energy inherent in the ratio function. For neutrons, R is unity to a good approximation for energies below 0.1 MeV. Above 1 MeV, considerable structure was present in R which made it difficult to fit well with simple functions. The slowly varying nature of the angular flux vs distance (Fig. 35) indicated that the ratio could be parameterized more efficiently by using distance as an independent variable. Thus, the following representation was used to model the ratio function of neutrons for each source energy:

$$R(E, r, \mu) = 1.0 \text{ for } E \leq 0.1 \text{ MeV}$$

$$R_E(r, \mu) = \exp \left| A_1(\mu) + A_2(\mu)r + A_3(\mu)r^2 \right| \text{ for } E > 0.1 \text{ MeV}$$

where

$$A(\mu) = B_1 \exp(B_2 \mu) \text{ for } -1.0 \leq \mu \leq 0.6178$$

$$= \exp(C_1 + C_2 \mu + C_3 \mu^2) \text{ for } 0.6178 < \mu \leq 1.0$$

This procedure increased the total number of neutron coefficients by less than a factor of 2 to represent 17 times the amount of data. Thus, the

54.
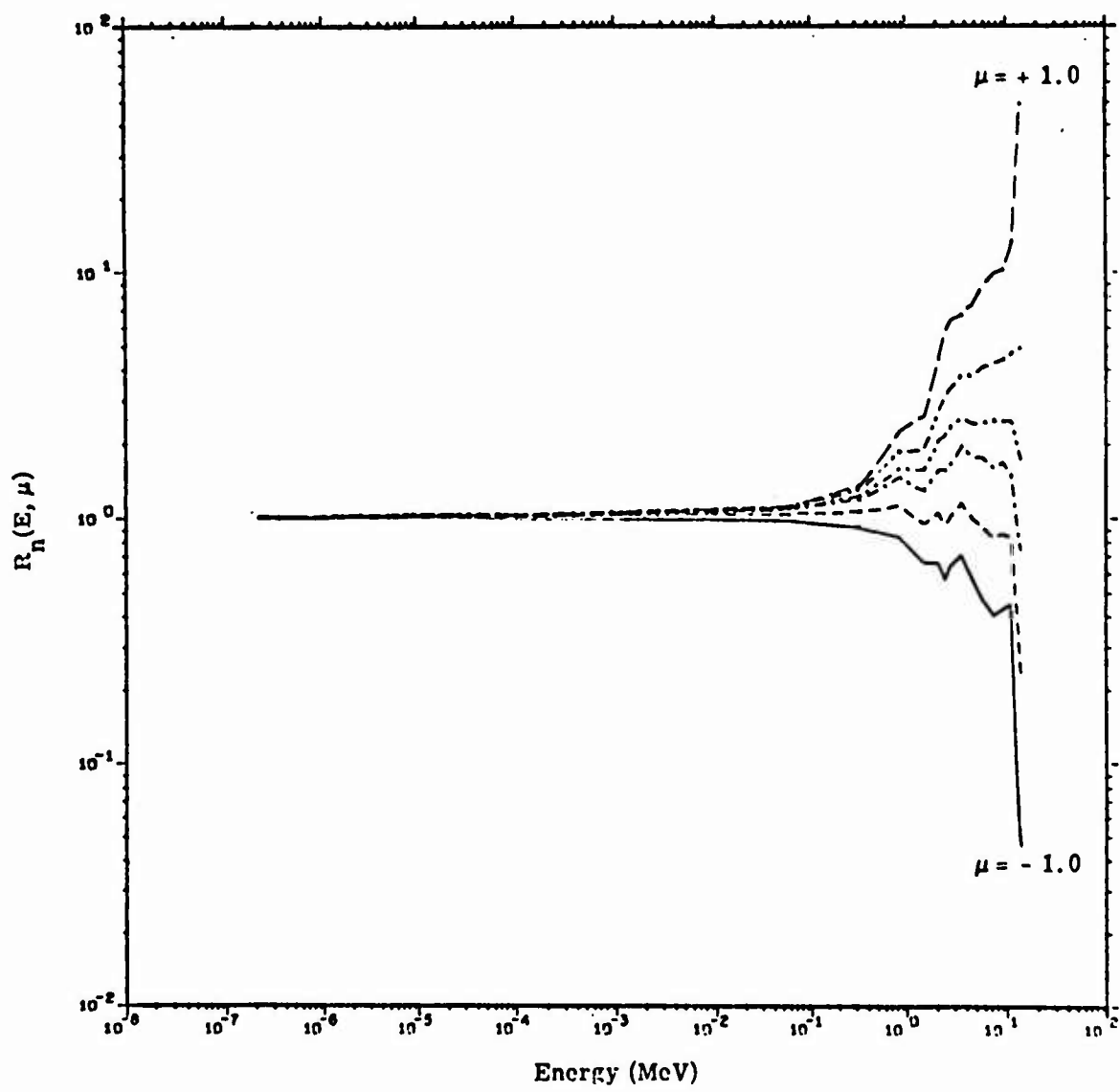
Fig. 36. Neutron ratio function for 14 MeV neutron source at 300 meters.
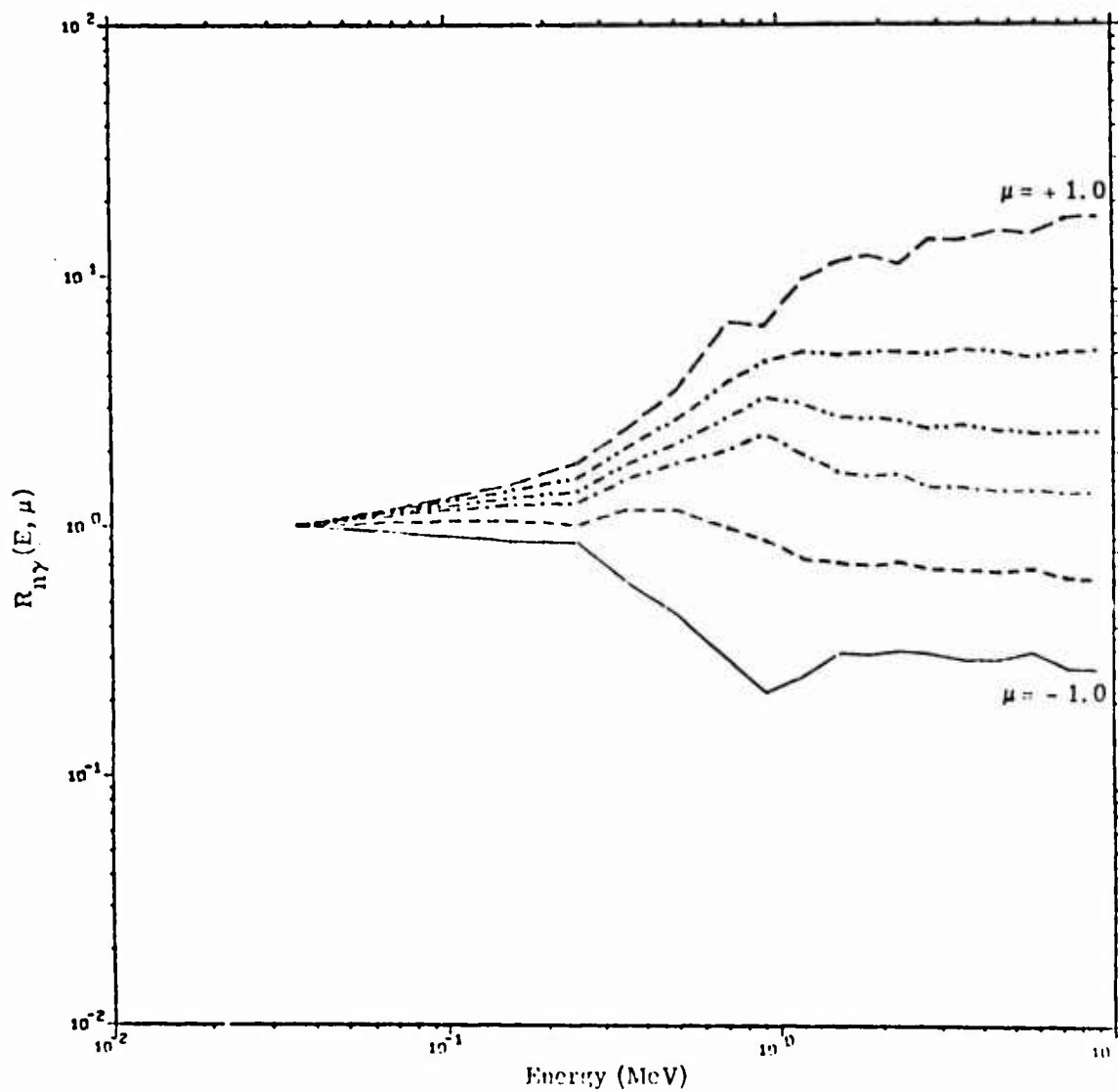
Fig. 37.   Secondary gamma-ray ratio function for 14 MeV neu-
tron source at 300 meters.

entire energy-angle data base for neutrons, representing over 10^6 flux values, required about 2000 coefficients.

The ratio function for secondary gamma-rays (Fig. 37) varied more smoothly with energy and was fit versus energy for each source by a five-order polynomial whose coefficients themselves were sub-polynomials in distance and angle. These parametric fits essentially doubled the number of coefficients in the secondary gamma-ray model for a 17-fold increase in flux information.

The accuracy of the neutron and secondary gamma-ray angular flux model is difficult to estimate because of the inherent limitation in the raw data base. Differences between the parametric model and the raw ANISN data base can be large for the small fluxes at high energies and in the backward directions, however, the raw data in this region are probably uncertain by a factor of 2. The agreement between the model and the "smoothed" angular flux data base is of course much better. The most meaningful estimate of the adequacy of the angular flux model is probably obtained by comparing partially integrated quantities with the raw ANISN data base. Thus, the total fluences integrated over energy and angle generally agreed within 5%; fluence distributions integrated over energy alone agreed to about 10%; and fluence distributions integrated over angle agreed to about 20%. Differential angular flux data calculated by the parametric model are shown in Figs. 38 and 39, for neutrons and secondary gamma-rays at 600 meters from a 14 MeV source. These curves
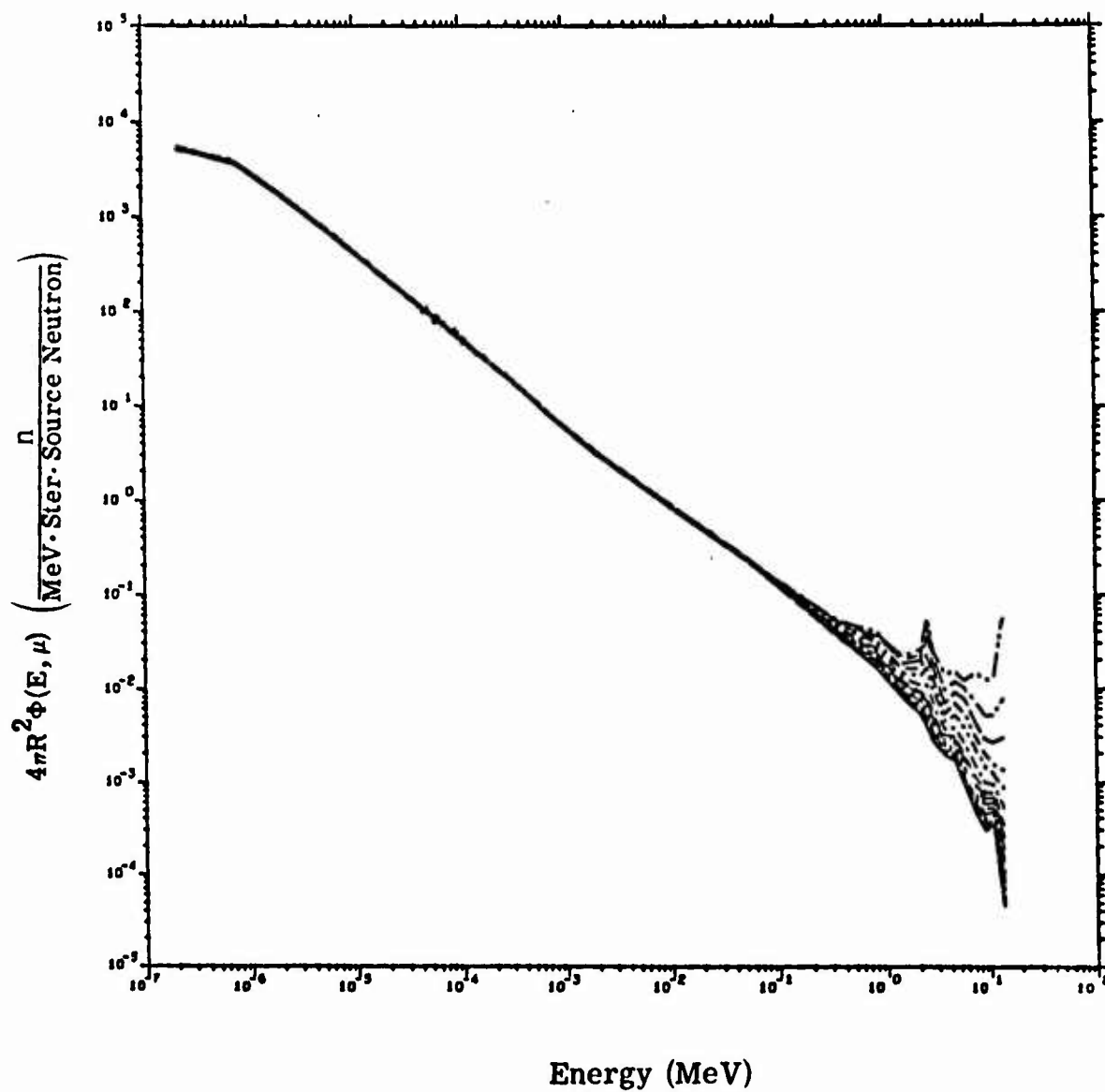
Fig. 38. Neutron energy-angle distributions calculated by ATR at 600 meters from a 14 MeV neutron source.
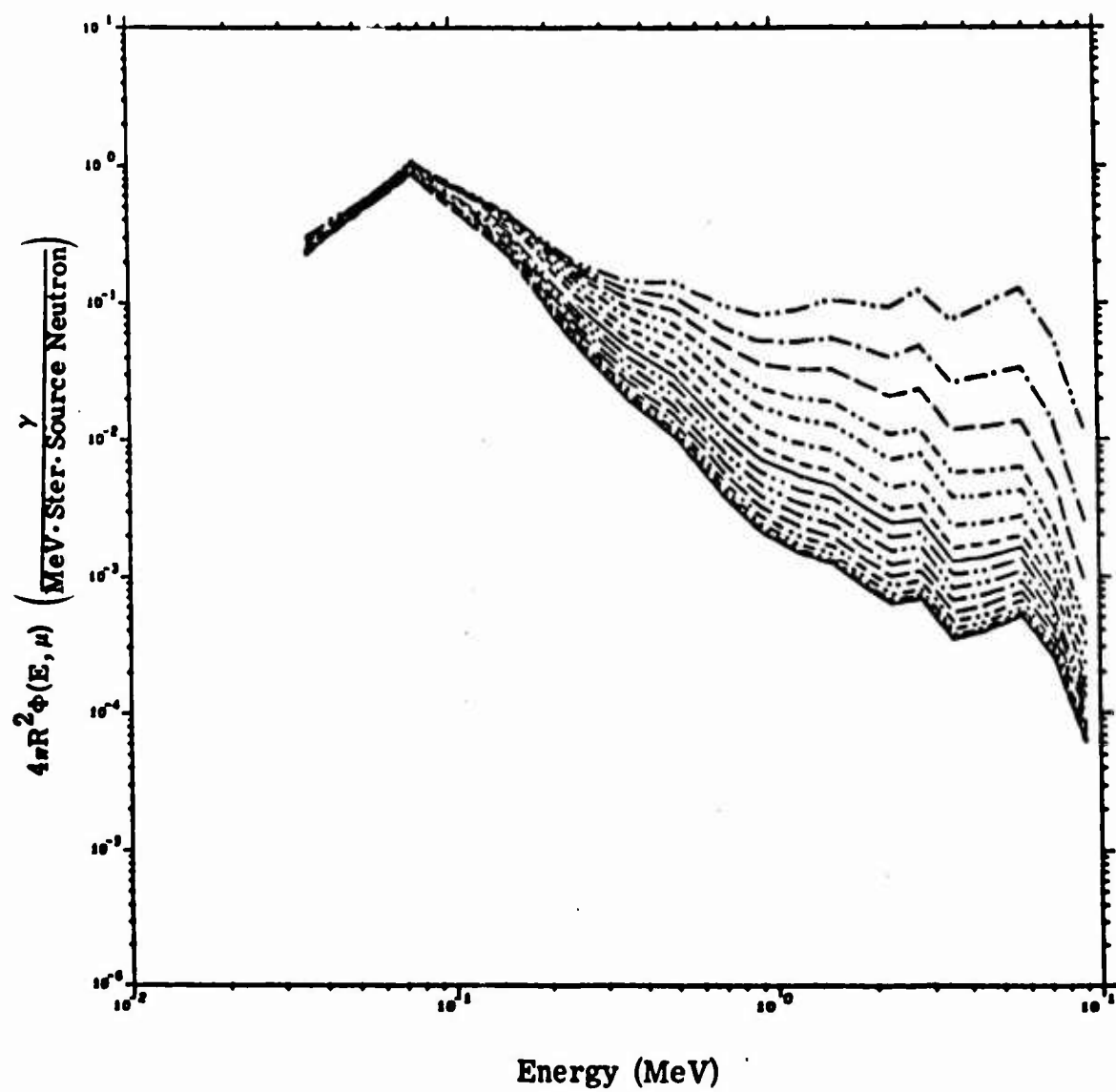
Fig. 39. Secondary gamma-ray energy-angle
distribution calculated by ATR at 600
meters from a 14 MeV neutron source.

59.

demonstrate the desired structure and the systematic behavior charac-
teristic of deep-penetration transport.

The extension of the angular-flux modeling to prompt photon
transport using a ratio function is expected to be a less tedius job due
to the lack of energy structure in the scalar flux shapes. Preliminary
estimates indicate that the angular dependence of prompt photon trans-
port will require approximately 1000 coefficients each for the low and
high-energy ranges.

IV. THE ATR CODE

The parametric models described in the previous section have been used as the basis for constructing ATR - a computer code for efficiently calculating the air transport of radiation for a variety of different problems at all altitudes in the atmosphere. Mass scaling is used to transform the parameterized results for homogeneous air from an air density of 1.11 mg/cm^3 to other air densities. Corrections are also included for air-ground interface and exponential air density effects. The code has been structured to allow the user a maximum degree of flexibility in calculating different problems, with a minimum number of restrictions on input data and format. The presently completed version of ATR calculates problems for neutron and secondary gamma-ray transport. Prompt photon transport for high and low energy photons will be included in the near future when modeling is completed on photon angular distributions.

4.1 Problem Geometry and Scaling Laws

The problem geometry for ATR is illustrated in Fig. 40, where the geometry coordinates are:

H_S = source altitude

H_T = target altitude

R_S = slant range

R_H = horizontal range

θ = slant angle
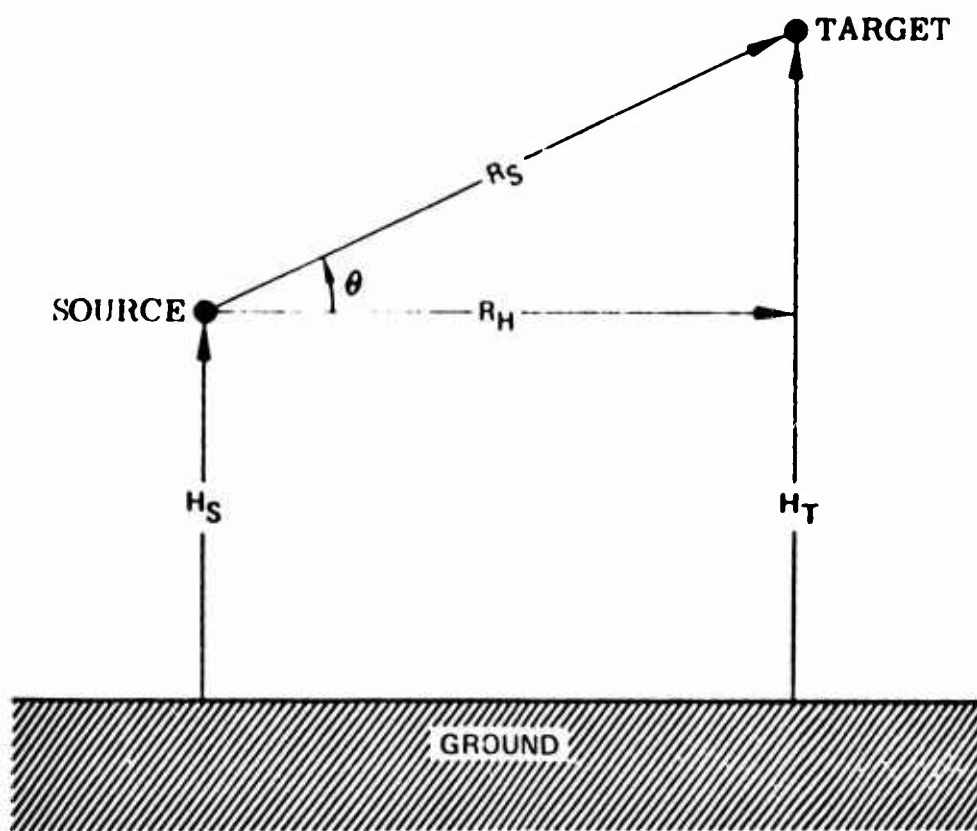
Fig. 40.   ATR problem geometry.

The fundamental calculation in ATR is to determine the free-field distribution for a given problem geometry and source spectrum. In order to calculate such problems for the actual atmosphere, two assumptions are made:

1.   The transport of radiation between source and target can be approximated by homogeneous air transport results for a density equal to the average density between the source and target altitudes.

2.   The corrections due to air-ground interface and exponential air density effects can be included as perturbations to homogeneous air results.

The general calculational scheme in ATR is therefore to scale transport results from the parametric model density of 1.11 mg/cm^3 to the average density of the problem and then to include correction factors for the effects of an air-ground interface and exponential air density. These correction factors were essentially negligible for altitudes from 1-20 KM. Density scaling laws for the Boltzmann equations are reviewed in Appendix B and show that the angular flux $\phi_t(E, \Omega, r)$ in the transformed system of density $\rho_t(r_t)$ is related to the flux in the original system at density $\rho(r)$ by

$$\phi(E, \Omega, r) = K^2 \phi_t(E, \Omega, r_t)$$

where

$$r_t = Kr \text{ and } \rho_t(r_t) = \rho(r)/K$$

i.e., for

$$\rho_t r_t = \rho r$$

This is the well known result that the $4\pi r^2$ flux depends only on the mass of air through which the neutrons and photons are being transported. The ATR parametric model is based on $4\pi r^2$ quantities as a function of penetration distance in grams/cm^2. The total mass of air between source and target for a given problem is calculated from $R_s \bar{\rho}$ and used to obtain $4\pi R_s^2$ quantities from the parametric data base, i.e.,

$$4\pi R_s^2 \phi_s = 4\pi R_o^2 \phi_o.$$

For

$$R_s \bar{\rho} = R_o \rho_o$$

where

$\bar{\rho}$ = average air density of the problem

ρ_o = air density of ATR data base (1.11 mg/cm^3)

ϕ_o = radiation free-field calculated by parametric equations at density ρ_o and distance R_o

ϕ_s = radiation free-field of the problem geometry

The average air density of the problem is calculated from

64.

$$\bar{\rho} = \frac{\int_{H_S}^{H_T} \rho(Z)dZ}{H_T - H_S}$$

where $\rho(Z)$ is the variation in the atmospheric density versus altitude above sea level.

The atmospheric-density was calculated for altitudes from 0-300 KM based on a model developed by Dupree.[74] Dupree's model consisted of a product of 32 exponential terms and was used for altitudes from 0-100 KM. Above, 100 KM, an empirical curve fit was used. The entire density model was based on data listed in the U. S. Standard Atmosphere.[76] Equations used for the model were:

$$\rho(h) = \frac{e^{-P_I(h-h_{I-1})}}{\rho_0} \left\{ \frac{}{\prod_{i=1}^{I-1}} e^{-P_i(h_i-h_{i-1})} \right\} \qquad 0 \le h \le 100 \text{ KM}$$

for $h_{I-1} \le h \le h_i$, with $h_0 = 0$ and $3 \le I \le 32$. The product is deleted for I=2, and ρ_0 is the sea level density value.

$$\rho(h) = \exp\left[C_1 + C_2 h + C_3 h^2 \right] \qquad 100 \text{ KM} < h \le 130 \text{ KM}$$

$$\rho(h) = \exp\left[C_1 + C_2 h + C_3 h^2 + \frac{C_4}{h-99} \right] \qquad 130 \text{ KM} < h$$

4.2 Air-Ground Interface Corrections

Corrections for air-ground interface effects were based on the first-last collision model of French.[75] In this model factors $F(H_S)$ and $F(H_T)$ are derived for correcting infinite air results according to

$$\phi(H_S, H_T, R) = F(H_S) F(H_T) \phi_0(R)$$

where $\phi_0(R)$ is the infinite air flux.

The model estimates $F(H_S)$ by calculating the effective fraction of first collisions about the source as a function of source altitude. $F(H_T)$ is determined by calculating the effective number of last-collisions in the vicinity of the target. The model was developed for fast neutrons and treats neutron reflection from the ground by an albedo approach. The correction factors are listed in Table II as a function of MFP from the ground.

Comparisons of the model prediction with Straker's two-dimensional transport calculations[12] of dose vs. distance showed that the model was more accurate in correcting from one source height to another than correcting infinite-air results. This was also true for correcting secondary gamma-rays where the model predictions alone gave results differing from Straker's calculations by as much as a factor of five. Correcting air-ground data from one source altitude to another, however, gave agreement to about 25%.

66.

TABLE II.

Air-ground correction factors from the
first-last collision model as a function
of MFP from the ground.

H(MFP)	$F(H_S)$	$F(H_T)$
0	0.434	0.697
0.01	0.466	0.717
0.02	0.478	0.728
0.05	0.506	0.750
0.10	0.546	0.781
0.25	0.632	0.841
0.50	0.724	0.902
0.75	0.798	0.934
1.00	0.862	0.953
1.50	0.941	0.977
2.00	0.972	0.987
2.50	0.987	0.990
3.00	0.993	0.993
3.50	0.996	0.995
4.00	0.997	0.997
H>4.0	1.00	1.00

On the basis of the above considerations, a scheme was developed for obtaining air-ground corrections to infinite air results by using the first-last collision model to extrapolate Straker's dose data to other altitudes, i.e., for $H_T \leqslant 100$ meters:

$$C(H_S, H_T, R_S) = \frac{F(H_S)F(H_T)}{F(H_S')F(H_T')} \quad \frac{D_0(H_S', H_T', \bar{\rho}R_S/\rho_0)}{D_{Inf.Air}(H_S, H_T, R_S)}$$

where

$H_S' = 15$ meters

$H_T' = 1$ meter

$D_0 =$ Henderson dose vs distance calculated by Straker at H_S' and H_T'

H_S, H_T and R_S are the problem coordinates

$\rho_0 = 1.11$ mg/cm^3

$\tilde{\rho} =$ average air density in problem geometry

The above correction factor is used in ATR to correct all differential results obtained by using mass scaling of the parametric model for target altitudes below 100 m. The two main assumptions in the above correction scheme are:

1.   The spatial, energy and angular distributions

of radiation near an air-ground interface can be approxi-

mated from infinite air results with a shift in intensity only.

2.   The intensity shift is proportional to ratio

of the air-ground dose to the infinite air dose cal-

culated for transport through the same mass of air.

For target altitudes above 100 meters, the infinite air results are
corrected using the first-last collision model alone, i.e., for $H_T > 100$
meters:

$$C(H_S, H_T, R_S) = F(H_S)F(H_T) \ .$$

The effect of the air-ground corrections is illustrated in Fig. 41, which

shows dose vs distance curves for the Hiroshima device obtained using

ATR and compared with the empirical results of Auxier et. al.[77] The

ATR results with air-ground corrections are approximately 50% lower

than scaled infinite air results, and are in fair agreement with Auxier's

values.

4.3   Exponential Air-Density Corrections

Corrections for non-uniform air density effects were obtained

by extending the first-last collision model to include the density varia-

tion versus altitude in the numerical integration scheme. The first-

collision correction factor for source altitude was obtained by numerical

integration of the equation below.

$$F(H_S) = \frac{\mu_T}{2} \int_0^\infty \int_{-H_S}^\infty \frac{W(Z) X \bar{\rho}(Z) e^{-\mu_T \bar{\rho}(Z) \sqrt{X^2 + Z^2}}}{X^2 + Z^2} \, dX dZ$$
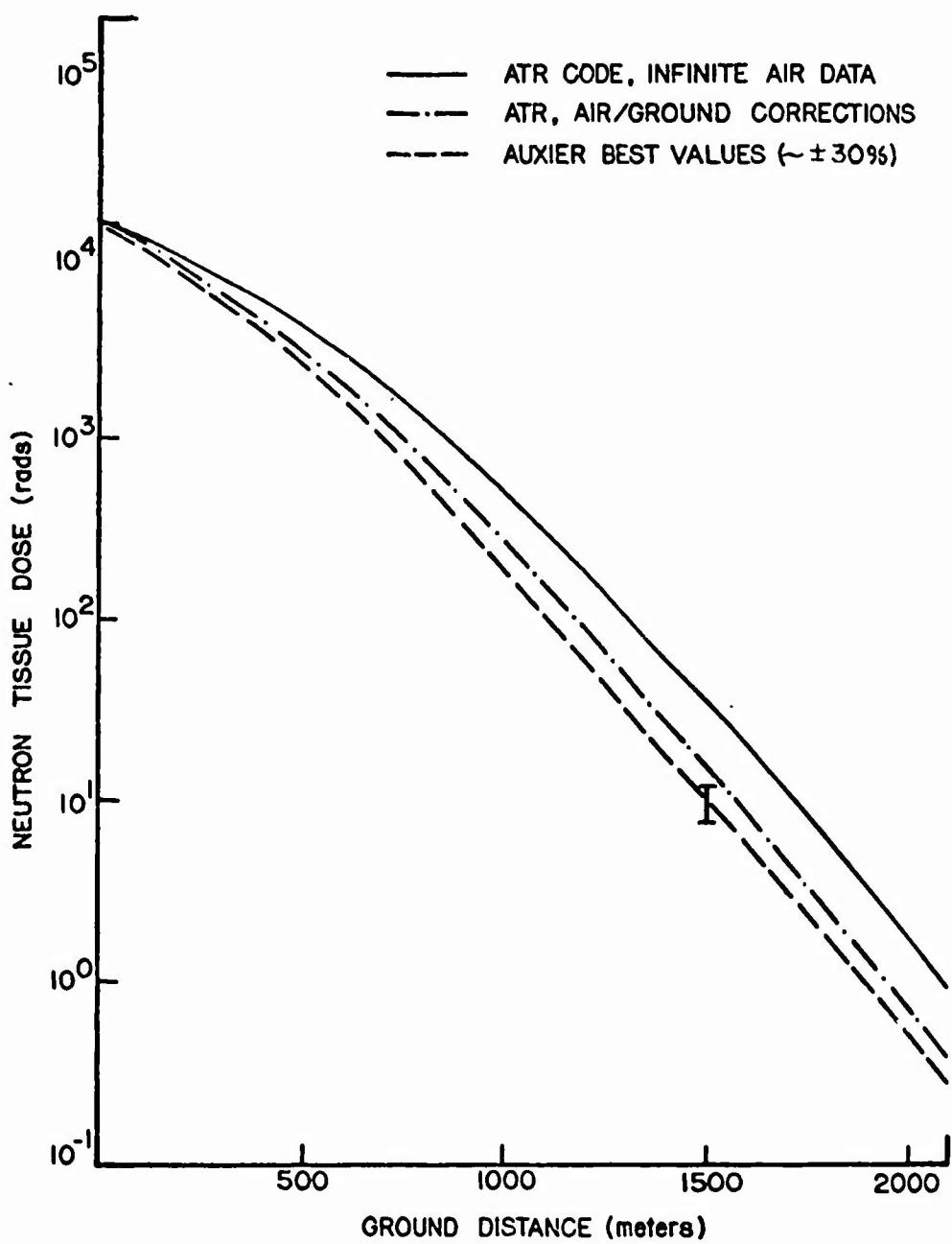
Fig. 41. Neutron dose from Hiroshima device (12.5 KT
yield, 579 m height-of-burst).

where μ_T is the total cross section in air in cm^2/gm. $W(Z)$ is a weighting factor given by $F(H_S + Z)$ to account for multiple scattering and is obtained by an iteration of the above equation.

The additional term used to account for reflection in the air-ground case is zero here since neutrons are not reflected from the top of the atmosphere.

The last-collision correction for target altitude was obtained from numerical evaluation of the above integral without the weighting function. The numerical results for $F(H_S)$ and $F(H_T)$ are listed in Table III as a function of altitude in terms of mean free path to the top of the atmosphere. These correction factors were applied uniformly to the scaled infinite-air results in ATR for both neutron and secondary gamma-rays. The validity of the model was checked against the two-dimensional Monte Carlo calculations of Keith[30] at the two source altitudes reported of 85 KFT and 110 KFT. The first-last collision model reduced the infinite-air flux by factors which approximated the average behavior of the Monte Carlo results, but did not predict the same relaxation lengths. At large distances where the model is expected to be a good approximation, the correction factors were in fairly good agreement with Monte Carlo results. At a co-altitude distance of 50 gm/cm^2, for example, the correction factors were .79 and .23 respectively, for a 14 MeV source at altitudes of 85

TABLE III.

Exponential air correction factor from the first-last
collision model as a function of MFP
from the top of the atmosphere.

H(MFP)	F(H$_S$)	F(H$_T$)
0	0	0
0.010	0.067	0.180
0.030	092	0.229
0.060	0.133	0.300
0.090	0.166	0.350
0.140	0.210	0.408
0.210	0.271	0.482
0.320	0.373	0.585
0.490	0.491	0.676
0.770	0.642	0.793
1.200	0.808	0.890
2.000	0.920	0.967
3.100	0.975	0.980
4.900	0.985	0.990
7.900	0.996	0.998
H>7.9	1.000	1.000

KFT and 110 KFT; these compared well with the corresponding ratios between the non-uniform and uniform air results determined from Keith's curves and were 0.69 and 0.23. Thus, the first-last collision model seems to predict the average effect of non-uniform air on neutron transport. Secondary gamma-ray data were not available for comparison.

The effect of the non-uniform air correction in ATR is demonstrated by the isodose curves in Fig. 42 which were calculated at a source altitude of 90 KFT for an isodose value of 2500 rads. The source was the unclassified thermonuclear spectrum of ORNL 4464 with a yield of 10^{26} neutron. The non-uniform air correction result in slant ranges which are smaller than for scaled homogeneous air since the corrected flux curve is shifted to smaller flux values.

4.4 ATR Control Commands

The list of control commands for setting up an ATR run is given in Fig. 43. For the most part, the order of control commands is immaterial for any given set of problems, i.e., between *EXC commands. The initialization routine contains some calculations on parameters which can be evaluated on the basis of other parameters as well as some storage initialization. When a command is read in and interpreted, the corresponding subroutine is called to interpret and properly place all of the parameters following the command.
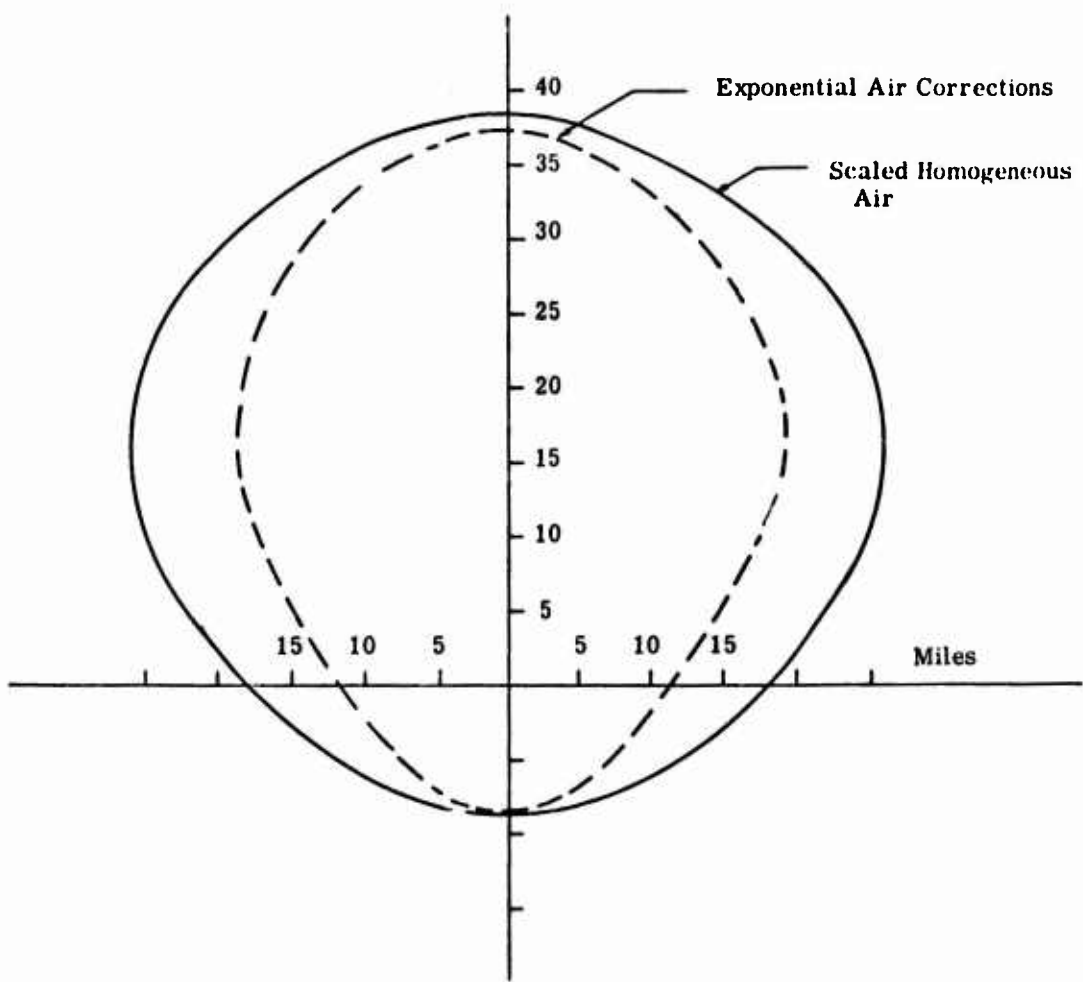
Fig. 42.   Isodose curves calculated with and without
non-uniform air correction for a source
altitude of 90 KFT.

ATR INPUT EXECUTIVE
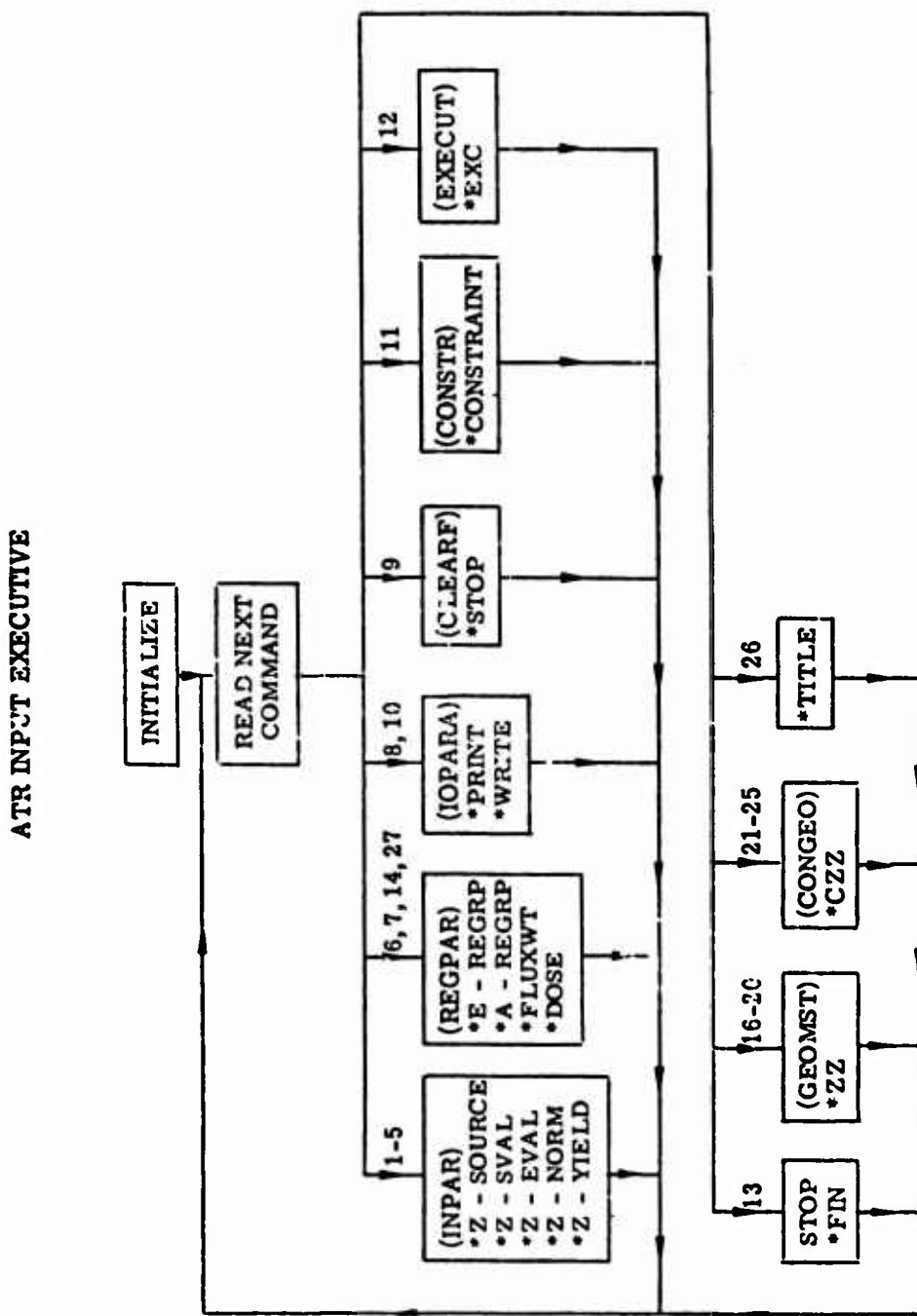
Fig. 43. Overall block diagram of the ATR code.

75.

Errors in control command format or structure are noted immediately but no other visible action is taken by the code until the *EXC command at which point output is generated which may be just a few numbers or hundreds of pages, depending on the input parameters.

The code also contains a set of subroutines which permit an essentially format-free placement of numbers. The reading of values is upward compatible in that real values need not contain decimal points. Standard FORTRAN-type real numbers in scientific notation are acceptable with or without the E; i.e., the number 400 can be written as 400 or 400. or 4.E+2 or 4.E2 or 4.+2. The blank character is used as a number delimiter, thus numbers must not contain blanks. Any number of blanks may separate numbers and a series of values may be continued on subsequent cards, but a number cannot be split between two cards. The major restriction is that since the real number and fractional parts as integers, neither the whole number nor the fractional part of any real number can exceed the integer capacity of the particular computer.

Control commands and their associated parameter values are cumulative so that even after the results of a particular problem have been displayed, the parameter values and flags remain the same for the next problem unless specified anew with another command of the same type. Consequently,

from one problem to the next, only the most essential parameters need to be specified. This feature allows multiple runs to be made easily which require only a few parameter changes to be made for each problem. Thus, the following sequence of commands is allowed:

.

.

.

    *EXC

    *EXC,4PIRSQ

This sequence executes the particular problem first without $4\pi R^2$ and then with $4\pi R^2$ included as a factor in the output quantities. The only command exempt from this is the *CONSTRAINT. In order to clear out unwanted parameters the *STOP command is used after which the problem must be completely respecified.

4.5   Input

The list of input control commands which were listed in Fig. 44 will be explained in detail in this section.

4.5.1   *Z-SOURCE(I)

Z = N, G, X and denotes neutron, prompt gamma or X-ray source, respectively, and has the same meaning for other source-related commands. I = 1, 2, 3, 4, 5, or 6 where 1-3 stands for internal

1.   *Z-SOURCE(I)

2.   *Z-SVAL, units, values

3.   *Z-EVAL, units, values

4.   *Z-NORM value

5.   *Z-YIELD value

6.   *XX, units, value(s)

7.   *E-REGRP/Z/, units, values

8.   *A-REGRP/Z/, units, values

9.   *PRINT/Z/(I1 I2 ...)

10.   *WRITE/Z/(I1 I2 ...)

11.   *CONSTRAINT/Z/(XX I Value), units

12.   *CXX, units, value(s)

13.   *FLUXWT/Z/, units, values

14.   *TITLE n

15.   *DOSE/Z/

16.   *EXC, 4PIRSQ

17.   *STOP

18.   *FIN

19.   *GROUND, units, value

Fig. 44. ATR input commands.

source selections, 4 denotes external histogram values, 5 denotes external nal point values and 6 specifies fission/fusion source. The internal source options taken from ORNL 4464 are fission spectrum (I=1), thermonuclear (I=2) and 12-15.2 MeV monoenergetic band (I=3) for neutrons. Options 4 and 5 require the use of the *Z-SVAL command to read in source values and a *Z-EVAL to read in energy values. If the internal source energy structure is used then only the *Z-SVAL command is necessary. The Value is the fraction (between 0 and 1) of 12-15.2 MeV neutrons in the internal fission spectrum and it is required for option 6 only.

Example: *N-SOURCE(4)

4.5.2 *Z-SVAL, Units[+], Values[++]

Units = PER MEV, PER KEV or PER GROUP and defines the source units. If units are not specified, the default choice is set internally to PER GROUP. Values = source values to be read in. These values must correspond to the energy values read in by the *Z-EVAL command. The order is assumed to be from low energy to high energy.

Example: *N-SVAL   .01   10   33   100   20.

[+]If units are designated with any of the commands, they must be delimited by commas; otherwise, default unit designations are used and commas must not appear.

[++]Values must be separated by at least one blank and may be continued on the next card.

4.5.3 *Z-EVAL, Units, Values

Units = MEV or KEV. A default in units specifies MEV for N and G, and KEV for X. Values = source energy boundary values if (4) is specified in 4.5.1, or source energy point values if (5) is specified in 4.5.1. The order is from low to high energy values.

Example: *N-EVAL, KEV, 3.35   12   50.5   120   170   235

4.5.4 *Z-NORM Value

Value = source normalization value in units of particle/KT. If this option is not specified then the source spectrum will not be normalized.

Example: *N-NORM 2.

4.5.5 *Z-YIELD Value

Value = source yield in KT. The total source output is the product of the YIELD value and the NORM value. Default value is 1.0.

Example: *N-YIELD 1.5E+23

4.5.6 *XX, Units, Value(s)

XX = one of RH, RS, HT, HS and AN. It denotes the horizontal range, slant range, target height, source height and slant angle respectively. Units = one of M, KM, MILE, YD, KFT, and FT for the distance and one of DEG, RAD, COS for the angle specification. Distance default unit is M and angle default unit is DEG. Values = up to 50 values of the geometry parameter. These values may be read in one at a time

80.

separated by blanks or in the format $n_1 (n)n_2$ signifying values from n_1 to n_2 in steps of n. In this case of the latter n_2 must be arithmetically greater than n_1. Three geometry values must be specified for a meaningful geometry configuration.

Two of the possible geometry configuration definitions result in ambiguities. One is when RH, RS and HT are specified. There is no inherent knowledge in this specification of whether HS should be placed above or below HT. In order to resolve the ambiguity the characters "+" or "−" should be used with the *HT command to indicate that HS is to be placed above or below HT, respectively. The other ambiguous configuration occurs when RH, RS and HS are specified. In this case the + or − should be used with the *HS command to place HT above or below HS respectively. If none of these characters are specified then + is assumed.

There is a special units option (GM) on RS which is allowed if the following geometry configuration is specified: HS, HT, RS. In that case the values following the "*RS,GM," command are interpreted as units of gm/cm^2 of the slant range. The GM units option is restricted to this configuration only.

Examples: *HT +, KM, 1.

*RS, KFT, .5(.5)10

*RH, KM, 10

4.5.7 *E-REGRP/Z/, Units, Values

Z = N, G, X, NG, GG for neutron, prompt gamma, X-ray, secondary gamma and combined prompt and secondary gammas, respectively. Units have the same options and meanings as in 4.5.3. Values = energy boundary values (low to high) which will be used to regroup output results.

Example: *E-REGRP/NG/ .1 .5 1. 2. 3. 5. 10

4.5.8 *A-REGRP/Z/, Units, Values

Z has the same options and meanings as in 4.5.7. Units has the same meaning as the angle specification in 4.5.6. Values - angle boundary values (low to high cosine values) which will be used to regroup output results.

Note that if angles are specified in degrees for this command then the angle values must be entered high to low.

Example: *A-REGRP/N/, COS, -1. -.5 0 .25 .5 .75 1.0

4.5.9 *PRINT/Z/(I1 I2 ---)

Z has the same meanings and options as in 4.5.7. I1, I2, etc. = integer values from 0 to 16, and will yield the following results on the print output unit:

0	=	summary
1	=	number fluence
2	=	number current
3		energy fluence

| 4 | = | energy current |

| 5-12 | = | internal dose responses |

| 13 | = | external flux weight as read in by *FLUXWT command |

| 14 | = | not used |

| 15 | = | results from *DOSE command |

| 16 | = | results from *CONSTRAINT commands |

If any of these appear with a negative sign, then the angle-energy distribution output will be suppressed for the particular case (applied to 1-13). The internal dose responses taken from ORNL-4464 correspond to the following specifications:

Neutron[+]

5 - Henderson Tissue Dose
6 - Snyder-Neufeld Dose
7 - Tissue Kerma
8 - Mid-Phantom Dose
9 - Concrete Kerma
10 - Air Kerma
11 - 1 MeV Silicon Equivalent
12 - Ionizing Silicon Kerma

Gamma[+]

5   - Henderson Tissue Dose
6   - Concrete Kerma
7   - Air Kerma
8   - Silicon Kerma
9-12 - not used

Example: *PRINT/NG/ (0 1 -3 2 6 -13)

Options 1-4 are defined in Section 4.6. The summary (option 0) includes total integrated quantities of currents, fluences, external flux weight, average energy, Henderson tissue dose and ionizing silicon dose.

[+]All responses are in units of $rad/(particle/cm^2)$.

Options 15 and 16 are automatically specified by the corresponding commands and need not be explicitly specified by the *PRINT command.

4.5.10 *WRITE/Z/(I1 I2 ---)

All of the options are the same as in 4.5.9.

Options 15 and 16 are automatically defined for *PRINT but must be explicitly specified for *WRITE.

Unit numbers are set up in a DATA statement where they can be easily modified for any particular computer system. The current values are:

> 5:input unit
>
> 6:print unit
>
> 8:write unit

The *WRITE command is included so that production runs generated by ATR can be saved on magnetic tape, drum or disk for future use.

Example: *WRITE/N/ (2 6 7 -8 15 16)

4.5.11 *CONSTRAINT/Z/(XX I Value), Units

Z has the same meanings and options as in 4.5.7 and I has the same meanings and options as in 4.5.9, but only options 1-13 are meaningful. Value is the fluence, current or dose value for which the constraint geometry is to be evaluated. This command only makes sense

84.

for response values that are not multiplied by $4\pi R^2$. Units has the same meanings and options as in 4.5.6 and it is a specification defining the geometry units printed in the output.

The *CONSTRAINT command calculates the value of coordinate XX which corresponds to a predetermined response level for given values of two other geometry coordinates specified. Version 1 of the code is restricted to XX = RS.

Example: *CONSTRAINT/N/ (RS 8 5E-20), MILE

4.5.12 *CXX, Units, Value(s)

*CXX defines the fixed coordinates and their values for a constraint calculation. All parameters have the same meaning and options as in 4.5.6.

Two *CXX commands combined with a *CONSTRAINT command define a constraint problem; of course, care must be taken to specify consistent and valid geometry configurations.

Examples: *CHS 1000

*CAN, DEG, -90 (10) 90

4.5.13 *FLUXWT/Z/, Units, Values

Z has the same meanings and options as in 4.5.7. Units = arbitrary (up to 16 characters) unit specification that will appear on the summary output. Values = flux weights to be used for weighting

the ATR energy spectrum and should correspond to the internal energy structure (low to high).

Examples:

*FLUXWT/NG/, CM**2 ERGS/GRAM, 5.9-8 1.2-8

8.-9 1.2-8 1.7-8 2.4-8 3.3-8 4.1-8 5.-8 6.15-8

7.15-8 8.4-8 9.8-8 1.2-7 1.5-7 1.8-7 2.2-7 2.65-7

4.5.14 *TITLE n

n may be up to 74 characters and is used as a problem title to identify the output.

Example: *TITLE AIR TRANSPORT PROBLEM

4.5.15 *DOSE/Z/

This command automatically prints dose values vs the running coordinate value specified. Z has the same meanings and options as in 4.5.7.

Examples: *DOSE/NG/

*DOSE/N/

4.5.16 *EXC, 4PIRSQ

This command is used to execute the problem defined by prior commands. If the comma appears after *EXC then resulting values will be multiplied by $4\pi R^2$ where R is the slant range.

86.

4.5.17 *STOP

This command clears the internal flags so that the next problem can be specified. All previous specifications are erased by this command, and it would normally follow a *EXC.

4.5.18 *FIN

This command terminates the program.

4.5.19 *GROUND, Units, Value

Units has the same meanings and options as in 4.5.6. Value is the ground level relative to sea level for the ATR problem geometry. If this command is not specified then sea level will be used for the ground level.

4.6 ATR OUTPUT AND SAMPLE RUNS

Five basic quantities can be calculated from ATR for each source-particle type:

Number Fluence: $\varphi(r, E, \mu)$ particles/MeV $\cdot$ cm^2 $\cdot$ steradian

Number Current: $\mu\varphi(r, e, \mu)$ particles/MeV $\cdot$ cm^2 $\cdot$ steradian

Energy Fluence: $E\varphi(r, E, \mu)$ particle-MeV/MeV $\cdot$ cm^2 $\cdot$ steradian

Energy Current: $E\mu\varphi(r, E, \mu)$ particle-MeV/MeV $\cdot$ cm^2 $\cdot$ steradian

DOSE: $D(E)\varphi(r, E, \mu)$ rads/MeV $\cdot$ steradian

The ATR control commands determine the type of output desired by the user, can consist of the differential quantities above, or any combination of the above integrated over energy or angle. A series of three sample ATR runs was made on a Univac 1108 computer to illustrate use of most of the input commands. The computer print-out is reproduced in this section and illustrates some of the output quantities available from ATR and the corresponding input required for each run.

```
VERSION 1. OF ATRNXG
*TITLE   SAMPLE ATR PROBLEM 1
*N=SOURCE(2)
*N=NORM  1.0+22
*N=YIELD 100
*GROUND,RF,1
*HS,KM,1
*HT,MI,0.621
*HS,KFT,6.56
*FLUXAT/N/,RADS, 1 1 1 1 1 1 1 1 1 1 1 1 1 1 1 1 1 1 1 1 1 1 1 1 1 1 1 1 1 1 1 1 1 1 1 1
*PRINT/N/(0)
*PRINT/NG/(0)
*EXC.
```

ATR PROBLEM NUMBER   1   SAMPLE ATR PROBLEM 1

• •

NEUTRON SOURCE   INTERNAL THERMONUCLEAR
NORMALIZATION= 1.000+22 NEUTRON /KT, YIELD= 1.000+02 KT
TOTAL OUTPUT= 1.000+24 NEUTRON

| | SOURCE SPECTRUM | ELD= 1.0 | | | |
ENERGY(MEV)	N/KT	N/KT*MEV	ENERGY(MEV)	N/KT	N/KT*MEV
1.07-05- 2.90-05	0.00	0.00	2.35+00- 2.46+00	5.00+21	4.55+22
2.90-05- 1.01-04	2.00+21	2.78+25	2.46+00- 3.01+00	1.90+22	3.45+22
1.01-04- 5.83-04	2.40+22	4.98+25	3.01+00- 4.07+00	2.60+22	2.45+22
5.83-04- 3.35-03	1.22+23	4.41+25	4.07+00- 4.97+00	1.70+22	1.49+22
3.35-03- 1.11-01	3.65+23	3.34+24	4.97+00- 6.36+00	1.80+22	1.29+22
1.11-01- 5.50-01	1.02+23	2.32+23	6.36+00- 8.19+00	1.47+22	8.03+21
5.50-01- 1.11+00	8.50+22	1.52+23	8.19+00- 1.00+01	1.41+22	7.79+21
1.11+00- 1.83+00	6.20+22	8.61+22	1.00+01- 1.22+01	2.56+22	1.16+22
1.83+00- 2.35+00	2.80+22	5.38+22	1.22+01- 1.50+01	7.06+22	7.52+22

• •

ATR PROBLEM NUMBER   1   SAMPLE ATR PROBLEM 1 • • • •

• •

```
 GROUND LEVEL     .305KM,   36.791GM/CM**2,  1.000KFT,   .190MILES
*HORIZ. RANGE RH= 1.999KM,  215.791GM/CM**2,  6.560KFT,  1.242MILES
 SLANT RANGE  RS= 1.999KM,  215.794GM/CM**2,  6.560KFT,  1.242MILES
 TARGET ALT.  HT=  .999KM,  115.273GM/CM**2,  3.279KFT,   .621MILES
 SOURCE ALT.  HS= 1.000KM,  113.537GM/CM**2,  3.281KFT,   .621MILES
*SLANT ANGLE  AN= -.017DEGREES (COS= 1.00000)
      *CALCULATED FROM OTHER COORDINATES
```

• •

NEUTRON   SUMMARY

		UNCOLL.	TOTAL	BUILDUP	BACKWARD	FORWARD
TISSUE DOSE (RADS*CM**2	)	3.91+09	5.08+12	1.30+03	1.65+12	3.42+12
SILICON DOSE (RADS*CM**2	)	4.01+08	9.60+10	2.39+02	1.99+10	7.62+10
NUMBER FLUENCE(N	)	9.05+17	8.22+21	9.08+03	3.54+21	4.61+21
NUMBER CURRENT(N	)	9.05+17	7.55+20	8.35+02	-1.72+21	2.48+21
ENERGY FLUENCE(N-MEV	)	6.14+18	3.15+21	5.13+02	8.20+20	2.33+21
ENERGY CURRENT(N-MEV	)	6.14+18	1.17+21	1.91+02	-3.74+20	1.55+21
EXT. FLX. WT. (RADS	)	9.05+17	8.15+21	9.01+03	3.54+21	4.61+21
AVERAGE ENERGY(MEV)		6.79+00	3.84-01	5.65-02	2.31-01	5.06-01

• •

NEUTRON GAMMA   SUMMARY

		UNCOLL.	TOTAL	BUILDUP	BACKWARD	FORWARD
TISSUE DOSE (RADS*CM**2	)	0.00	5.54+12	0.00	4.82+11	5.05+12
SILICON DOSE (RADS*CM**2	)	0.00	6.03+12	0.00	7.41+11	5.29+12
NUMBER FLUENCE(G	)	0.00	1.39+22	0.00	5.53+21	9.96+21
NUMBER CURRENT(G	)	0.00	3.63+21	0.00	-2.66+21	6.29+21
ENERGY FLUENCE(G-MEV	)	0.00	1.55+22	0.00	1.04+21	1.44+22
ENERGY CURRENT(G-MEV	)	0.00	1.23+22	0.00	-4.54+20	1.27+22
EXT. FLX. WT. (	)	0.00	0.00	0.00	0.00	0.00
AVERAGE ENERGY(MEV)		0.00	1.11+00	0.00	1.87-01	1.45+00

• •

**EXECUTION COMPLETED
*STOP

```
*TITLF   SAMPLE ATR PROHLEM 2
*N-SOURCE(3)
*HS.KM.20
*AN 45
*HS.KM.10
*PRINT/N/(-2)
*EXC
```

ATR PROBLEM NUMBER   1   SAMPLE ATR PROBLEM 2

• •

NEUTRON SOURCE   INTERNAL 14MEV
NORMALIZATION= 1.000+00 NEUTRON /KT, YIELD= 1.000+00 KT
 TOTAL OUTPUT= 1.000+00 NEUTRON

SOURCE SPECTRUM

ENERGY(MEV)		N/KT	N/KT*MEV	ENERGY(MEV)		N/KT	N/KT*MEV
1.07-05-	2.90-05	0.00	0.00	2.35+00-	2.46+00	0.00	0.00
2.90-05-	1.01-04	0.00	0.00	2.46+00-	3.01+00	0.00	0.00
1.01-04-	5.83-04	0.00	0.00	3.01+00-	4.07+00	0.00	0.00
5.83-04-	3.35-03	0.00	0.00	4.07+00-	4.97+00	0.00	0.00
3.35-03-	1.11-01	0.00	0.00	4.97+00-	6.36+00	0.00	0.00
1.11-01-	5.50-01	0.00	0.00	6.36+00-	8.19+00	0.00	0.00
5.50-01-	1.11+00	0.00	0.00	8.19+00-	1.00+01	0.00	0.00
1.11+00-	1.83+00	0.00	0.00	1.00+01-	1.22+01	0.00	0.00
1.83+00-	2.35+00	0.00	0.00	1.22+01-	1.50+01	1.00+00	3.57-01

• •

ATR PROBLEM NUMBER   1   SAMPLE ATR PROBLEM 2

• •

```
 GROUND LEVEL        .000KM.      .000GM/CM**2,   .000KFT.    .000MILES
*HORIZ. RANGE  RH= 7.071KM.   62.329GM/CM**2, 23.199KFT,  4.394MILES
 SLANT RANGE   HS= 10.000KM.   52.984GM/CM**2, 32.808KFT,  6.214MILES
*TARGET ALT.   H1= 27.071KM,1016.634GM/CM**2, 88.816KFT, 16.821MILES
 SOURCE ALT.   HS= 20.000KM,  979.169GM/CM**2, 65.617KFT, 12.427MILES
 SLANT ANGLE   AN=  45.000DEGREES (COS=  .70711)
       *CALCULATED FROM OTHER COORDINATES
```

• •

ATR PROBLEM NUMBER   1   SAMPLE ATR PROBLEM 2

• •

  NEUTRON   NUMBER CURRENT

DISTRIBUTION OVER ANGLE

ANG	DEGREES		COSINE		SUM OVER ENERGY (N/CM**2 *STER)	CUMULATIVE SUM (N/CM**2)
1	180.0 -	166.6	-1.0000 -	-.9728	-7.324-15	-1.249-15
2	166.6 -	155.6	-.9728 -	-.9106	-7.072-15	-4.016-15
3	155.6 -	144.6	-.9106 -	-.8154	-6.614-15	-7.970-15
4	144.6 -	133.7	-.8154 -	-.6908	-5.940-15	-1.262-14
5	133.7 -	122.8	-.6908 -	-.5412	-5.040-15	-1.756-14
6	122.8 -	111.8	-.5412 -	-.3720	-3.904-15	-2.151-14
7	111.8 -	100.9	-.3720 -	-.1894	-2.523-15	-2.440-14
8	100.9 -	90.0	-.1894 -	.0000	-8.994-16	-2.547-14
9	90.0 -	79.1	.0000 -	.1894	9.533-16	-2.434-14
10	79.1 -	68.2	.1894 -	.3720	2.499-15	-2.090-14
11	68.2 -	57.2	.3720 -	.5412	5.189-15	-1.517-14
12	57.2 -	46.3	.5412 -	.6908	8.419-15	-7.258-15
13	46.3 -	35.4	.6908 -	.8154	1.195-14	2.101-15
14	35.4 -	24.4	.8154 -	.9106	1.707-14	1.231-14
15	24.4 -	13.4	.9106 -	.9728	2.563-14	2.233-14
16	13.4 -	.0	.9728 -	1.0000	6.796-14	3.393-14

• •

```
                    DISTRIBUTION OVER ENERGY
     ENERGY(MEV )        SUM OVER ANGLE   CUMULATIVE SUM
                  (    N/CM**2  *MEV   ) (   N/CM**2      )
  1   0.00    - 4.14-07       1.583-10        5.728-17
  2   4.14-07- 1.12-06        9.524-11        1.245-16
  3   1.12-06- 3.06-06        4.241-11        2.068-16
  4   3.06-06- 1.07-05        1.562-11        5.261-16
  5   1.07-05- 2.90-05        5.766-12        4.520-16
  6   2.90-05- 1.01-04        1.570-12        5.734-16
  7   1.01-04- 5.83-04        5.402-13        8.302-16
  8   5.83-04- 3.35-03        1.059-13        1.122-15
  9   3.35-03- 1.11-01        1.673-14        2.277-15
 10   1.11-01- 5.50-01        4.089-15        4.072-15
 11   5.50-01- 1.11+00        4.553-15        6.622-15
 12   1.11+00- 1.83+00        2.818-15        8.651-15
 13   1.83+00- 2.35+00        5.464-15        1.071-14
 14   2.35+00- 2.46+00        7.752-15        1.157-14
 15   2.46+00- 3.01+00        4.230-15        1.349-14
 16   3.01+00- 4.07+00        1.394-15        1.537-14
 17   4.07+00- 4.97+00        2.313-15        1.745-14
 18   4.97+00- 6.36+00        1.452-15        2.017-14
 19   6.36+00- 8.19+00        1.134-15        2.224-14
 20   8.19+00- 1.00+01        5.909-16        2.331-14
 21   1.00+01- 1.22+01        8.581-15        2.520-14
 22   1.22+01- 1.50+01        3.118-15        3.193-14

 . . . . . . . . . . . . . . . . . . . . . . . . . . . . . . .
 **EXECUTION COMPLETED
 *STOP
```

```
*TITLE   SAMPLE ATR PROBLEM 3
*"-SOURCE(4)
*"-SVAL   0 0 0 0 .0155 .143 .198 .218 .12 .023 .089 .107 .035 .035 .014
.003 .00089 .00018
*-S 3000
*RM 1500
*HT.KM. 3 4 5 7 10 15 20
*DOSE/NG/
*EXC.



ATR PROBLEM NUMBER    1              SAMPLE ATR PROBLEM 3

* * * * * * * * * * * * * * * * * * * * * * * * * * * * * * * * * * * *

NEUTRON SOURCE    EXTERNAL HISTOGRAM
NORMALIZATION= 1.002+00 NEUTRON /KT. YIELD= 1.000+00 KT
 TOTAL OUTPUT= 1.002+00 NEUTRON /KT. YI

                    SOURCE SPECTRUM
ENERGY(MEV )    N/KT    N/KT*MEV    ENERGY(MEV )     N/KT    N/KT*MEV
1.07-05- 2.90-05  0.00      0.00    2.35+00- 2.46+00  2.30-02  2.09-01
2.90-05- 1.01-04  0.00      0.00    2.46+00- 3.01+00  8.90-02  1.62-01
1.01-04- 5.83-04  0.00      0.00    3.01+00- 4.07+00  1.07-01  1.01-01
5.83-04- 3.35-03  0.00      0.00    4.07+00- 4.97+00  3.50-02  3.89-02
3.35-03- 1.11-01  1.55-02  1.44-01  4.97+00- 6.36+00  3.50-02  2.52-02
1.11-01- 5.50-01  1.43-01  3.26-01  6.36+00- 8.19+00  1.40-02  7.65-03
5.50-01- 1.11+00  1.98-01  3.54-01  8.19+00- 1.00+01  3.00-03  1.66-03
1.11+00- 1.83+00  2.18-01  3.03-01  1.00+01- 1.22+01  8.90-04  4.05-04
1.83+00- 2.35+00  1.20-01  2.31-01  1.22+01- 1.50+01  1.60-04  5.71-05

* * * * * * * * * * * * * * * * * * * * * * * * * * * * * * * * * *

ATR PROBLEM NUMBER    1              SAMPLE ATR PROBLEM 3

* * * * * * * * * * * * * * * * * * * * * * * * * * * * * * * * * *
GROUND LEVEL       .000KM,     .000GM/CM**2,     .000KFT,   .000MILES
HORIZ. RANGE  RH= 1.500KM, 136.371GM/CM**2,    4.921KFT,  .932MILES
*SLANT RANGE   HS= 1.500KM, 136.371GM/CM**2,    4.921KFT,  .932MILES
TARGET ALT.   HT= 3.000KM, 318.462GM/CM**2,    9.842KFT, 1.864MILES
SOURCE ALT.   HS= 3.000KM, 318.462GM/CM**2,    9.842KFT, 1.864MILES
*SLANT ANGLE  AN=   .000DEGREES (COS= 1.00000)
        *CALCULATED FROM OTHER COORDINATES

* * * * * * * * * * * * * * * * * * * * * * * * * * * * * * * * * *

  NEUTRON GAMMA    DOSE  VS.  TARGET ALT.    (RADS*CM**2 )
                  DOSE 1= HENDERSON TISSUE
                  DOSE 2= CONCRETE
                  DOSE 3= AIR
                  DOSE 4= IONIZING SILICON

TARGET ALT.     DOSE 1    DOSE 2    DOSE 3    DOSE 4
  3.000+00 KM   1.87-11   2.05-11   1.64-11   2.00-11
  4.000+00 KM   1.23-11   1.35-11   1.08-11   1.32-11
  5.000+00 KM   4.02-12   4.46-12   3.52-12   4.33-12
  7.000+00 KM   3.00-13   3.32-13   2.62-13   3.22-13
  1.000+01 KM   1.20-14   1.32-14   1.04-14   1.28-14
  1.500+01 KM   5.06-16   5.58-16   4.42-16   5.43-16
  2.000+01 KM   1.17-16   1.28-16   1.02-16   1.25-16

* * * * * * * * * * * * * * * * * * * * * * * * * * * * * * * * * *
**EXECUTION COMPLETED
*HT 3000
*RM,KM, .5 1 1.5 2 2.5 3 4 5
*EXC.
```

ATR PROBLEM NUMBER   2   SAMPLE ATR PROBLEM 3

• •
    GROUND LEVEL   .000KM.   .000GM/CM**2.   .000KFT.   .000MILES
    HORIZ. RANGE RH= .500KM.   45.457GM/CM**2.   1.640KFT.   .311MILES
   *SLANT RANGE   RS= .500KM.   45.457GM/CM**2.   1.640KFT.   .311MILES
    TARGET ALT.   HT= 3.000KM. 318.462GM/CM**2. 9.842KFT.   1.864MILES
    SOURCE ALT.   HS= 3.000KM. 318.462GM/CM**2. 9.842KFT.   1.864MILES
   *SLANT ANGLE   AN=   .000DEGREES (COS= 1.00000)
            *CALCULATED FROM OTHER COORDINATES

• •
    NEUTRON GAMMA   DOSE VS. HORIZ. RANGE   (RADS*CM**2)
                    DOSE 1= HENDERSON TISSUE
                    DOSE 2= CONCRETE
                    DOSE 3= AIR
                    DOSE 4= IONIZING SILICON

HORIZ. RANGE   DOSE 1   DOSE 2   DOSE 3   DOSE 4
   5.000-01 KM   5.60-11   5.95-11   4.96-11   5.89-11
   1.000+00 KM   4.54-11   4.92-11   4.01-11   4.83-11
   1.500+00 KM   1.87-11   2.05-11   1.64-11   2.00-11
   2.000+00 KM   6.86-12   7.61-12   6.02-12   7.39-12
   2.500+00 KM   2.42-12   2.69-12   2.12-12   2.61-12
   3.000+00 KM   8.40-13   9.32-13   7.34-13   9.03-13
   4.000+00 KM   9.99-14   1.11-13   8.73-14   1.07-13
   5.000+00 KM   1.24-14   1.37-14   1.08-14   1.33-14

• •
**EXECUTION COMPLETED
*STOP

```
*TITLE   SAMPLE ATR PROBLEM 4
*N-SOURCE(3)
*N-NORM 1.0+22
*N-YIELD 100
*CHS,KM,10
*CAN -90(10)90
*CONSTRAINT/N/(RS 5 2500)
*EXC      :
```

ATR PROBLEM NUMBER   1   SAMPLE ATR PROBLEM 4

* *

NEUTRON SOURCE   INTERNAL   14MEV
NORMALIZATION= 1.000+22 NEUTRON /KT, YIELD= 1.000+02 KT
 TOTAL OUTPUT= 1.000+24 NEUTRON

                     SOURCE SPECTRUM

ENERGY(MEV)	N/KT	N/KT*MEV	ENERGY(MEV)	N/KT	N/KT*MEV
1.07-05- 2.90-05	0.00	0.00	2.35+00- 2.46+00	0.00	0.00
2.90-05- 1.01-04	0.00	0.00	2.46+00- 3.01+00	0.00	0.00
1.01-04- 5.83-04	0.00	0.00	3.01+00- 4.07+00	0.00	0.00
5.83-04- 5.35-03	0.00	0.00	4.07+00- 4.97+00	0.00	0.00
5.35-03- 1.11-01	0.00	0.00	4.97+00- 6.36+00	0.00	0.00
1.11-01- 5.50-01	0.00	0.00	6.36+00- 8.19+00	0.00	0.00
5.50-01- 1.11+00	0.00	0.00	8.19+00- 1.00+01	0.00	0.00
1.11+00- 1.83+00	0.00	0.00	1.00+01- 1.22+01	0.00	0.00
1.83+00- 2.35+00	0.00	0.00	1.22+01- 1.50+01	1.00+24	3.57+23

* *

ATR PROBLEM NUMBER   1   SAMPLE ATR PROBLEM 4

* *

NEUTRON   CONSTRAINT FOR SLANT RANGE   AND HENDERSON TISSUE= 2.50+03

*HORIZ. RANGE	SLANT RANGE	*TARGET ALT.	SOURCE ALT.	SLANT ANGLE
6.1570-05	1.9994+03 M	8.0006+03	1.0000+04	-90.000 DEG
3.4710+02	1.9983+03 M	8.0421+03	1.0000+04	-80.000 DEG
6.8262+02	1.9959+03 M	8.1243+03	1.0000+04	-70.000 DEG
1.0070+03	2.0140+03 M	8.2558+03	1.0000+04	-60.000 DEG
1.3030+03	2.0271+03 M	8.4471+03	1.0000+04	-50.000 DEG
1.5600+03	2.0402+03 M	8.6880+03	1.0000+04	-40.000 DEG
1.7862+03	2.0606+03 M	8.9076+03	1.0000+04	-30.000 DEG
1.9611+03	2.0882+03 M	9.2862+03	1.0000+04	-20.000 DEG
2.0788+03	2.1109+03 M	9.6534+03	1.0000+04	-10.000 DEG
2.1400+03	2.1400+03 M	1.0000+04	1.0000+04	.000 DEG
2.1356+03	2.1665+03 M	1.0376+04	1.0000+04	10.000 DEG
2.0605+03	2.1927+03 M	1.0750+04	1.0000+04	20.000 DEG
1.9204+03	2.2172+03 M	1.1109+04	1.0000+04	30.000 DEG
1.7162+03	2.2404+03 M	1.1440+04	1.0000+04	40.000 DEG
1.4529+03	2.2602+03 M	1.1731+04	1.0000+04	50.000 DEG
1.1373+03	2.2746+03 M	1.1970+04	1.0000+04	60.000 DEG
7.8390+02	2.2920+03 M	1.2154+04	1.0000+04	70.000 DEG
4.0011+02	2.3042+03 M	1.2269+04	1.0000+04	80.000 DEG
7.1039-05	2.3069+03 M	1.2307+04	1.0000+04	90.000 DEG

            *CALCULATED FROM OTHER COORDINATES
**EXECUTION COMPLETED
*N-YIELD 1000
*EXC

ATR PROBLEM NUMBER   2   SAMPLE ATR PROBLEM 4

• •

NEUTRON SOURCE   INTERNAL 14MEV
NORMALIZATION= 1.000+22 NEUTRON /KT, YIELD= 1.000+03 KT
 TOTAL OUTPUT= 1.000+25 NEUTRON

```
                    SOURCE SPECTRUM
ENERGY(MEV )    N/KT    N/KT*MEV    ENERGY(MEV )    N/KT    N/KT*MEV
1.07-05- 2.90-05  0.00    0.00     2.35+00- 2.46+00  0.00    0.00
2.90-05- 1.01-04  0.00    0.00     2.46+00- 3.01+00  0.00    0.00
1.01-04- 5.83-04  0.00    0.00     3.01+00- 4.07+00  0.00    0.00
5.83-04- 3.35-03  0.00    0.00     4.07+00- 4.97+00  0.00    0.00
3.35-03- 1.11-01  0.00    0.00     4.97+00- 6.36+00  0.00    0.00
1.11-01- 5.50-01  0.00    0.00     6.36+00- 8.19+00  0.00    0.00
5.50-01- 1.11+00  0.00    0.00     8.19+00- 1.00+01  0.00    0.00
1.11+00- 1.83+00  0.00    0.00     1.00+01- 1.22+01  0.00    0.00
1.83+00- 2.35+00  0.00    0.00     1.22+01- 1.50+01  1.00+25  3.57+24
```

• •

ATR PROBLEM NUMBER   2   SAMPLE ATR PROBLEM 4

• •

NEUTRON   CONSTRAINT FOR SLANT RANGE   AND HENDERSON TISSUE= 2.50+03

```
*HORIZ. RANGE   SLANT RANGE   *TARGET ALT.    SOURCE ALT.    SLANT ANGLE
 8.9643-05    2.9110+03 M      7.0890+03      1.0000+04      -90.000 DEG
 5.0633+02    2.9158+03 M      7.1285+03      1.0000+04      -80.000 DEG
 1.0020+03    2.9297+03 M      7.2470+03      1.0000+04      -70.000 DEG
 1.4768+03    2.9537+03 M      7.4420+03      1.0000+04      -60.000 DEG
 1.9277+03    2.9991+03 M      7.7026+03      1.0000+04      -50.000 DEG
 2.3232+03    3.0321+03 M      8.0586+03      1.0000+04      -40.000 DEG
 2.6725+03    3.0860+03 M      8.4570+03      1.0000+04      -30.000 DEG
 2.9581+03    3.1480+03 M      8.9233+03      1.0000+04      -20.000 DEG
 3.1680+03    3.2149+03 M      9.4414+03      1.0000+04      -10.000 DEG
 3.2984+03    3.2984+03 M      1.0000+04      1.0000+04        .000 DEG
 3.3276+03    3.3789+03 M      1.0587+04      1.0000+04       10.000 DEG
 3.2529+03    3.4617+03 M      1.1184+04      1.0000+04       20.000 DEG
 3.0680+03    3.5436+03 M      1.1772+04      1.0000+04       30.000 DEG
 2.7897+03    3.6416+03 M      1.2341+04      1.0000+04       40.000 DEG
 2.3654+03    3.7110+03 M      1.2865+04      1.0000+04       50.000 DEG
 1.9006+03    3.8012+03 M      1.3292+04      1.0000+04       60.000 DEG
 1.3254+03    3.8751+03 M      1.3641+04      1.0000+04       70.000 DEG
 6.7718+02    3.8997+03 M      1.3840+04      1.0000+04       80.000 DEG
 1.2034-04    3.9094+03 M      1.3909+04      1.0000+04       90.000 DEG
          *CALCULATED FROM OTHER COORDINATES
```
**EXECUTION COMPLETED
*FIN

REFERENCES

1. E. A. Straker, "Calculations of the Transport of Neutrons from Fission and 14-MeV Point Sources in an Infinite Medium of Air," ORNL-TM-1547 (1966).

2. E. A. Straker, "Sensitivity of Neutron Transport in Oxygen to Various Cross-Section Sets," ORNL (1968).

3. E. A. Straker, "Time-Dependent Neutron and Secondary Gamma-Ray Transport in Infinite Air and in Air Over Ground," ORNL-TM-2781 (1970).

4. W. M. Webster, "Neutron Air Transport Calculations," UCRL-50570 (1969).

5. L. F. Hansen, J. D. Anderson, E. Goldberg, J. Kammerdienes, E. Plechaty, and C. Wong, "Predictions for Neutron Transport in Air Based on Integral Measurements in Nitrogen and Oxygen at 14 MeV," UCRL-71838 (1969).

6. J. R. Keith and F. H. Shelton, "Neutron Transport in Uniform Air by Monte Carlo Calculations," Kaman Nuclear, KN-774-68-2 (1968).

7. L. F. Hansen, private communication, July 1970.

8. L. F. Hansen, J. D. Anderson, E. Goldberg, E. F. Plechaty, M. L. Stelts, and C. Wong, "Time Spectra from Spheres Pulsed with 14-MeV Neutrons and Their Analysis," UCRL-71124 (1968).

9. P. Brown, et al., to be published.

10. J. L. Russell, Jr., "Measurement and Analysis of Fast Neutrons in Liquid Nitrogen," Gulf General Atomic, GA-9081 (1968).

11. R. J. Harris, Jr., "Neutron Spectrum Measurements in Liquid Nitrogen," Gulf General Atomic, GA-9886 (1969).

REFERENCES (continued)

12. E. A. Straker, "Time-Dependent Neutron and Secondary Gamma-Ray Transport in an Air-Over-Ground Geometry. Vol. II. Tabulated Data," ORNL-4289 (1968).

13. E. A. Straker and M. L. Gritzner, "Neutron and Secondary Gamma-Ray Transport in Infinite Homogeneous Air," ORNL-4464 (1969).

14. T. R. Jeter, A. D. Coates, and J. A. Devanney, "Program 2, Operation HENRE, Part 1, Free-Field Spectral and Dose Determinations," Ballistic Research Laboratory, BRL 1420 (1968).

15. J. L. Pigg and J. L. Russell, Jr., "Neutron Penetration Measurements Program" Gulf General Atomic, AEC Report GA-8485 (1968).

16. G. M. Reynolds, "Gamma-Ray Transport in Liquid Nitrogen," Gulf General Atomic, DASA Report, GA-4929 (1969).

17. F. F. Haywood, T. E. Fronenyano, and J. A. Auxier, "Operation Plan-Operation HENRE," U. S. Atomic Energy Command Report CEX-65.03.

18. H. Goldstein and J. E. Wilkins, Jr., "Calculations of the Penetration of Gamma Rays," NYO-3075 (1954).

19. F. H. Shelton and J. R. Keith, "X-Ray Air Transport (U)," DASA Report No. 1981 (1967) S/RD.

20. F. H. Shelton and J. R. Keith, "Final Report--Time Dependent X-Ray Air Transport (U)," DASA Report No. 2138 (1968) S/RD.

21. A. D. Krumbein, "Angular Distribution of Scattered X-Rays Transported in a Homogeneous Atmosphere," UNC-5153 (1966) S/RD.

REFERENCES (continued)

22. A. D. Krumbein, "Additional Time, Energy and Angular Distributions of X-Rays in Air and at Air-Ground Interface (U)," UNC-5186 (1967) S/RD).

23. R. J. Harris, Jr., "Atmospheric Transport of X-Rays," Gulf General Atomic, GA-10165, to be published (1970).

24. E. E. Morris and A. B. Chilton, "Build-Up Factors in Water for Gamma Rays of 1 MeV and Lower Energy," Nucl. Sci. Eng. 40, 128 (1970).

25. M. Alberg, H. Beck, K. O'Brien and J. E. McLaughlin, "An Investigation of Differential Energy and Angle Spectra for ^{137}Cs Gamma Rays in Water and Air," Nucl. Sci. Eng. 30, 65 (1967).

26. C. W. Garrett, "The Low-Energy Component of the Total Dose for Deep Gamma-Penetrations in Air and Water," Trans. of Am. Nucl. Soc., Winter Meeting (1965).

27. A. B. Chilton, in Engineering Compendium on Radiation Shielding, Vol. I, R. G. Jaeger, et al., p. 210-226, Springer-Verlag, New York (1968).

28. M. J. Berger, "Energy Deposition in Water by Photons from Point Isotropic Sources," MIRD Pamphlet No. 2, Journal of Nuclear Medicine, Supplement No. 1 (February 1968).

29. B. Bennett and H. Beck, "Solutions of the One-Dimensional Gamma-Ray Transport Equation Using Full and Half Range Legendre and Tschelyscheff Polynomial Approximations," HASL-185, Health and Safety Laboratory, USAEC (1967).

30. J. R. Keith and F. H. Shelton, "Neutron Transport in Non-Uniform Air by Monte Carlo Calculations," Kaman Nuclear, KN-774-69-1 (1969).

REFERENCES (continued)

31. R. L. French, Health Physics **8**, 299 (1962).

32. D. D. Babb, "Curve Fits of Gamma-Ray Differential Energy Spectra," HARF-59-36T (1959).

33. E. A. Straker, W. W. Engle, Jr., and P. N. Steven, "Some Calculated Milestone Solutions to Time-Dependent Radiation Transport Problems," ORNL-TM-2499 (1969).

34. J. L. Abbott, R. L. Berger and H. A. Sandmeier, "Computed Neutron Flux at Coaltitude Ranges in Uniform Sea-Level Air," NWEF 1021 (1968).

35. S. Holland, Jr. and P. I. Richards, J. Appl. Phys. **27**, 1042 (1956).

36. C. D. Zerby, ORNL-2277 (1957).

37. M. B. Wells, FZK-9-147 (1958).

38. C. R. Mehl, SC-4174(TR) (1958).

39. F. L. Keller, C. D. Zerby and W. W. Dunn, ORNL-2462 (1958).

40. W. A. Biggers, L. J. Brown and K. C. Kohr, LA 2390 (1960).

41. E. M. Hippelli, D. L. Summers, and A. E. Anthony, Jr., AFSWC-TN-60-38 (1960).

42. J. I. Marcum, RM-2556 (1960).

43. M. B. Wells, MR-N-197 (1960)

44. R. H. Ritchie and V. E. Anderson, ORNL-3189 (1961).

45. D. Speilberg, NDA 2106-10 (1961).

REFERENCES (continued)

46. A. E. Anthony, Jr., AFSWC-TR-61-85 (1961).

47. R. E. Beissner, FZK-9-151 (1961).

48. W. E. Kinney, ORNL-3287 (1962).

49. C. Marotta and W. Guber, UNC-5006 (1962).

50. J. J. Marcum, RM-3531-PR (1963).

51. II. A. Sandmeier, G. E. Hansen, R. B. Lazarus and R. J. Howerton, LA 3415 (1965).

52. G. A. Husman, Jr. and F. N. Wimenity, HDL-TR-1305 (1965).

53. W. A. Biggers and M. R. Hemmendinger, LA-2390 (1963).

54. J. I. Marcum, RM-4385 (1965).

55. J. P. George and A. Lavagnino, DASA-1820-II (1966).

56. R. H. Karcher, Nucl. Sci. Eng. $\underline{27}$, 367 (1967).

57. M. D. Marshall and M. B. Wells, Trans. Am. Nucl. Soc. $\underline{9}$, No. 2, 343 (1966).

58. L. B. Engle and P. C. Fisher, LAMS-2642 (1962).

59. Reactor Handbook, Second Edition, Vol. III, Part 15, New York Interscience Publishers, 1962, p. 189-205.

60. M. Heusinkneld, 1958 Interum Internal Report, published as UCRL-50259 (1967).

61. R. H. Ritchie and G. S. Hurst, Health Physics $\underline{1}$, 390 (1959).

REFERENCES (continued)

62. J. A. Auxier, F. F. Haywood and L. W. Gilley, "General Correlative Studies--Operation BREN," U. S. Atomic Energy Command Report CEX-62.03 (1963).

63. P. A. Yampol'skii, et al., Soviet Journal of Atomic Energy, Vol. 21, #4926-930 (1966).

64. A. E. Fritzsche, et al., EGG-1183-1438, TR-L-943 (1969).

65. C. E. Clifford, Can. J. Phys. 42, 2373 (1964).

66. C. Sybesma, Nucl. Instr. Methods 21, 167 (1963).

67. J. Celnik, "Infinite-Medium Neutron Air Transport Build-Up and Corrections for an Exponential Atmosphere," Trans. Am Nucl. Soc. 12 (2), 955 (1969).

68. Detailed results of R. H. Ritchie and V. E. Anderson (not published but made available by private communication).

69. T. W. DeVries, "United States/Federal Republic of Germany Joint Main Bettle Tank Radiological Armor Program--Development of Free-Field Radiation Data for Nuclear Weapons Final Report," FZK-323 (April 15, 1967).

70. J. R. Keith and F. H. Shelton, "Interim Report--14 MeV Neutron Transport Results," KN-774-68-1 (September 19, 1968).

71. A. E. Straker and F. R. Mynatt, "Calculations of the Effect of the Air-Ground Interface on the Transport of Fission Neutrons through the Atmosphere," ORNL-TM-1819 (November 1, 1967).

72. E. A. Straker, "Time-Dependent Neutrons and Secondary Gamma-Ray Transport in an Air-over-Ground Geometry, Vol. II, Tabulated Data," ORNL-4289, Vol. II (September, 1968).

73. C. F. Johnson, "Radiological Armor Program Methods and Data Compilation, Vol. 2, Radiation Environments," General Dynamics/Fort Worth Report FZK 200-2 (August 31, 1965).

74. S. A. Dupree, "Calculations of Radiation Envelopes About Point Sources in the Atmosphere: Program Slant," NWEF 1044 (1969), Weapons Evaluation Facility.

75. R. L. French, "A First-Last Collision Model of Air-Ground Interface Effects on Fast Neutron Distribution", Nuclear Science and Engineering 19, 151 (1964).

76. U.S. Standard Atmosphere, 1962. U. S. Government Printing Office, Washington, D. C., December 1962.

77. J. A. Auxier, et. al., Health Phys. 12, 425 (1966).

78. J. H. Hubbell, "Photon Cross Sections, Attenuation Coefficients, and Energy Absorption Coefficients from 10 keV to 100 GeV," NBS 29, August 1969.

79. W. H. McMaster, N. Kerr Del-Grande, J. H. Moilett, J. H. Hubbell (NBS), " Compilation of X-Ray Cross Sections," UCRL-50174 Sec. II Rev. 1, May 1969.

80. The OGRE Calculations of 60 keV-Photon Transport in Liquid Nitrogen were made by W. A. Coleman at Science Applications.

81. The OGRE Calculation of Low-Energy Photon Transport in Air were Sponsored by BRL and made by N. Banks (BRL) and W. A. Coleman (SAI). These results to be published soon.

APPENDIX A

A bibliography of basic data for radiation transport in air has been compiled during the course of this work from published and unpublished works which have resulted during the past fifteen years. This compilation represents the major comprehensive works of which the authors are aware, based on a systematic document search by computer, personal communications and private files.

A summary of references on theoretical and experimental work is listed in Tables I and II, respectively, in chronological order, according to type of radiation considered. Tables III-V give details of the calculational problems considered for exponential air, infinite uniform air and for an air-ground interface, respectively.

Table 1. Summary of References on Calculational Air-Transport Data

Year	Neutrons	Secondary Gamma-Rays	Photons
1954			Goldstein and Wilkins[16]
1956	Holland[35]		
1957	Zerby[36]		
1958	Wells, [38] Mehl, [38] Keller[39]	Wells[37]	Lynch[59]
1960	Biggers, [40] Hippell, [40] Marcum, [42] Wells[43]		
1961	Ritchie, [44] Speilberg, [45] Anthony, [46] Beissner[47]	Speilberg[45]	
1962	Kinney, [48] Marotta[49]		Engle and Fisher[56]
1963	Biggers, [53] Marcum[50]		
1965	Sandmeier, [51] Ausman[52] Marcum[54]		
1966	George, [55] Straker[1]		Marshall, [57] Krumbein[21]
1967	Karcher[55]		Krumbein, [22] Keith[19]
1968	Straker, [12] Keith[6]	Straker[12]	Keith[20]
1969	Straker, [13] Keith, [30] Webster, [4] Hansen[5], Celnik[67]	Straker[13]	
1970	Straker[3]	Straker[2]	

Table II. Summary of References on Experimental Air-Transport Data

Year	Neutrons	Secondary Gamma-Rays	Photons
1958	Heusinkneld[60]	Heusinkneld[60]	
1959	Ritchie[51]		
1965	Haywood (Operation HENRE[17] and BREN[62])	Haywood (Operation HENRE[17] and BREN[62])	Sybesma, [66] Clifford[55]
1966	Yampolski[63]		
1968	Jeter, [14] Russell, [10] Hansen[8]	Jeter, [14] Russell[10]	Alberg[25]
1969	Harris, [11] Fritzsche[64]	Reynolds[16]	
1970	Brown[9]		Harris[23]

Table III. List of Calculations for Exponential Air

Investigator	Date	Method	Source Energy	Source Height	Pages	Results*	Code
Marcum[42]	1963	Monte Carlo	14 MeV	100,000 200,000	40	$\phi(r,E)$	RAND
Marcum[54]	1965	Monte Carlo	14 MeV Fission	33,000 158,000	24	$S_g(r,t)$	RAND
George and Lavagnino[55]	1966	Monte Carlo	17 Mono. Energies	30,000 50,000 80,000	788	$\phi(r,E,t)$	AUGEAS
Shelton and Keith[30]	1968	Monte Carlo	8 Energy Intervals	110,000 85,000	131	$\phi(r,E,\Omega)$	NHAT
Celnik[67]	1969	Monte Carlo	7 Energy Intervals	65,000 to 250,000	3	$\phi(r,E,t)$	UNC-SAM2

* ϕ denotes fluence; S denotes source term, g denotes secondary gamma ray, D denotes dose.

Table IV. List of Calculations for Infinite Air

Investigator	Date	Method	Source Energy	Pages	Results*	Code
Holland and Richards[55]	1955	Moments	Monoenergetic	113	$\phi(r,E)$	
Mehl[38]	1958	Monte Carlo	8 Energies	135	$\phi(r,E,\Omega)$	
Wells[37]	1960	Monte Carlo	Fission 8 Energies	276	$\phi(r,E,\Omega)$	K-74
Spielberg[45]	1961	Moments	Fission	33	$\phi(r,E)$	RENUPAK
Kinney[48]	1962	Monte Carlo	6 Energies	17	$\phi(r,E)$	O5R
Ritchie and Anderson[44,68]	1962	Monte Carlo	14 Energies	9	$\phi(r,E)$ $D(r,\Omega)$	
Marcum[50]	1963	Monte Carlo	14 MeV	40	$\phi(r,E)$	
Eisenhauer	1965	Moments	Fission 14 MeV	N.P.	$\phi(r,E)$	
Johnson[73]	1965	Monte Carlo	14 MeV Fission 5 Energies	41	$\phi(r,E,\Omega)$	K-74
Sandmeier[51]	1965	Discrete Ordinates	12-14 MeV	69	$\phi(r,E)$	DTF-IV
Straker[1]	1965	Monte Carlo	Fission 14 MeV	7	$\phi(r,E)$ $D(r)$	O5R

* ϕ denotes fluence, g denotes secondary gamma ray, D denotes dose.

109.

Table IV. (continued)

Investigator	Date	Method	Source Energy	Pages	Results*	Code
Straker[1]	1965	Discrete Ordinates	Fission 14 MeV	7	$D(r)$ $\phi(r,E)$	ANISN
Trubey	1965	Moments	14 MeV Fission	N.P.	$\phi(r,E)$ $D(r)$	RENUPAK
Karcher[56]	1966	Monte Carlo	Spectrum	44	$\phi(r,E)$ $\phi(r,\Omega)$	OSR
DeVries[69]	1967	Monte Carlo	14 MeV	75	$\phi(r,E,\Omega)$ $\phi_g(r,E,\Omega)$	COHORT
Yampolskii[63]	1967	Monte Carlo	9 Energies	10	$\phi(r,E)$	
Keith and Shelton[70]	1968	Monte Carlo	14 MeV	15	$D(r)$	NHAT
Keith and Shelton[6]	1968	Monte Carlo	12 Energies	155	$\phi(r,E)$ $\phi(r,t)$	NHAT
Webster[4]	1969	Monte Carlo	12 Energies	67	$\phi(r,E)$	SORS
Straker and Gritzner[13]	1969	Discrete Ordinates	8 Energies Fission	410	$\phi(r,E,\Omega)$ $\phi_g(r,E,\Omega)$	ANISN
Hansen et al.[1]	1970	Monte Carlo	14 MeV	50	$\phi(r,E)$ $D(r)$	SORS

* ϕ denotes fluence, g denotes secondary gamma ray, D denotes dose.

Table V. List of Calculations for Air/Ground

Investigator	Date	Method	Source Energy	Source Height	Pages	Results*	Code
Biggers, Brown, Kohr[40]	1960	Monte Carlo	12 Energies Weapons Leakage	300 ft	173	$\phi(r,E,t)^\dagger$	NHM
Marcum[42]	1960	Monte Carlo	3, 14 MeV	300 ft	55	$\phi(r,E)$	RAND
Kinney[48]	1962	Monte Carlo	6 Energies	0	17	$\phi(r,E)$	05R
Ritchie, Anderson[44,66]	1962	Monte Carlo	14 Energies	300 ft 650 ft	18	$\phi(r,E)$ $D(r,\Omega)$	NHM
Marcum[42]	1963	Monte Carlo	14 MeV	0, 750, 3,000	40	$\phi(r,E)$ $D(r)$	CAPS
DeVries[69]	1967	Monte Carlo	14 MeV	116 ft	75	$\phi(r,E,\Omega)$ $\phi_g(r,E,\Omega)$	COHORT
Straker and Mynatt[71]	1967	Discrete Ordinates	Fission	300 ft	19	$\phi(r,E)$ $D(r)$	DOT
Straker[72]	1968	Monte Carlo	9 Energy Bands	50 ft	250	$\phi(r,E,\Omega,t)$ $D(r,t)$ $\phi_g(r,E,\Omega,t)$ $D_g(r,t)$	06R
Straker[72]	1968	Discrete Ordinates	9 Energy Bands	50 ft	250	$\phi(r,E,\Omega)$ $D(r,\Omega)$ $\phi_g(r,E,\Omega)$ $D_g(r,E,\Omega)$	DOT

*ϕ denotes fluence, g denotes secondary gamma ray, D denotes dose.

†Shock wave included.

Table VI. Comprehensive infinite Uniform Air Calculations

Year	Investigator	Computer Codes	Cross-Sections	Results
1965	Sandmeier (LASL)	Discrete ordinates DTF-IV	Howerton	$\Phi_n(E, r, \theta)$
1968	Keith and Shelton (Kaman Nuclear)	Monte Carlo HAT	Howerton	$\Phi_n(E, r, \theta, t)$
1969	Webster (LRL)	Monte Carlo SORS	Modified Howerton	$\Phi_n(E, r, \theta)$
1969	Straker (ORNL)	Discrete ordinates ANISN	ENDF/B	$\Phi_n(E, r, \theta)$
				$\Phi_\gamma(E, r, \theta)$

APPENDIX B

DENSITY-SCALING SOLUTIONS TO THE BOLTZMANN TRANSPORT EQUATION.

Given an arbitrary scattering medium and particle source configuration, the corresponding transport problem solution can be obtained from an equivalent (in that the solutions to Boltzmann's equation are identical) density-scaled configuration. Relationships are given here between the solution to the given arbitrary configuration and the solution to the transformed configuration.

The Boltzmann transport equation can be written

$$\frac{\partial N(E, \vec{\Omega}, \vec{r}, t)}{\partial t} = S(E, \vec{\Omega}, \vec{r}, t) - \vec{v}(E, \vec{\Omega}) \cdot \nabla N(E, \vec{\Omega}, \vec{r}, t)$$

$$- \sigma_t(E, \vec{r}) \cdot \rho(\vec{r}) \cdot N(E, \vec{\Omega}, \vec{r}, t) \cdot |\vec{v}(E)|$$

$$+ \int\int N(E', \vec{\Omega}', \vec{r}, t)\, \sigma_p(E', \vec{r}) \cdot \rho(\vec{r}) \cdot |\vec{v}(E')|$$

$$\cdot G(E', \Omega', E, \Omega)\, dE'\, d\Omega'$$

This equates the time rate of change of the particle differential number density, $N(E, \vec{\Omega}, \vec{r}, t)$, to the source strength minus the losses due to convection and scattering plus the gain due to scattering from other energy and direction groups.

N is the number of particles per meter^3-Mev-steradian

S is the source of particles per meter^3-Mev-steradian

σ_t is the total particle cross section in meter^2/target

σ_p is the particle-producing cross section in meter^2/target

ρ is the target density in targets/meter^3

v is the particle velocity in meters/second

G is the probability that given a collision, the particle scatters from E´, Ω´ to E, Ω.

If we perform the transformation

$$\rho_t(\vec{r}_t) = \rho(\vec{r})/K$$

$$\vec{r}_t = K \vec{r}$$

$$t_t = K t$$

$$N_t(E, \vec{\Omega}, \vec{r}_t, t_t) = K^{-3} N(E, \vec{\Omega}, \vec{r}, t)$$

$$S_t(E, \vec{\Omega}, \vec{r}_t, t_t) = K^{-4} S(E, \vec{\Omega}, \vec{r}, t)$$

then the transport equation is merely multiplied on both sides by K^{-4}. In other words, if $N(E, \vec{\Omega}, \vec{r}, t)$ is a solution of Boltzmann equation given $\rho(\vec{r})$, $S(E, \vec{\Omega}, \vec{r}, t)$, then $N_t(E, \vec{\Omega}, \vec{r}_t, t_t)$ is a solution given the configuration ρ_t and $S_t(E, \vec{\Omega}, \vec{r}_t, t_t)$ as defined in the above transformation.

Information about the particle density $o(r, t)$ in the initial problem is equivalent to information about the particle density at a scaled time and position in the transformed (scaled) problem. The scaling of specific quantities derived from the number density follows from their definitions.